CRC/EI Research report

Charge generation and dissipation in aviation fuel handling with filter monitors

CRC Project Number AV-22-15

CRC/EI RESEARCH REPORT

CHARGE GENERATION AND DISSIPATION IN AVIATION FUEL HANDLING WITH FILTER MONITORS

Harold L. Walmsley (Harold Walmsley Electrostatics Ltd),
Daniel Taylor (Afton Chemical Corporation)

September 2017

Published by
Energy Institute, London
The Energy Institute is a professional membership body incorporated by Royal Charter 2003
Registered charity number 1097899

and the
Coordinating Research Council, Inc.
5755 North Point Parkway, Suite 265, Alpharetta, GA 30022

The Energy Institute (EI) is the chartered professional membership body for the energy industry, supporting over 23 000 individuals working in or studying energy and 250 energy companies worldwide. The EI provides learning and networking opportunities to support professional development, as well as professional recognition and technical and scientific knowledge resources on energy in all its forms and applications.

The EI's purpose is to develop and disseminate knowledge, skills and good practice towards a safe, secure and sustainable energy system. In fulfilling this mission, the EI addresses the depth and breadth of the energy sector, from fuels and fuels distribution to health and safety, sustainability and the environment. It also informs policy by providing a platform for debate and scientifically-sound information on energy issues.

The EI is licensed by:
- the Engineering Council to award Chartered, Incorporated and Engineering Technician status;
- the Science Council to award Chartered Scientist status, and
- the Society for the Environment to award Chartered Environmentalist status.

It also offers its own Chartered Energy Engineer, Chartered Petroleum Engineer and Chartered Energy Manager titles.

A registered charity, the EI serves society with independence, professionalism and a wealth of expertise in all energy matters.

This publication has been produced as a result of work carried out within the Technical Team of the EI, funded by the EI's Technical Partners. The EI's Technical Work Programme provides industry with cost-effective, value-adding knowledge on key current and future issues affecting those operating in the energy sector, both in the UK and internationally.

For further information, please visit **http://www.energyinst.org**

The EI gratefully acknowledges the financial contributions towards the scientific and technical programme from the following companies

Apache North Sea
BP Exploration Operating Co Ltd
BP Oil UK Ltd
Centrica
Chevron North Sea Ltd
Chevron Products Company
CLH
ConocoPhillips Ltd
DCC Energy
DONG Energy
EDF Energy
ENGIE
ENI
E. ON UK
ExxonMobil International Ltd
Innogy
Kuwait Petroleum International Ltd
Maersk Oil North Sea UK Limited
Nexen CNOOC
Phillips 66
Qatar Petroleum
Repsol Sinopec
RWE npower
Saudi Aramco
Scottish Power
SGS
Shell UK Oil Products Limited
Shell U.K. Exploration and Production Ltd
SSE
Statkraft
Statoil
Tesoro
Taqa Bratani
Total E&P UK Limited
Total UK Limited
Tullow Oil
Uniper
Valero
Vattenfall
Vitol Energy
Woodside
World Fuel Services

However, it should be noted that the above organisations have not all been directly involved in the development of this publication, nor do they necessarily endorse its content.

The Coordinating Research Council, Inc. (CRC) is a non-profit corporation supported by the petroleum and automotive equipment industries. CRC operates through the committees made up of technical experts from industry and government who voluntarily participate. The four main areas of research within CRC are: air pollution (atmospheric and engineering studies); aviation fuels, lubricants, and equipment performance, heavy-duty vehicle fuels, lubricants, and equipment performance (e.g., diesel trucks); and light-duty vehicle fuels, lubricants, and equipment performance (e.g., passenger cars). CRC's function is to provide the mechanism for joint research conducted by the two industries that will help in determining the optimum combination of petroleum products and automotive equipment. CRC's work is limited to research that is mutually beneficial to the two industries involved. The final results of the research conducted by, or under the auspices of, CRC are available to the public.

ISBN 978 0 85293 975 8

Published by the Energy Institute

Hard copy and electronic access to EI and IP publications is available via our website, **https://publishing.energyinst.org**.
Documents can be purchased online as downloadable pdfs or on an annual subscription for single users and companies.
For more information, contact the EI Publications Team.
e: **pubs@energyinst.org**

CONTENTS

Contents continued

Page

Contents continued

LIST OF FIGURES AND TABLES

Page

Figures

Tables

List of figures and tables continued

Page

SUMMARY

This report describes experiments done to examine charge generation and dissipation in aviation kerosene during the filling of tanks via filter monitor units. There have been changes to both fuels and filter monitor element design since the last publicly reported studies of these processes more than 12 years ago. The principal aim of the work was to see if these changes had any impact on the charge densities that could be delivered to tanks. A secondary aim was to investigate the electric fields these charge densities could be expected to generate within a receiving tank. A range of fuel charging behaviours is present globally in aviation fuel distribution systems and it was not practicable to test every potential situation. The conditions chosen for testing seek to provide the industry with a fair insight into the expected behaviour within the limitations of the programme.

The test rig was designed to measure charging in commercial filter monitor elements up to 6" in diameter at their maximum rated flow. The pipe residence times, tank fill times and charge densities due to pipe charging were matched, as closely as was practicable, to representative values for a selected full-scale scenario. The measured charge densities should then everywhere be comparable to those in the equivalent real system. This equivalence can be used to scale the medium-scale test data to full size conditions. Appropriate scaling laws are suggested. Details of fuel properties and test equipment (conductivities, charge decay times, flow rate, pipe dimensions, residence times etc) are also provided to allow for the approximate adjustment of the measured data to predict the behaviour of full scale systems with different parameters.

For each condition tested, a fuel was charged by passing it from a metal source tote[1] through a filter monitor vessel and into a metal receiving tote. Between the filter and the receiving tote the charge was allowed to relax in two successive sections of fuel hose. The filter vessel, the two hose sections and the receiving tote were electrically isolated from each other and from ground. By connecting the isolated sections to ground via sensitive ammeters the currents generated in the filter unit, dissipated in the hoses and delivered to the tote could be measured. The streaming currents carried by the fluid across the interfaces between these sections were reconstructed from the measured currents and converted into charge densities (charge density = streaming current/flow rate) using the measured flow rate. The receiving tote was fitted with an internal electric field meter to measure the electric field in the vapour space both during and immediately after the flow period.

The measurements were done in two phases. Phase 1 principally covered the charging, at full rated flow, of EI 1583 6th edition filter monitor elements from each of the three known manufacturers (Parker Velcon, Faudi Aviation and Peco Facet)[2]. Each test used three 2" x 30" elements from one manufacturer. A few comparative tests using one type of 4th edition element were also done. Each type of element was tested in its as-received dry state and after water-wetting to a maximum level set so that the pressure drop at rated flow was around 10 psi/69 kPa.

The Phase 1 results were obtained with an aviation kerosene (Jet A) and a Green diesel. Each fuel was tested as received, after clay filtration, after additisation with varying doses of SDA and after additisation with a specified dose of a pro-static agent. The pro-static agent was chosen from the results of preliminary testing with a mini-static tester. This was the only screening test available, although it was not expected to correlate closely with the behaviour of commercial filter monitor elements. The concentration of pro-static agent was set to maximise charge generation without increasing the conductivity beyond the range that could give a significant level of charge accumulation in the receiving tank.

1 'Totes' are known in Europe as Intermediate Bulk Containers or IBCs.
2 The report does not link any individual results to the specific manufacturer.

In Phase 2 an approximate worst-case fuel and additive combination was chosen from Phase 1 and used with both 2" and a full range of 6" element types at flow rates ranging from 50 % to 100 % of rated flow. These results primarily indicate the influence of flow rate and the differences between 2" and 6" elements.

The maximum charge densities observed with both dry and water-wetted elements were similar to the highest values reported in earlier work on 2" filter monitor charging. The differences are regarded as too small to be significant.

In Phase 2 no significant differences were found between 2" and 6" monitors and the charge densities either remained constant or increased approximately linearly with flow rate.

1 INTRODUCTION

This report describes a work programme initiated jointly by the Energy Institute (EI) and the CRC to measure charge generation and dissipation in a representative aviation fuel handling test rig using commercial filter monitor elements. Although there has been recent, commercially-motivated work in this area, much of the detail is confidential. Charging in filter monitors was last reported on publicly more than 12 years ago [1,2] and most published work [e.g. 3,4] pre-dates that. There have been changes to fuels and filter element design since these publicly-reported measurements. The principal aim of the work was to see if these changes had any impact on the charge densities that could be delivered to tanks. During the work, the opportunity was also taken to measure the electric fields in the roof space of the receiving tank to also evaluate the benefit of in-tank relaxation processes.

The rig was designed to match, as closely as was practicable, the specific flow rate in the filter monitor elements, the pipe residence times, the pipe flow charge densities and the tank fill times to the equivalent processes in a representative full-scale set-up, whilst using the smallest practicable test scale that would allow the testing of 6" elements at full rated flow. With the chosen test parameters the measured charge densities and decay times should then be as close as possible to those in the equivalent real system. This fact can be used to scale the parameters that do change with equipment scale (currents, total in-tank charge, voltages and electric fields) from the test-rig scale to the equivalent full size conditions. The necessary scaling laws are described in Annex A. In the final design it was necessary to compromise on tank fill time, which is a little longer than in the real world scenario the rig was trying to simulate.

This report describes the test rig design, test conditions, measurement methods and test procedures and presents the results in terms of streaming current, charge density, in-pipe charge dissipation, in-tank electric field and post-fill electric field decay time.

Although we tried to match a specific real world scenario, all necessary fuel properties and test rig data (conductivities, charge decay times, flow rates, pipe dimensions, residence times, fill times, etc.) are provided to allow the approximate adjustment of the measured data to predict the behaviour of systems with different full-scale parameters.

The general electrostatic aspects of rig design and the data analysis were carried out by Harold Walmsley Electrostatics Limited. The detailed rig design and construction and the experimental test programme itself were carried out by Afton Chemical Corporation. There was much valuable feedback on all aspects of the work from the other members of the project team.

2 OUTLINE OF TEST PROCEDURE

As an aviation fuel flows through a fuel handling system, electrostatic charge is generated and produces an electric current, known as the streaming current, that is the product of the volumetric flow rate and the charge density generated by the flow. The highest charge densities are generated by flow through fine filters. The present tests consisted of a series of runs carried out to investigate the streaming currents and charge densities produced by EI 1583 6th edition filter monitors.

Each test run involved transferring a 180 USG (0,698 m^3) batch of fuel between two metal totes via a filter monitor unit and two successive sections of 2" aviation fuel hose. Electrostatic charge was generated on the fuel as it passed through the filter monitor and then partially relaxed as it continued through the fuel hoses to the second ('receiving') tote. The filter vessel, the two hose sections and the receiving tote were electrically isolated from each other and from ground so that, by connecting the isolated sections to ground via sensitive ammeters, the currents generated in the filter unit, dissipated in the hoses and delivered to the tote could be measured. The streaming currents carried by the liquid were reconstructed from the measured currents as described in Annex B. The flow rate was also measured so that the streaming currents could be converted into charge densities. The receiving tote was fitted with a field meter to measure the electric field in the vapour space both during and immediately after the flow period. This enabled both the measurement of the vapour space electric field and the determination of the electric field decay time.

The testing was done in two phases. Phase 1 tests covered the charging produced at full rated flow (90 USGPM, 340 l/min) in a filter vessel housing three 2" x 30" (50 mm x 762 mm) filter monitor elements qualified to EI 1583 6th edition. At every chosen test condition, two repeat test runs were done using a set of elements produced by each of the three current aviation filter manufacturers (Parker Velcon, Faudi Aviation and Peco Facet). For the presentation of Phase 1 data, the manufacturers are randomly assigned the labels A, B and C. Each element was tested in its as-received dry state and again after water-wetting to a maximum level set so that the pressure drop at rated flow was around 10 psi/69 kPa. For comparison, a limited number of tests were done with some elements qualified to EI 1583 4th edition 2" that were still available. These happened to be from manufacturer B.

The Phase 1 tests were done with two different fuels, an aviation kerosene (Jet A) and a 100 % hydrocarbon Green diesel. Each fuel was tested as received, after clay filtration, after additisation with varying doses of static dissipater additive (SDA) and/or after additisation with a specified dose of a pro-static agent. The pro-static agent was chosen from the results of preliminary testing with a mini-static tester. This was the only screening test available, although it was expected to correlate fairly poorly with the behaviour of filter monitor elements in commercial operations. The concentration of pro-static agent was chosen to maximise charge generation without increasing the conductivity beyond the range that could give significant in-tank electric fields.

The Phase 2 work was all done in a single, approximately worst-case condition (Jet A plus pro-static agent, dry elements) chosen from the Phase 1 results. It involved testing both the 2" x 30" 6th edition elements used in Phase 1 and a full set of 6" x $28\frac{7}{8}$" (152 mm x 727 mm) elements qualified to EI 1583 4th edition at flow rates from 50 % to 100 % of the rated flow. These results primarily indicate the differences between 2" and 6" elements and the influence of flow rate. When reporting Phase 2 results the manufacturers are labelled X, Y and Z.

3 THE TEST RIG AND INSTRUMENTATION

3.1 THE LIQUID HANDLING SYSTEM

Figure 1 shows a photograph of the main liquid handling equipment and a schematic diagram is shown in Figure 2. The key components are:

- A source container (tote).
- A filter monitor housing (with bypass) containing, in Phase 1, three 2" x 30" elements or, in Phase 2, a single 6" element or four 2" x 30" elements.
- Two 120" (3 048 mm) lengths of 2" aviation fuel hose plus short lengths of linking pipe, flanges and valves connecting the filter to a receiving tote that is part-filled during each test.
- A receiving container (tote) that has an electric field meter mounted to an access chamber cover in the centre of the roof to permit electric field measurement in the vapour space.
- A clay filter that can be used for treating the fuel between tests and cleaning up the rig.

Figure 1: Photograph of the test rig

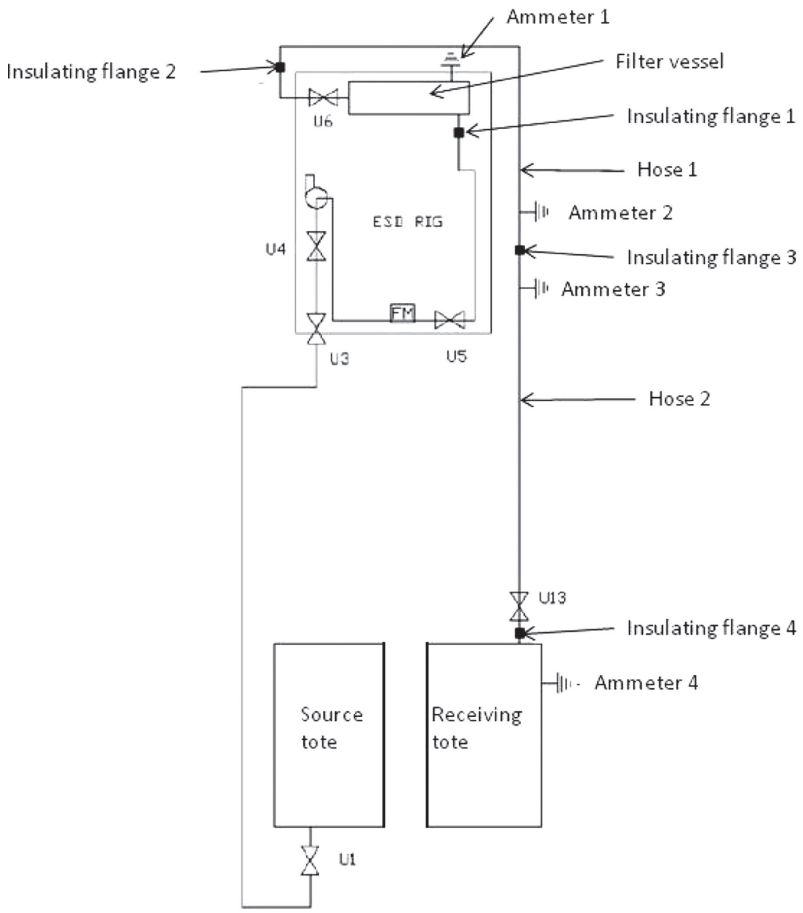

Figure 2: Schematic diagram of the test rig

The flow speeds, tank fill times and residence times in the system aimed to give charge densities, pipe/hose residence times and tank fill times representative of the worst cases that would be encountered in commercial jet fuel handling (i.e. highest charge density, shortest residence and fill times), although for tank fill time a compromise was necessary on tank fill time in order to get adequate test flow time at full rated flow. A discussion of operating conditions and the selection of rig parameters is given in Annex A, which includes the recommendation that pipe charging should be considered to scale as velocity/pipe diameter (*v/d)* [5,6]. Table 1 lists the dimensions of key parts of the system and includes the flow speeds, *v/d* values and residence/fill times at a standardised flow rate of 100 USG/min. Maximum flow rates were 90 USGPM for Phase 1 2" element tests, 120 USGPM for Phase 2 2" element tests and 115 USGPM for Phase 2 6" element tests so the tabulated data for residence time, flow speed and *v/d* are approximately correct for all tests. Accurate values are readily derived, if required, by scaling the tabulated *v* and *v/d* values by (flow rate/100) and the tabulated times by (100/flow rate).

The flow rates per element quoted here are the upper limits for these filter types and the *v/d* values in the pipes and hoses are close to the typical recommended maxima for full-scale systems. For example 5 m/s in a 4" line, which is a widely used upper limit in road tanker loading, gives $v/d = 50\ s^{-1}$, so filter charge densities and pipe charge densities are expected, in respect of the influence of flow speed, to be representative of those in full scale systems.

Table 1: Lengths/heights and volumes plus residence times and fill times for a flow rate of 100 USGPM

Item	Length, mm	Diameter, *d*, or Width w, mm	Height, mm	Flow speed, *v*, m/s	*v/d*, s^{-1}	Volume, m^3	Residence time or fill time, s
Element exit to insulating flange 2	965	52,5		2,91	55,5	2,09e-3	0,33
Filter vessel exit to insulating flange 2	813	52,5		2,91	55,5	1,76e-3	0,28
Hose 1 (inc fittings) between insulating flanges 2 and 3	3 048	50,8		3,11	61,3	6,18e-3	0,98
Hose 2 (inc fittings) between insulating flanges 3 and 4	3 048	50,8		3,11	61,3	6,18e-3	0,98
Pipe between hose 2 and insulating flange 4	470	52,5		2,91	55,5	1,02e-3	0,16
Hose 2 and pipe between insulating flanges 3 and 4						7,2e-3	1,14
Total between insulating flanges 2 and 4	6 566					1,34e-2	2,12
Insulating flange 4 to tote inlet	305	779		1,32		1,45e-3	0,23
Receiving tote	1 219	1 067	1 041			1,35	215[1)]
Notes: [1] This is the time to fill the tote completely. The test time is shorter.							

3.2 INSTRUMENTATION

3.2.1 Streaming currents

To enable the streaming currents to be measured, the filter housing, both hose sections and the receiving tote were electrically insulated from each other and from earth with insulating flanges and supports (insulation resistance >100 MΩ). Each insulated section was then connected to earth via a sensitive Keithley ammeter. The locations of the insulating flanges and meter connections are indicated in Figure 2.

During a test, no liquid leaves the receiving tote so the tote meter measures the total current received. The other two meters measure the difference between the streaming currents entering and leaving the section to which the meter is connected (see Annex B). By working upstream from the receiving tote all individual streaming currents can be determined from the differences. In practice, the current flowing out of the filter section is usually[3] much greater than that flowing in, so the filter meter often essentially records the current generated on the element minus whatever dissipation occurs between the element and the downstream end of the filter test section. The hose meters record the loss of streaming current due to charge dissipation in the hoses.

The standard accuracy of the logged electrometer outputs is adequate for the measurement of filter charging currents except at extremely high conductivity, when most of the filter charge dissipates before the fuel emerges from the filter section. In this case the measured currents are dominated by pipe charging and the results show that in-tank electric fields are extremely low.

It is, however, a useful bonus if, as noted in Annex B, we can use the current imbalance to derive the inlet streaming current at the entry to the filter section. The imbalance is usually much smaller than the measured currents and consequently, for it to be reliably measured, the calibration of the logged meter outputs must be more accurate than the standard. The ammeter calibrations were therefore checked and correction factors for the logged values were derived to increase the accuracy. The calibration procedure is described in Annex B, which also includes details of the meter types and procedures for ensuring the adequacy of the insulation of the test sections.

3.2.2 Electric field at the centre of the tank roof

When a streaming current carries charge into a tank, charge accumulates in the liquid and generates electric fields and potentials inside the tank. We measured the electric field in the centre of the tote roof using a Boltek EFM 100 field meter protruding down from an access chamber cover in the centre of the tote roof. The local meter geometry is shown in Figure 3. Experimental calibration tests and theoretical calculations were done to estimate what the field would have been with a flush-mounted meter or a flat roof (see Annex C). These suggested that the field at a flat roof would a factor of x0,31 lower than the field measured by the protruding meter. This factor was independent of liquid depth to two figures.

3 Except at high conductivity when the charge generated on the filter element is all dissipated before the liquid reaches the end of the filter housing section.

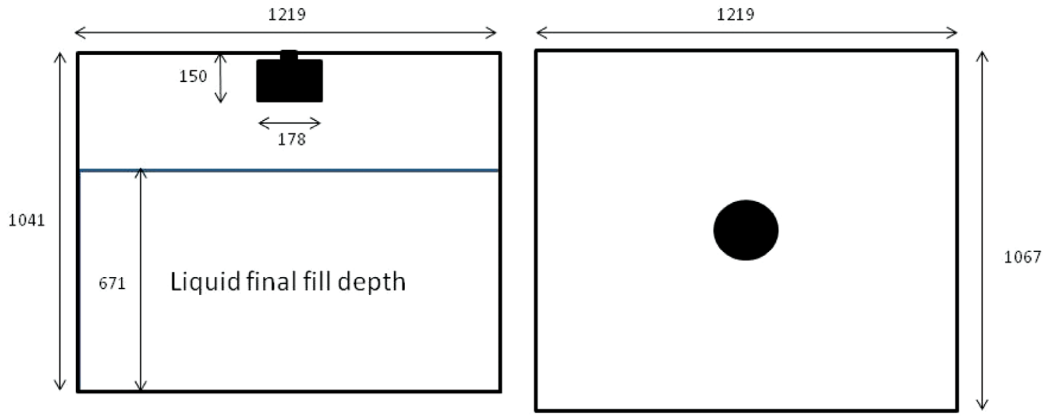

Figure 3: Field meter geometry (dimensions in mm)

At maximum sensitivity the Boltek meter reads 20 kV/m full scale and produces a ±20 V full scale analogue output. The digitiser had a maximum input voltage of ±10 V so only the lower half of the analogue range could be used. This limited the full range value for the logged data to 10 kV/m. For fields above 10 kV/m the meter sensitivity was reduced by inserting a plug-in resistor as described in Annex B, see B.2.1. The attenuation resistor value was noted in the header of the logged data[4].

At measured conductivities below about 20 pS/m, in-tank electric field decay times could be determined from the field meter readings. At higher conductivities, the charge decay was too rapid to measure (comparable to or faster than the shutdown time of the flow or the decay of streaming current). Also, at high conductivity the relationship between roof field and liquid surface voltage becomes less certain due to changes in the charge distribution, which becomes more localised around the inlet due to rapid dissipation. However, calculations show that the ratio of on-axis roof field to maximum surface potential varies by less than 10 percent for a wide range of charge distributions. Hence the extremely low fields encountered at higher conductivity provide very strong evidence that the surface voltages were also very low even though accurate values cannot be assigned.

3.2.3 Flow rate

The flow rate was measured with a Micromotion F-series Coriolis flow meter and the flow meter output was logged throughout each test. The recorded flow decline time in a run with rapid current decay suggested a first order response time constant of 0,43 s.

3.2.4 Fuel temperature

The fuel temperature was measured with an Ace glass thermocouple located at the centre of the fluid in the source tote. The fuel temperature was logged during each test.

4 The absence of a resistor is indicated by the manually entered value '0' which indicates open circuit rather than 0 Ω.

3.2.5 Data logging

The analogue outputs from the current meters, field meter, flow meter and fuel temperature sensor were digitised and logged on a laptop PC using an Afton in-house data acquisition system. Data were averaged over 1 s intervals and the averages were recorded.

3.2.6 Supporting measurement: electrical conductivity of fuel

An Emcee type 1153 dipcell conductivity meter was used to obtain fuel conductivity readings for each test. The measurement sample was taken from the source tote after each test. For this instrument any reading below about 1 pS/m registers as 0 pS/m.

4 FUELS AND ADDITIVES

The fuels were commercial samples of Jet A and Green diesel. The Green diesel was a hydrocarbon fuel (no FAME) from renewable sources. Although not an aviation fuel, it was included in the programme as a potentially higher charging fuel than Jet A to compensate for being unable to test enough jet fuel samples to find a worst case. The fuel properties are given in Annex D.

The SDA was a commercial sample of neat STADIS® 450. The pro-static agent was a proprietary material supplied by Innospec after a preliminary screening programme with a mini-static tester. It was used at a treat rate of 5 g/m^3, which was expected to give a conductivity of around 5 pS/m in Jet A.

5 TEST PROCEDURE

The standard test procedure commenced with the throttling valves already set to give the required maximum flow rate and with 50 USG (0,19 m^3) of fuel initially present in the receiving tote. A run then consisted of:

– start logging;
– record baseline data for a few seconds;
– start the flow quickly and run at the full test flow rate until 180 USG (0,68 m^3) has been transferred, and
– stop the flow quickly but continue logging data until the electric field in the receiving tote has fallen to zero.

A few runs were started with an empty tote. In this case 230 USG (0,87 m^3) of fuel was transferred in the test to give the same final liquid level.

Fuller details of the test run and liquid/rig preparation procedures are given in Annex E.

6 CONDITIONS TESTED AND TEST SEQUENCE

6.1 PHASE 1

Phase 1 consisted of the main test sequence and a few supplementary tests. In the main test sequence, Jet A and Green diesel fuels were tested with three different commercial filter monitor elements qualified to EI 1583 6th edition. Each element was tested dry and in a 'water-wetted' condition where 'water-wetted' means wetted until the pressure drop at full rated flow could cause them to be removed from service. A pressure drop of at least 10 psi/69 kPa was used for this criterion as above this the pressure drops tend to rise rapidly and could lead to unstable flow rates. The fuels were tested as received, after clay filtration and after additising with the SDA or the pro-static agent. All fuel, additive and filter monitor element combinations are shown in chronological order of testing in Table 2, which also notes the procedures used between tests to clean up the fuel/rig, add additives, etc. These procedures are labelled as Fill, Drain, Flush, Add Water, Clay Treat/Clean and Add Additive. Fill and Drain (the rig) and are self-explanatory; the other procedures are described in Annex E.

Two analysed runs were done sequentially for each test condition. In a few cases, due to problems with one of the runs (e.g. signal unexpectedly out of range), a third run was done. When an extra run was done many of the data points on the problem run were actually well-recorded and these data were always found to match the other runs within the usual data spread. However, beyond checking that this was the case, the third run was not usually analysed.

Individual run data have been archived. The main summary data presented in the analysis use either the maximum or the average of the two runs as appropriate. In Phase 1, individual runs are identified using labels of the format TCnnAj where TCnn is the test condition ID from Table 2, A is the element manufacturer code and j is the run number (1 or 2).

Table 2: Phase 1: Main test sequence: three 2" x 30" elements per test at rated flow[a)]

Condition ID[b)]	Fuel	Fuel condition	Element condition	Additive	Conductivity, pS/m Target/ Measured[c)]
Flush with pre-test liquid, Drain, Fill with Jet A, Insert New Element[c)]					
TC01	Jet A	As received	Dry	None	-/1,0
Add Water[d)]					
TC02	Jet A	As received	Wet	None	-/1,0
Clay Treat/Clean					
TC17	Jet A	Clay treated	Dry	None	-/0
TC18	Jet A	Clay treated	Wet	None	-/0
Add STADIS® 450					
TC05	Jet A	Clay treated	Dry	STADIS® 450	20/20
TC06	Jet A	Clay treated	Wet	STADIS® 450	20/18
Add STADIS® 450					
TC07	Jet A	Clay treated	Dry	STADIS® 450	200/192
TC08	Jet A	Clay treated	Wet	STADIS® 450	200/193

Table 2: Phase 1: Main test sequence: three 2" x 30" elements per test at rated flow[a)] (continued)

Condition ID[b)]	Fuel	Fuel condition	Element condition	Additive	Conductivity, pS/m Target/ Measured[c)]
Clay Treat/Clean, Add STADIS® 450					
TC03	Jet A	Clay treated	Dry	STADIS® 450	5/3,3
TC04	Jet A	Clay treated	Wet	STADIS® 450	5/3
Add STADIS® 450					
TC09	Jet A	Clay treated	Dry	STADIS® 450	600/576
TC10	Jet A	Clay treated	Wet	STADIS® 450	600/576
Clay Treat/Clean, Add pro-static agent					
TC19	Jet A	Clay treated	Dry	Pro-static	5/8
TC20	Jet A	Clay treated	Wet	Pro-static	5/4,7
Drain, Flush, Fill with Green diesel					
TC11	Green diesel	As received	Dry	None	-/0
TC12	Green diesel	As received	Wet	None	-/0
Clay Treat/Clean, Add STADIS® 450					
TC13	Green diesel	Clay treated	Dry	STADIS® 450	600/605
TC14	Green diesel	Clay treated	Wet	STADIS® 450	600/601
Clay Treat/Clean, Add pro-static agent					
TC15	Green diesel	Clay treated	Dry	Pro-static	5/4,3
TC16	Green diesel	Clay treated	Wet	Pro-static	5/2,3

Notes:

[a] All three makes of element were tested at each condition, rated flow is 30 USGPM (114 l/min) per element.

[b] The table rows are in the chronological order in which the tests were performed. For convenience of liquid handling this differs from the original test plan so test condition numbers do not rise sequentially.

[c] There were minor differences in conductivity from run to run: see Table 9 for details.

[d] The Insert New Element procedure was carried out before the first test on each element type in each dry condition. After a set of dry runs was completed, the Add Water procedure was used to wet the elements and the wet element test runs for that element were done. When these were complete the next Insert New Element cycle was started. The Insert New Element and Add Water stages are only shown once in the table to avoid undue repetition. The capitalised test procedures are all described in Annex E.

The Phase 1 supplementary tests are listed in Table 3. They consisted of three tests done with one specific example[5] of an older type of 2" filter monitor element (EI 1583 4th edition) for comparison with the newer elements tested in the main sequence and a test with no filter monitor elements to measure the underlying pipe charging. All the supplementary tests were carried out immediately after the TC20 tests and the conditions are as for TC 19 and 20 (i.e. clay treated Jet A containing only the pro-static agent).

5 All that was available.

Table 3: Phase 1: Supplementary Phase 1 tests

Test ID	Test	Fuel	Fuel condition	Element condition	Additive(s)	Conductivity, pS/m Target/Measured
S01	4th ed	Jet A	Clay treated	Dry	Pro-static	5/15
S02	4th ed	Jet A	Clay treated	Wet	Pro-static	5/5
S03	4th ed empty tank	Jet A	Clay treated	Wet	Pro-static	5/5
S04	No element	Jet A	Clay treated	–	Pro-static	5/5
Note: These tests are listed in chronological order. They were conducted after test condition TC20 of the main sequence.						

6.2 PHASE 2

The Phase 2 work covered both 2" and 6" monitors using conditions as for TC 19 (i.e. clay treated Jet A with pro-static agent and dry elements). Differences from Phase 1 were:

- The use of 6" as well as 2" elements.
- The flow rate was varied in stages from 50 % to 100 % of maximum rated flow.
- Four rather than three 2" elements were used giving a maximum rated 2" element flow of 120 USGPM rather than 90 USGPM. This was done to overcome problems with turning down the flow rate to below 50 USGPM.

6" monitors can have either in-to-out or out-to-in flow direction. Both types were tested. Most tests used the standard procedure of starting a run with a residual 50 USG of fuel in the receiving tote but a final run at each condition was added with maximum flow rate and no initial fuel in the receiving tote. In reporting the Phase 2 tests the filter manufacturers are labelled X, Y and Z.

7 ANALYSIS METHODS

The analysis consisted of:

- General
  - Identifying start and stop times from the flow data.
  - Applying calibration factors and subtracting zero offsets obtained from the pre-flow data.
- Current and charge density analysis:
  - Converting the measured currents into streaming currents (see B.1.4).
  - Applying a correction where a tote current error was evident (see B.1.8).
  - Determining the absolute maximum and final measured 'raw' values of the streaming currents. These were determined as follows: the maximum raw current is the maximum absolute value between the time when the flow rate first exceeds 5 gallons per minute and the time five samples before the flow rate last exceeds 5 gallons per minute. This interval is chosen to eliminate the transient effects of starting and stopping the flow. The final raw current is obtained by averaging the current over the last 25 % of the sampling domain described here. The tabulated values are the highest obtained in all runs done at the given condition.
  - Brief transient currents do not transfer enough charge into the receiving tank to significantly raise the charge or potential. Hence the in-tank charges, fields and potentials depend on a current averaged over the in-tank charge decay time rather than on the raw current. We derived this average current, which we have called the effective current, I_{eff}, at the exit from each measurement section. Mathematical details are given in B.1.9. For summary purposes, we focus on the maximum and final (end of flow period) I_{eff} values. The maximum value is the most important summary value but the final value, is also recorded because it is useful to explore the link between the final effective current and the maximum electric field which usually occurred at the end of the flow.
  - Deriving maximum and final charge densities from the raw and effective currents and the flow rates.
  - Deriving the effective timescale for hose dissipation from the streaming currents at the hose inlets and exits (see B.1.10).
- Electric field analysis:
  - Selecting the maximum field magnitudes from each run.
  - Deriving the electric field that would have existed at the tote roof in the absence of the meter from the measured electric field using the theoretical calibration factor described in Annex C.
  - Calculating the electric field decay times by differentiation of both the raw data and curve fits to these data as described in B.2.2)[6].

6 The decay time of the electric field after the fill was found to be a function of time (i.e. the field decay was not strictly exponential).

8 RESULTS

8.1 PHASE 1

8.1.1 Aims of Phase 1

The aims of Phase 1 were to indicate the maximum level of charging and the degree of charge dissipation (in both hoses and receiving tank) produced by the flow of each of the two test fuels (Jet A and Green diesel) through 2" filter monitor elements in a rig for which residence times were well documented and representative of full-scale practice and in which the pipe-charging charge density was expected to be representative of full-scale working practice. The influence of absorbed water on the elements, SDA (STADIS® 450) in the fuels and a potential pro-static agent (identified by mini static testing) in the fuels were investigated to probe worst-case conditions.

8.1.2 Test identification codes

In reporting Phase 1 data, individual runs are identified, where necessary, using labels of the format TCnnAj where TCnn is the test condition ID from Table 2, A is the element manufacturer code and j is the run number (1 or 2).

8.1.3 Currents

8.1.3.1 Shapes of measured current vs time plots

An unexpectedly wide range of time dependences was observed in the plots of test current. In Figure 4 we present a selection that illustrates this variety. All the individual streaming current vs time plots are reproduced in Annex G.

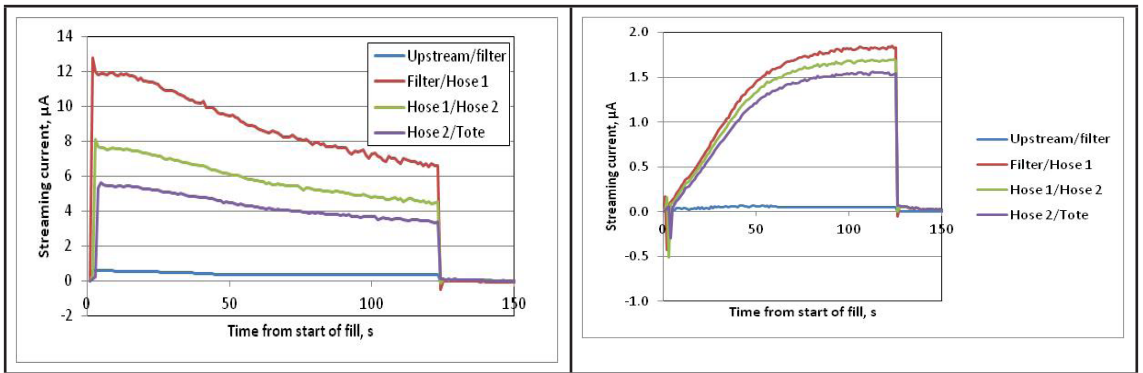

a) Rapid rise then steady decline (TC01a2)	b) Initial transient then rise to a constant level (TC01 c1)

Figure 4: Selected streaming current vs time profiles showing the range of behaviour encountered

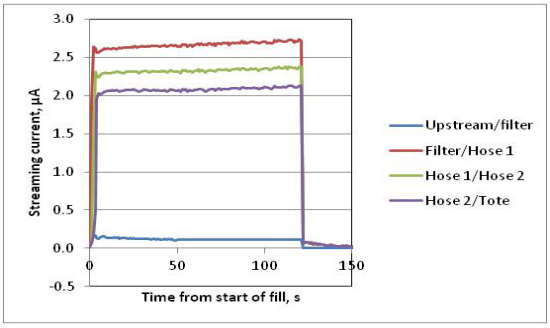

c) Rapid rise then almost constant (TC02a1)

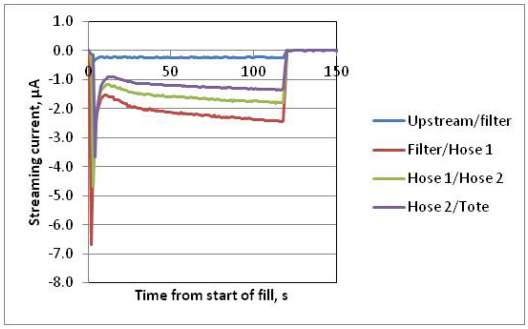

d) Spike then slow rise towards steady value

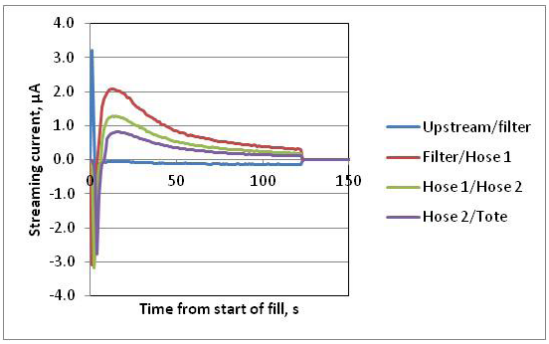

e) Spike, peak of opposite sign then decline

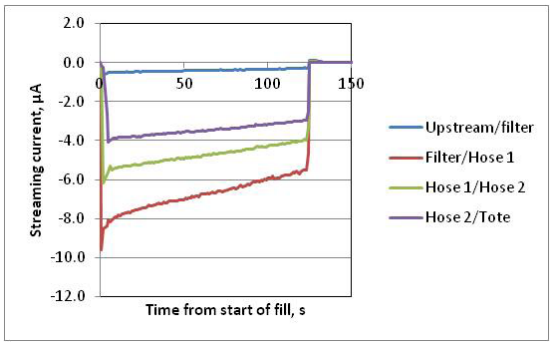

f) Spike then near linear decline

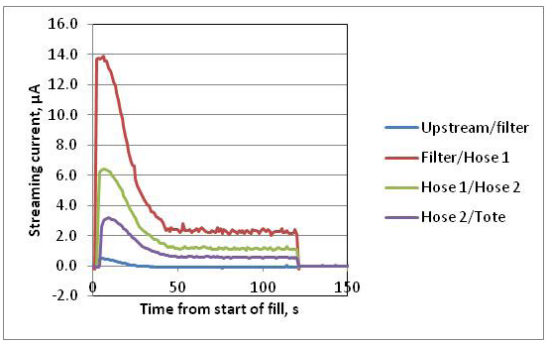

g) Peak then sharp decline to steady level

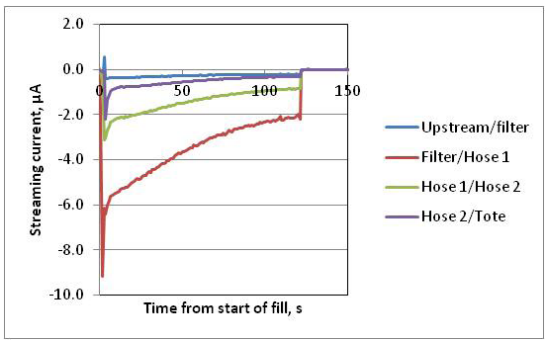

h) Spike then 'exponential' marked decline

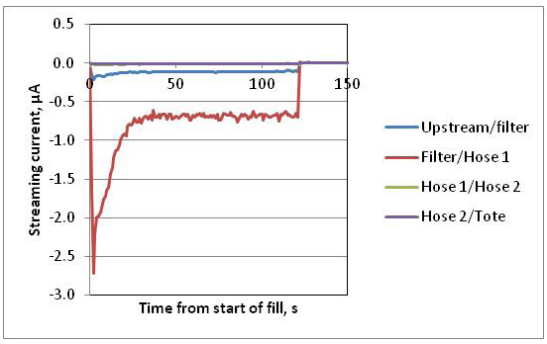

i) Spike then decline to steady, strong dissipation

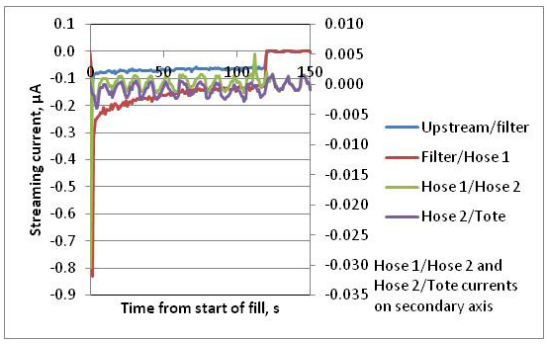

j) Similar to i) but hose and tote currents shown on expanded scale (noise levels ~5 nA pk to pk)

Figure 4: Selected streaming current vs time profiles showing the range of behaviour encountered continued

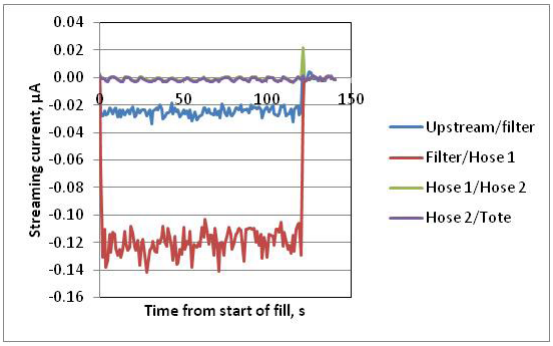

k) Small, fluctuating but measurable current at high conductivity (~600 pS/m)

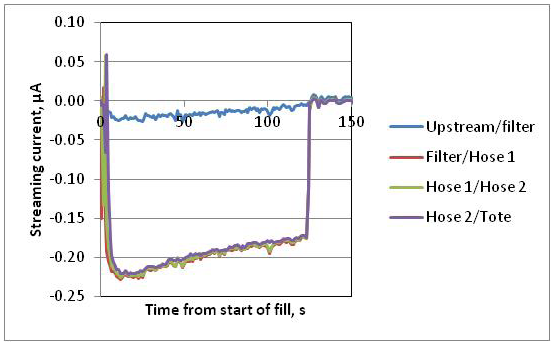

l) Low current, early peak and almost no dissipation at low conductivity

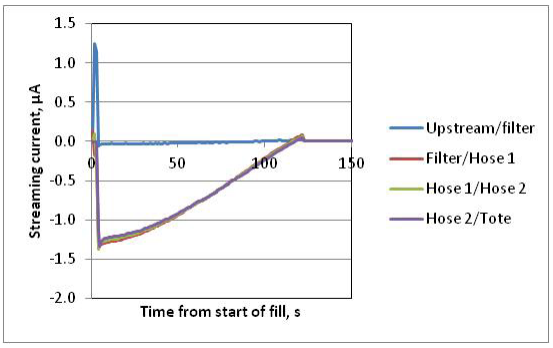

m) Almost no dissipation, currents change sign near end of run, very low conductivity

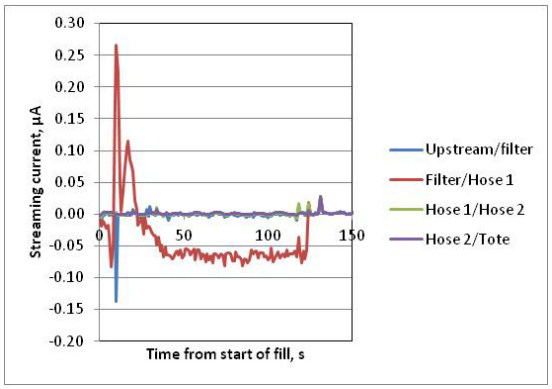

n) Small current changing polarity, high conductivity

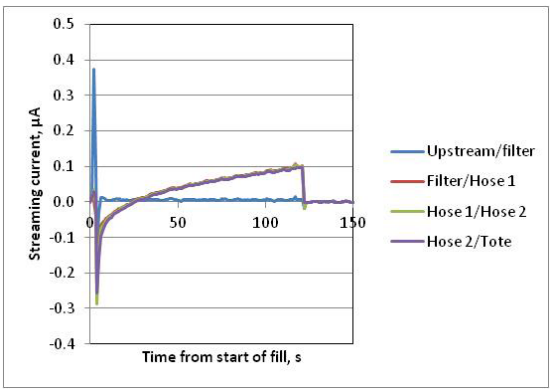

o) Spike then change in polarity of charging

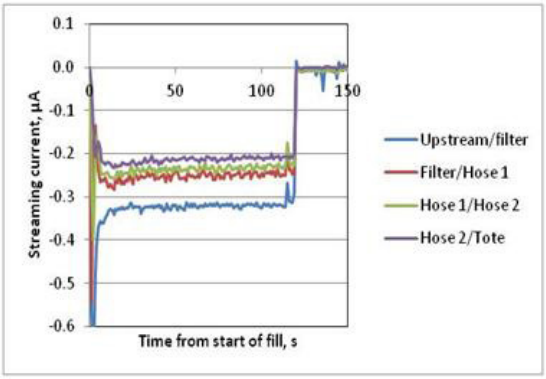

p) Streaming currents with no element

Figure 4: Selected streaming current vs time profiles showing the range of behaviour encountered continued

In some conditions [e.g. Figure 4 case c)] the current rose rapidly then remained almost constant; in many others [e.g. cases f) to i), l) and m)] it rose to a maximum then declined (sometimes declining throughout the fill and sometimes reaching a constant value). In yet others, it started small or went through a dip after an initial spike and then rose gradually throughout the fill [e.g. case d)]. In a few it changed polarity during a fill [e.g. cases e), n) and o)].

At very low conductivity [e.g. cases l), m) and o)], the residence time in the hose was much less than the charge relaxation time, dissipation in the hose sections was small and the current delivered to the drum was almost equal to the filter current. Conversely, at high conductivity, [e.g. cases i) and j)] the key residence times are all longer than the charge relaxation time. In these cases, the Hose 1 dissipation current is comparable (equal and opposite) to the filter section current and the subsequent streaming currents (at the Hose 1/Hose 2 and Hose 2/ Tote interfaces) are small. In the low and high conductivity extremes only limiting values can be placed on the effective conductivity for charge dissipation in the hoses but in intermediate cases, effective conductivities can be estimated via equation (B.7).

Although Figure 4 shows filter charging currents that often change considerably during a run, the individual test-run data in Annex G demonstrate that repeat runs at a given condition are very similar. Thus, in the periods between runs, which were typically 5 to 15 minutes, the elements recovered from any changes that occurred during the runs.

8.1.3.2 Overall magnitudes of effective currents and charge densities at the filter exit and into the tote

The higher of the maximum effective streaming currents from the two runs at each condition[7] (to get a worst-case) and the average of the final effective currents (for comparison with the average final field) are listed in Annex H, Table H.1. Due to the unsteadiness of the filter streaming currents, the impact of the averaging in the effective current calculation is different for nearly every run. For some applications, it may be useful to avoid this complication. The maximum and final raw currents provide additional guidance to cover such cases and are therefore recorded in Table H.2.

Table 4: Streaming currents at high conductivity

Fuel	Conductivity, pS/m	Average current, nA			
		Upstream	Filter exit	Hose 1 exit	Hose 2 exit
Jet A	~200	–187,9	–543,9	–80,2	–21,5
Jet A	~600	–50,4	–235,7	(–0,6)	(–1,4)
Diesel	~600	–3,8	–25,1	(–1,0)	(0,3)

7 Averages rather than maxima at >25 pS/m.

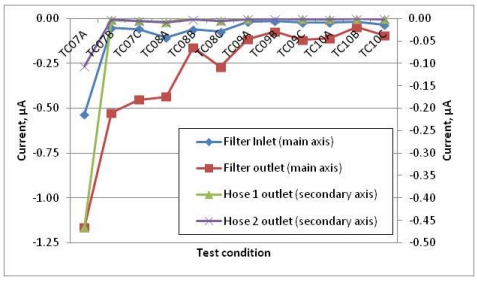

a) Jet A at 200 pS/m (TC07, TC08) and 600 pS/m (TC09, TC10)

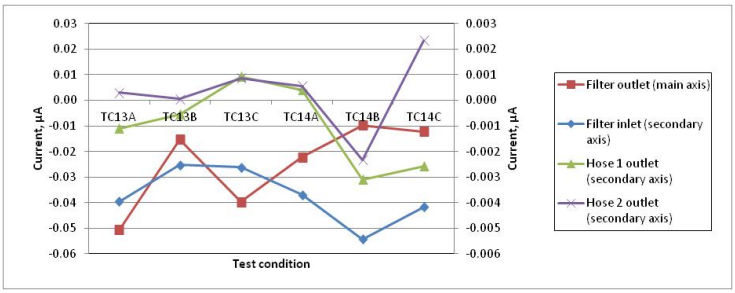

b) Green diesel at 600 pS/m (TC13, TC14)

Figure 5: Average streaming currents for high conductivity conditions (~200 pS/m and 600 pS/m)

We now discuss the main features of the effective current data starting with the high conductivity cases: that is, the data obtained with conductivities around 200 pS/m and 600 pS/m. In these cases, the measured currents were small and only values averaged over the entire test run are given to provide an indication of the magnitude. Averages over all element types and both wet and dry conditions for Jet A at 200 pS/m and 600 pS/m and diesel at 600 pS/m are given in Table 4; data points for individual conditions are shown in Figure 5.

The filter section exit currents are always larger than the other currents and should represent reliable data. There were generally also non-zero measured values for the upstream current but these may be affected by leakage current issues across Insulating Flange 1. Hose 1 and Hose 2 exit currents were noisier and smaller, especially at 600 pS/m, and the measurements in brackets in Table 4 are probably unreliable although they do indicate the maximum order of magnitude of the currents. Noise levels were typically about 1,5 nA peak to peak at a predominant frequency of about 0,08 Hz although this may have been a beat frequency; at 600 pS/m the hose currents were only of a similar magnitude to the noise. In a few cases there was no significant difference between the readings with and without flow or the apparent difference was of opposite polarity to the filter charging. In other cases differences of order nA could be seen between flow and non-flow periods despite the noise.

Based on the measured conductivity, the relaxation time of the fuel would be between about 0,1 s at 200 pS/m and 0,03 s at 600 pS/m whilst the residence time of the fuel between the element exit and Insulating Flange 2, which isolates the filter section from the hose, was 0,37 s. Thus T/τ varies from 3,7 at 200 pS/m to 12,3 at 600 pS/m. However, there is often a factor of x0,5 difference between effective and measured conductivity. This would modify the loss factors at 200 pS/m and 600 pS/m by so much as to make the estimates of element current at these conductivities completely unreliable. The residence times in the hoses are such that at both 200 S/m and 600 pS/m the filter currents would have almost completely dissipated so the tote inlet currents would arise virtually entirely from hose charging.

We now consider the more safety-critical data, which are those obtained at 25 pS/m and below. The maximum effective and final effective filter exit currents for each test condition in this range are plotted as a function of measured liquid conductivity in Figure 6.

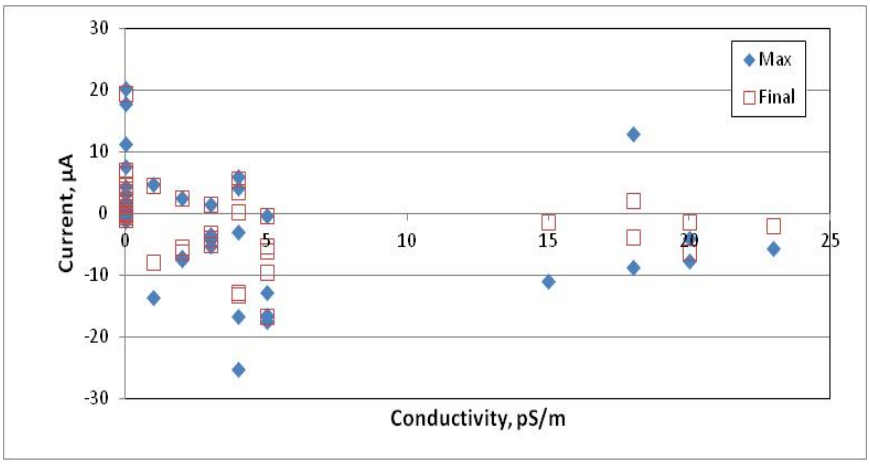

Figure 6: Maximum effective and final effective filter exit currents, data below 25 pS/m

Note that if the abscissa were to be extended to 600 pS/m, the currents at 200 pS/m and 600 pS/m would all look like zeros on this ordinate scale. The highest currents all occur at conductivities below 5 pS/m and there is a trend from positive charging at the very lowest conductivities (those measuring '0' pS/m in the dip cell) to negative charging at 5 pS/m.

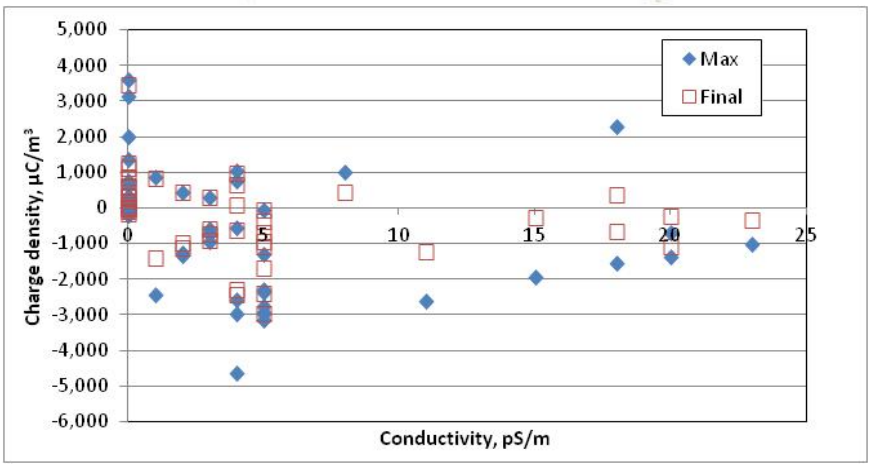

Figure 7: Charge density corresponding to the currents in Figure 6

The filter exit charge densities corresponding to the currents in Figure 6 are shown in Figure 7. The highest positive and negative charge densities are +3 610 µC/m^3 and –4 640 µC/m^3 respectively.

Table 5 gives the maximum and final effective currents and charge densities at the filter exit for several subsets of the data in Figures 6 and 7. The most important results are the positive

and negative maxima for Jet A with 6th edition elements. Figures 8 and 9 show, respectively, the streaming currents and charge densities passing from the exit of Hose 2 into the tote. The effects of charge dissipation in the hoses can be seen by comparing Figures 6 and 8 or 7 and 9. Even at low conductivities the maximum values are reduced by about a factor of 2 from the filter exit values and bigger reductions are evident at higher conductivities.

Table 5: Highest effective filter exit streaming currents and charge densities

	Highest effective filter exit current, μA /charge density, μC/m³			
	Max		**Final**	
Fuel, polarity and filter class	**Test**	**Value**	**Test**	**Value**
Diesel, positive, 6th edition	TC11A	20,4/3 610	TC11A	19,4/3 440
Diesel, negative, 6th edition	TC16C	–25,4/–4 640	TC15C	–16,6/–2 980
Jet A, positive, all	TC05A	12,9/2 290	TC01A	7,0/1 240
Jet A, negative, all	TC19 4th edition	–17,5/–3 130	TC19C	–13,7/–2 420
Jet A, positive, 6th edition	TC05A	12,9/2 290	TC01A	7,0/1 240
Jet A, negative, 6th edition	TC19C	–15,6/–2 750	TC19C	–13,7/–2 420

Comparing the highest values at 0 pS/m in Figures 6 and 8 or 7 and 9 suggests that some dissipation occurred in the hoses (residence time 2,1 s) even at the lowest conductivity. This, however, is misleading. The dissipation apparent in the highest values hides the fact that some of the less extreme currents did not dissipate much at all. This issue mainly arises because the method adopted for conductivity measurement does not satisfactorily discriminate between different conductivities of less than a few pS/m. Thus, all conductivities below about 1 pS/m are classed as '0' pS/m even though the dissipation behaviour expected would be very different between, say, 0,95 pS/m and 0,03 pS/m. A better representation of the data is therefore obtained by plotting them as a function of the effective conductivity derived from the tote electric field dissipation time. This is done in Figure 10 for the filter exit charge density data.

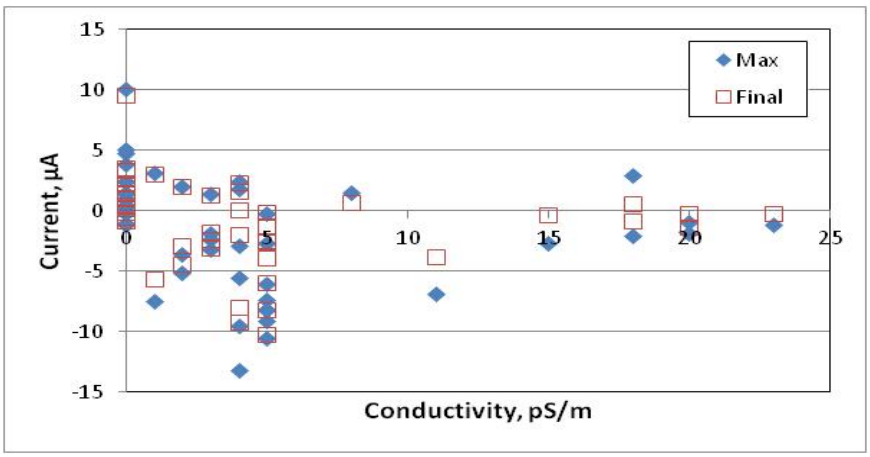

Figure 8: Maximum effective and final effective streaming currents into the tote

The effective conductivity was generally about a factor of 2 lower than the measured conductivity and the displayed conductivity range is reduced accordingly.

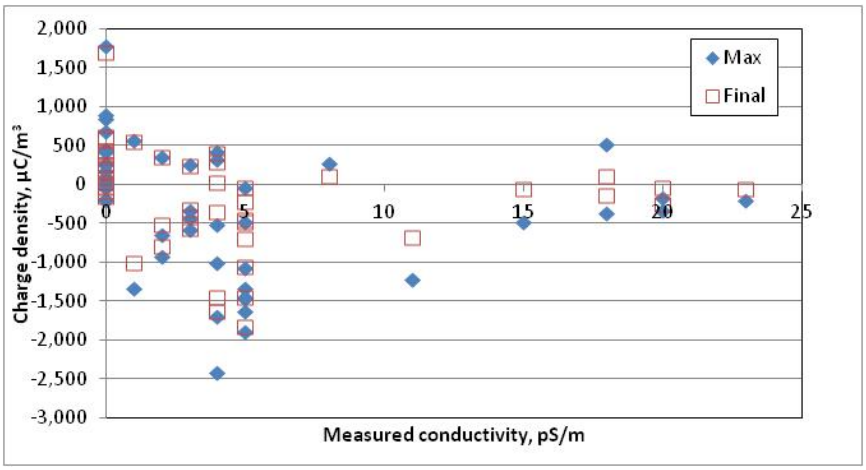

Figure 9: Maximum effective and final effective charge densities into the tote

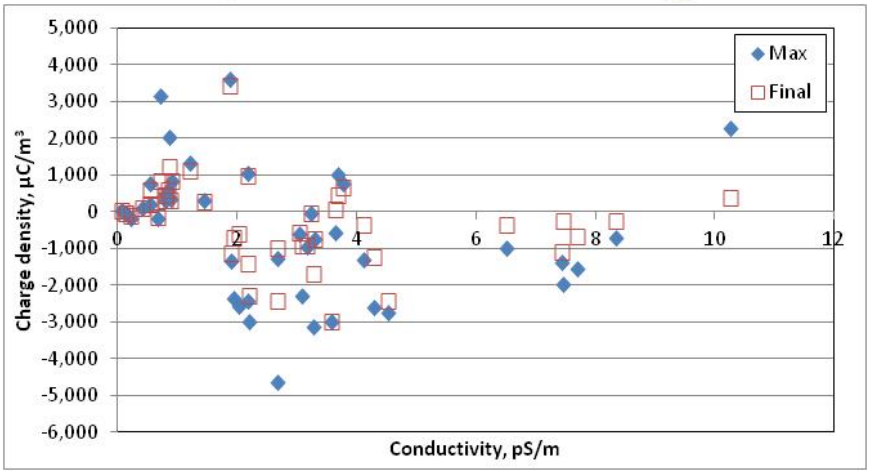

Figure 10 Filter section exit charge densities as a function of effective conductivity derived from the electric field decay

With this presentation it appears as though the highest exit charge density from the filter section occurs between effective conductivities of 1 pS/m and 3 pS/m (i.e. measured conductivities between about 2 pS/m and 6 pS/m) with positive charging predominating below 2 pS/m effective and negative charging above 2 pS/m effective.

8.1.3.3 Comparison of 4th edition and 6th edition elements

The results of the comparison between 4th and 6th edition elements are given in Table 6. The 4th edition elements gave a maximum filter segment exit charge density of –3 140 µC/m³ whilst the 6th edition elements gave a maximum filter segment exit charge density of –2 800 µC/m³. The difference is regarded as too small to be significant.

Table 6: Comparison of maximum effective filter exit charge densities with 4th and 6th edition Elements

Element	Maximum filter section exit charge density, μC/m³	
	Dry	Wet
4th edition	–3 140	–2 930
6th edition A	+1 000	–2 400
6th edition B	–2 600	–1 300
6th edition C	–2 800	–2 600

8.1.3.4 Comparison of element brands

The charge densities generated by Faudi, Parker and Peco elements are compared in Figure 11 with the brands identified only in coded form.

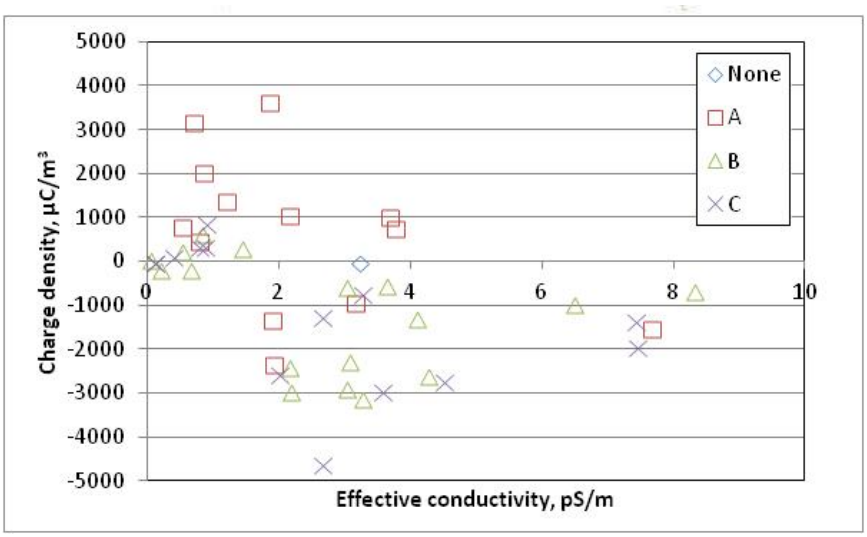

Figure 11: Charge densities with different filter element types as a function of effective conductivity from initial field decay time

All give a similar magnitude of maximum charging although there are differences between brands. Thus the highest charge densities were A: +3 610 μC/m³, B: –3 130 μC/m³, C: –4 640 μC/m³. The differences seem to correspond as much to shifts between positive and negative charging tendencies as to differences in the magnitude of charging. Thus element A charges highest below 2 pS/m where charging tended to be positive, whereas element C charges highest above 2 pS/m where charging tended to be negative. It is perfectly possible that a different fuel would charge negatively at the lowest conductivities and, in such a fuel, element A might give the lowest charging whilst another fuel might charge more positively and leave element C as the lowest charging.

When evaluating hazards, in addition to considering the absolute charging tendency, it should be noted that brush discharges from charged fuel surfaces can cause ignition at lower voltages with negatively charged fuel [7].

8.1.3.5 Comparison of charging by dry and wet elements

The charging of fuels passing through dry elements and wetted elements is compared in Figure 12.

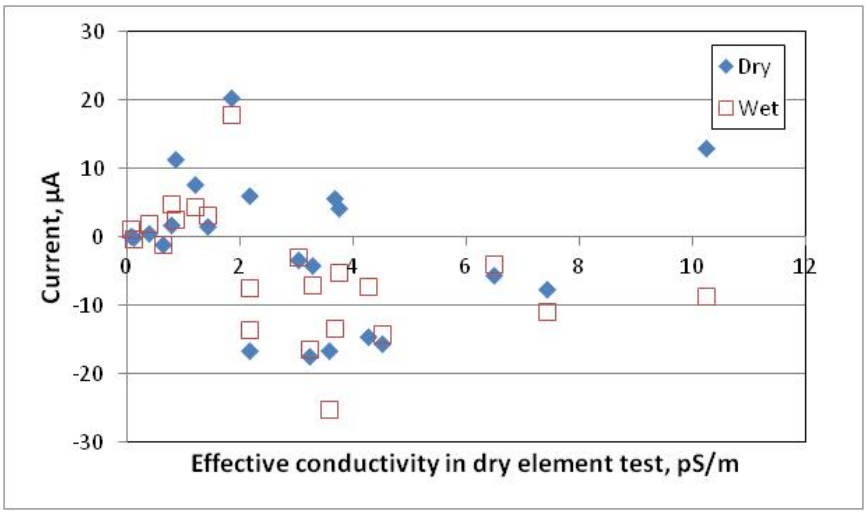

Figure 12 Filter exit charging currents with wet and dry elements

Contrary to expectations, wetting the elements did not appear to produce a significant change in the generated charge. However, on average, it shifted the charging negative by about 16 % of the maximum positive current. The standard deviation of the difference between the means is about 15 % so the difference is barely significant.

8.1.3.6 The influence of fuel type

The influence of fuel type is shown in Figure 13, which gives the charge density at the exit of the filter section as a function of the effective conductivity from the final field decay.

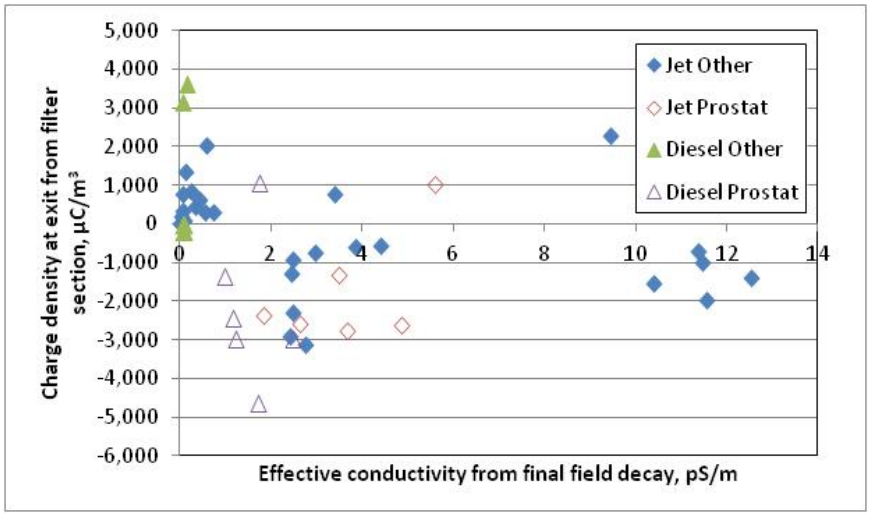

Figure 13: The influence of fuel type and pro-static agent

The Green diesel tended to charge more strongly than the Jet A. Thus, the positive maxima at very low conductivity are 3 600 μC/m³ and 2 000 μC/m³, respectively, and the negative maxima at around 2 pS/m are 4 600 μC/m³ and 3 100 μC/m³. Thus, the diesel was found to charge 1,5 to 1,8 times higher. It is not clear how much of this is a systematic difference between the product types (e.g. due to the viscosity difference) and how much is a random difference between individual fuel samples.

8.1.3.7 The influence of the pro-static agent

Figure 13 also shows the influence of the pro-static agent in both Green diesel and Jet A. The Green diesel data do not provide an ideal comparison because the tests with and without the pro-static agent were at different conductivities, nevertheless, the data with the pro-static agent seem to follow the general trend from positive charging at low conductivity to negative charging at 2 pS/m[8] and there is little evidence of any substantial increase in the magnitude of charging. For Jet A, there are charge density measurements with and without pro-static agent at effective conductivities between 2 pS/m and 6 pS/m. In this range the highest charge density is –3 100 μC/m³ without pro-static agent and –2 750 μC/m³ with pro-static agent. The standard deviation of the difference between the means is 830 μC/m³. Thus, the pro-static agent did not have a significant effect on the maximum charging of Jet A in filter monitor elements.

8.1.3.8 Effective dissipation time and conductivity from current decay measurements

Figure 14 shows the effective conductivity derived from the current decay in the hoses as a function of the effective conductivity derived from the electric field decay time (see 8.1.4.2 and B.2.2).

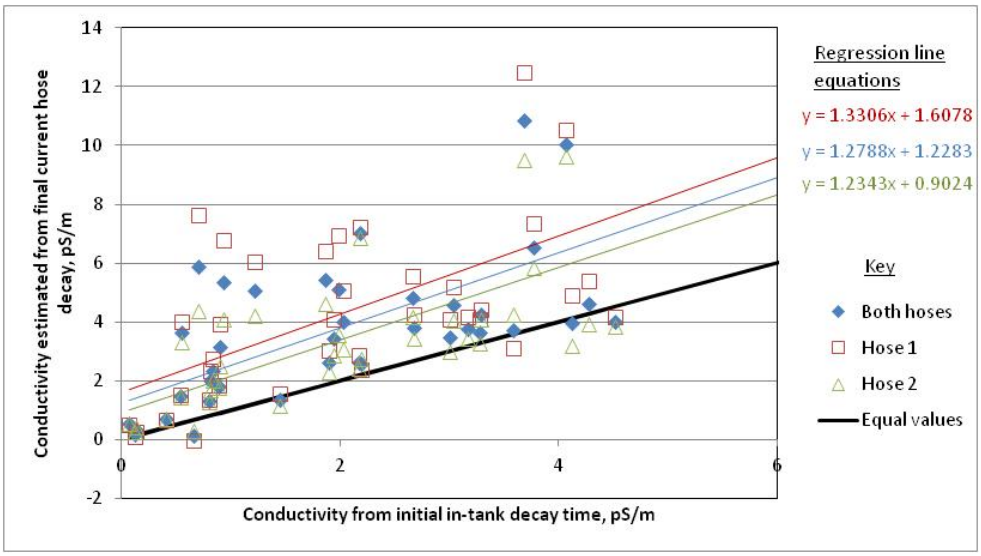

Figure 14: Effective conductivity from initial in-tank electric field decay time

8 The observed dependence of charging polarity on conductivity may be dependent on fuel type and conditioning. There is no evidence that it is universal.

The regression lines (equations shown on the figure) indicate that the ratio of effective conductivity for charge decay in the hoses to the effective conductivity for electric field decay in the tank does stay fairly close to one as the effective conductivity for field decay tends to zero (i.e. there is no hose dissipation at the lowest conductivities even though there appears to be when the assessment is based on the dip-cell conductivity data as when comparing Figures 6 and 8 for current or 7 and 9 for charge density). Generally, the effective conductivity in the hoses is greater than in the tote and the effective conductivity in Hose 1 is greater than in Hose 2. This is consistent with a form of generalised hyperbolic decay although detailed comparisons with hyperbolic decay models reveal inconsistencies.

8.1.4 Electric field

8.1.4.1 Logged values

Figure 15 shows a typical low conductivity measured electric field vs time plot. In nearly all cases the maximum field was recorded at the end of the fill although in a few cases, when the current dropped particularly markedly through the run and the dissipation time was relatively short, it occurred earlier. A full set of maximum electric field values is given in Annex I.

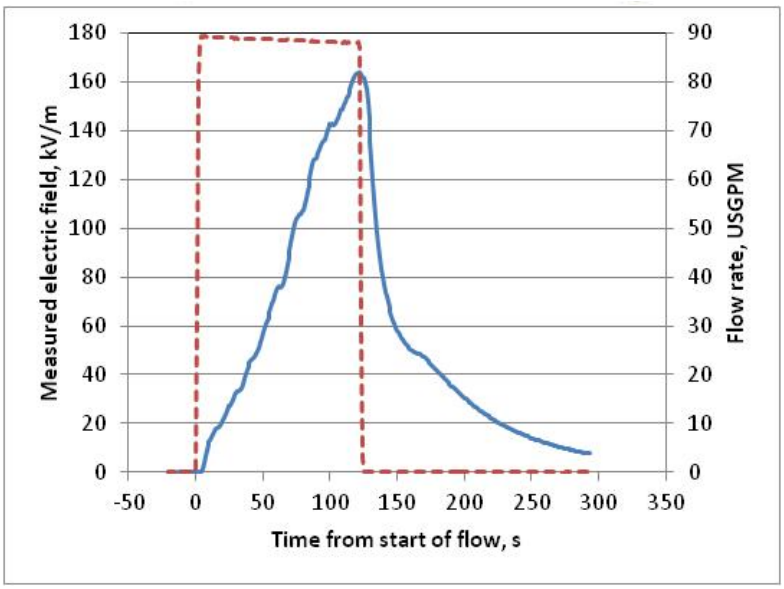

Figure 15: Raw measured electric field

Features to be noted in Figure 15 are:

- There is a short delay after the start of flow before the field begins to rise. This probably relates to the time taken for the first highly charged liquid to reach the tote from the filter monitor.
- After the initial delay, there is a short period of rapid field increase. Some Phase 2 fills started with an empty tote. The rapid rise was missing in those fills. If, with an initial 50 USG in the tote, the incoming charge remained stratified at the bottom, the fields with and without the initial 50 USG would be similar. The difference suggests that the rapid increase is associated with the mixing of the incoming liquid with the initial 50 USG of uncharged liquid in the tote.

– After the mixing period, the field rises somewhat more slowly and almost linearly with time. On low conductivity test runs, such as in Figure 15, the rate of rise of field tended to increase until the end of the fill but at higher conductivities it was usually constant or falling. Although both behaviours were influenced by the variation of incoming current over the fill, the effect of higher conductivity is also important. The total charge in the tank approaches a constant on a timescale set by the charge relaxation time and at high conductivity this charge is confined to an increasingly localised volume around the liquid entry jet. Both factors tend to suppress the rate of rise of field. At low conductivities, the charge in the tank increases for longer and the charge spreads throughout the liquid.
– There is usually a delay of 5 s to 10 s after the end of flow before the field begins to drop. The reason for this is not known. It may be linked to the influence of flow plus non-uniform bulk charge distributions or to the formation of surface charge layers.
– There is often a rather 'wavy' field decay with a decay time that is far from constant (e.g. a clear kink can be seen at about 170 s in Figure 15). Under some conditions the decay was close to exponential but much of the analysis had to deal with cases like Figure 15 using the curve fitting process discussed in B.2.2.

The maximum flat-roof-corrected fields[9] for each test condition are plotted in Figure 16 as a function of the effective conductivity measured from the initial rate of field decay and listed in Table 7.

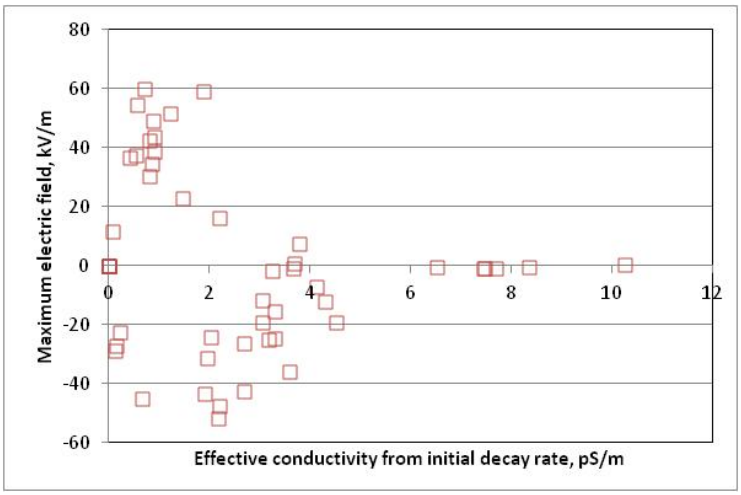

Figure 16: Maximum 'flat-roof' electric field as a function of effective conductivity from initial field decay rate

The highest fields (>50 % of the maximum) occur with an effective conductivity of between 0,1 pS/m and 3,6 pS/m. As with the charge density (not surprisingly but gratifying that there is a match), there is a predominance of positive charging below 2 pS/m and a predominance of negative charging above. The maximum flat-roof positive and negative fields are +59 kV/m and –52 kV/m.

9 Using a recorded field to flat roof field calibration factor of 0,31. See section 7 and Annex C for details of derivation.

Table 7: Maximum flat roof field for each test condition (the maximum of the two runs)

Test condition	Filter element	Maximum field at a flat roof, kV/m	Test condition	Filter element	Maximum field at a flat roof, kV/m
S01	None	–1,5	TC11	A	59,3
S02	D	–24,7	TC11	B	–45,1
S03	D	–20,1	TC11	C	–27,0
TC01	A	49,3	TC12	A	60,0
TC01	B	23,2	TC12	B	–22,6
TC01	C	30,4	TC12	C	–28,8
TC02	A	42,5	TC13	A	–29,2
TC02	B	34,8	TC13	B	–
TC02	C	39,0	TC13	C	–
TC03	A	7,8	TC14	A	–
TC03	B	–11,8	TC14	B	–
TC03	C	–15,4	TC14	C	–
TC04	A	–25,1	TC15	A	16,5
TC04	B	–0,93	TC15	B	–47,4
TC04	C	–26,0	TC15	C	–35,6
TC05	A	0,59	TC16	A	–43,5
TC05	B	–0,13	TC16	B	–51,6
TC05	C	–0,62	TC16	C	–42,3
TC06	A	–0,90	TC17	A	51,9
TC06	B	–0,16	TC17	B	11,6
TC06	C	–0,75	TC17	C	36,8
TC07	A	–	TC18	A	54,7
TC07	B	–	TC18	B	37,6
TC07	C	–1,6E-03	TC18	C	44,0
TC08	A	–	TC19	A	0,94
TC08	B	–	TC19	B	–12,2
TC08	C	–	TC19	C	–19,1
TC09	A	–1,0E-03	TC20	A	–31,0
TC09	B	1,5E-03	TC20	B	–6,8
TC09	C	–	TC20	C	–24,3
TC10	A	3,4E-03			
TC10	B	–			
TC10	C	–			

Note: Dashes indicate fields below the noise level, which could be up to about 0,005 kV/m.

8.1.4.2 Electric field decay time in the tank

The initial and final decay times generated by the curve fit method (see B.2.2) are shown in Table 8 and the corresponding effective conductivities are given in Table 9. Because the meter measurements do not register below 1 pS/m we need to use one of these effective values as the abscissa for plots that discriminate the lower end of the conductivity range. The final effective conductivity is expected to be the closest to reflecting the measurable conductivity of the uncharged liquid whilst the initial effective conductivity is expected to be closest to the decay rate of the charged liquid in a tank. In Figure 17 we plot the measured conductivity and the initial effective conductivity from the field decay time as a function of the final effective conductivity.

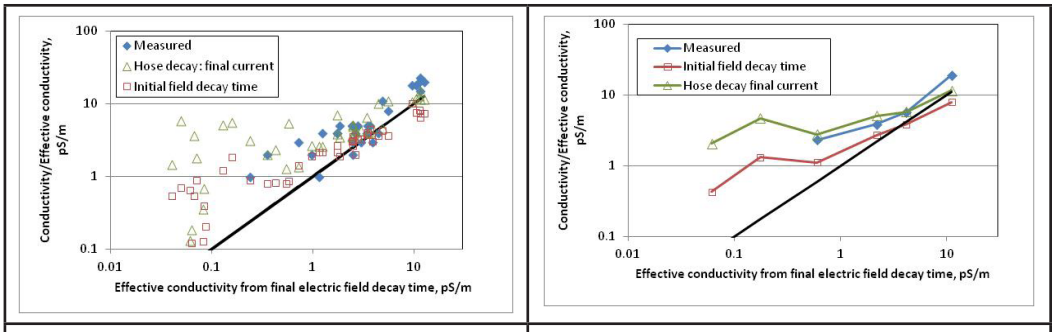

a) Data points | b) Averaged values

Figure 17: Measured conductivity and final effective conductivity for electric field decay versus initial effective conductivity for field decay

Figure 17 includes both a plot of individual data points and one of clusters of points averaged over conductivity ranges. The black lines indicate equality with the final effective conductivity. The effective conductivity from the hose measurements (both hoses) is included on both plots for comparison. At around 10 pS/m the measured conductivity is about a factor of two higher than the final effective conductivity whilst the effective conductivity from hose decay is about equal to it and the initial effective conductivity is lower. The latter difference probably reflects the difficulty of separating out the influence of the delay period in this conductivity range in which the measurable decay period was very short.

Table 8: Initial and final decay times using the curve fit method

Test condition	Filter element	Initial decay time, s	Final decay time, s	Test condition	Filter element	Initial decay time, s	Final decay time, s
S01	None	5,8	5,5	TC12	A	26,3	375,0
S02	D	5,7	6,7	TC12	B	90,0	215,0
S03	D	6,1	7,7	TC12	C	150,9	296,5
TC01	A	21,4	32,1	TC15	A	8,5	10,7
TC01	B	12,9	25,9	TC15	B	8,5	15,2
TC01	C	23,3	34,2	TC15	C	5,2	7,5
TC02	A	23,1	53,1	TC16	A	9,8	19,2

Table 8: Initial and final decay times using the curve fit method (continued)

Test condition	Filter element	Initial decay time, s	Final decay time, s	Test condition	Filter element	Initial decay time, s	Final decay time, s
TC02	B	22,3	43,5	TC16	B	8,6	16,2
TC02	C	20,6	77,4	TC16	C	6,9	10,8
TC03	A	4,9	5,5	TC17	A	15,3	144,6
TC03	B	6,1	4,8	TC17	B	258,9	1897,0
TC03	C	5,7	6,3	TC17	C	46,1	224,1
TC04	A	5,9	7,5	TC18	A	34,0	277,1
TC04	B	5,1	4,2	TC18	B	34,6	464,7
TC04	C	7,0	7,6	TC18	C	20,8	264,5
TC05	A	1,8	2,0	TC19	A	5,0	3,3
TC05	B	2,9	1,6	TC19	B	4,3	3,8
TC05	C	2,5	1,5	TC19	C	4,1	5,1
TC06	A	2,4	1,8	TC20	A	9,6	10,2
TC06	B	2,2	1,6	TC20	B	4,5	5,3
TC06	C	2,5	1,6	TC20	C	9,2	7,1
TC11	A	10,0	117,1				
TC11	B	28,2	305,2				
TC11	C	145,3	224,8				

A slightly increasing factor of difference is maintained between the measured and final effective conductivity right down to the point at which the meter fails to register measured values. Both the hose decay conductivity and the initial field decay conductivity become larger multiples of the final effective conductivity for field decay as the conductivity declines. This probably reflects the increasing role of hyperbolic relaxation effects. With this explanation, the higher charge densities existing in the hose compared to the tote could explain the higher effective hose conductivity. In this respect, it would be interesting, in a more detailed future analysis of the data, to see how the excess conductivities correlate with excess charge levels and fuel viscosity.

The differences between measured and final effective conductivity may arise from a combination of measurement error charge redistribution during the decay period and the hindering of charge dissipation by the free surface of the liquid. The sensitivity of the conductivity meter is only a few pS/m so it was working at the bottom end of its range and accurate readings could not be expected[10]. Furthermore, contamination errors tend to make conductivity measurements read high.

10 That is why the measured readings do not extend below 1 pS/m.

Table 9: Measured conductivity and effective conductivities from initial and final decay times

Test condition	Filter element	Measured	From initial decay time	From final decay time	Test condition	Filter element	Measured	From initial decay time	From final decay time
S01	None	5	3,2	3,4	TC12	0,71	0	0,71	0,050
S02	D	5	3,3	2,8	TC12	0,21	0	0,21	0,086
S03	D	5	3,0	2,4	TC12	0,12	0	0,12	0,063
TC01	A	0	0,9	0,6	TC15	2,2	4	2,2	1,7
TC01	B	3	1,4	0,7	TC15	2,2	4	2,2	1,2
TC01	C	0	0,8	0,5	TC15	3,6	5	3,6	2,5
TC02	A	2	0,8	0,4	TC16	1,9	2	1,9	1,0
TC02	B	0	0,8	0,4	TC16	2,2	1	2,2	1,1
TC02	C	1	0,9	0,2	TC16	2,7	4	2,7	1,7
TC03	A	4	3,8	3,4	TC17	1,2	0	1,2	0,13
TC03	B	3	3,0	3,9	TC17	0,07	0	0,07	0,010
TC03	C	3	3,3	3,0	TC17	0,40	0	0,40	0,083
TC04	A	3	3,2	2,5	TC18	0,55	0	0,55	0,067
TC04	B	4	3,6	4,4	TC18	0,54	0	0,54	0,040
TC04	C	2	2,7	2,5	TC18	0,89	0	0,89	0,070
TC05	A	18	10,3	9,5	TC19	3,7	8	3,7	5,6
TC05	B	23	6,5	11,5	TC19	4,3	11	4,3	4,8
TC05	C	20	7,4	12,5	TC19	4,5	5	4,5	3,7
TC06	A	18	7,7	10,4	TC20	1,9	5	1,9	1,8
TC06	B	20	8,3	11,4	TC20	4,1	5	4,1	3,5
TC06	C	15	7,5	11,5	TC20	2,0	4	2,6	7,1
TC11	A	0	1,9	0,16					
TC11	B	0	0,66	0,061					
TC11	C	0	0,13	0,083					

8.2 PHASE 2

8.2.1 Aims of Phase 2

The aims of the Phase 2 measurements were to use one of the higher charging configurations identified in Phase 1 to investigate:

– the influence of flow rate on charging, and
– the charging of 6" elements relative to 2" elements.

A repeat of condition TC 19 (Jet A plus pro-static agent) was selected for the Phase 2 tests and the influence of flow rate was investigated by measuring at a series of flow rates between 50 % and 100 % of the rated flow for each element set. To turn down the flow to 50 % of the rated flow, it was necessary to use four 2" monitors elements in the housing rather than three. This increased the full rated flow from 90 USGPM to 120 USGPM and reduced the residence times in the hoses and the fill time of the tote to 3/4 of the times that occurred in TC19. It may be possible to extract information about the hose and tank relaxation processes from these differences, but in this report we focus on the stated aims and report how the measured currents, charge densities and potentials varied with flow rate and element type. Charge decay data are obtained and compared with the Phase 1 data without detailed interpretation.

8.2.2 Element identification codes

In reporting Phase 2 data, individual elements are identified using labels of the format Xnaa where X is the element manufacturer code, n is the element diameter in inches (2 or 6), aa is the flow direction code (OI for Out-to-In, io for in-to-out and omitted for 2" monitors as these are all out-to-in). Thus, typical Phase 2 codes would be Y6oi meaning a 6" element from manufacturer Y with out-to-in flow or X2 meaning a 2" monitor element from manufacturer X.

8.2.3 Charge densities relative to equivalent Phase 1 data

The maximum effective filter segment exit charge densities at rated flow for the 2" elements are compared to the Phase 1 values for the same element types and test conditions in Table 10.

Table 10: 2" element comparisons: Phase 1 TC19 maximum effective filter exit charge density compared to Phase 2 at full rated flow with the same element type

Element	Phase 1 charge density, μC/m³	Phase 2 charge density at rated flow, μC/m³
X	+1 010	–1 540
Y	–2 610	–1 240
Z	–2 710	–380
Average	–1 440	–1 060

The charge density averaged over all the 2" elements is reasonably similar between Phase 1 and Phase 2 (both within about 15 % of the mean) but there is considerable scatter on the individual results. The Phase 2 work was done several weeks later than Phase 1 and the liquid

conductivities in Phase 2 covered a wider range than in Phase 1 (values from final field decay range from 0,8 pS/m to 9 pS/m rather than 3 pS/m to 5 pS/m) so there may have been some underlying differences in the conditioning of the fuel.

8.2.4 Charge density versus flow rate and comparisons of charge density from 2" and 6" elements

Figure 18 shows the measured filter segment maximum exit charge densities of both 2" and 6" elements as a function of flow rate. It includes the equations of linear regression lines to each segment.

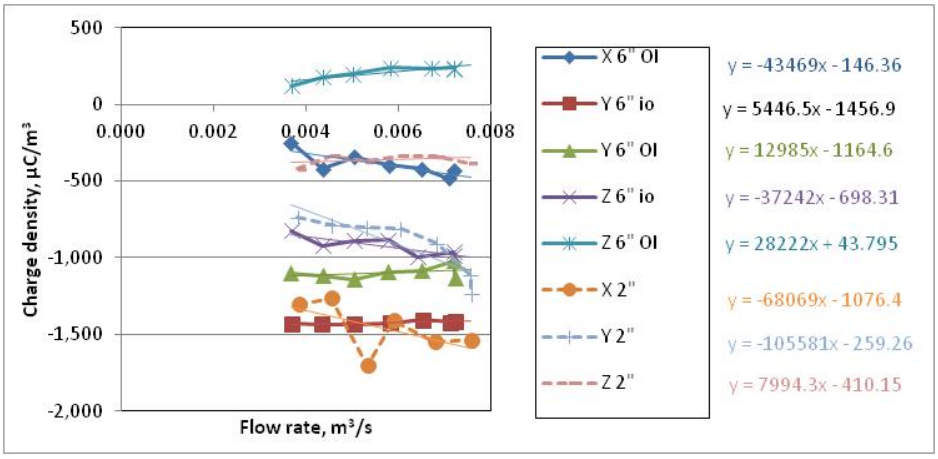

Figure 18: Exit charge density from filter segment as a function of flow rate

Some curves are almost horizontal, others are almost linear rises. We distinguish between these on the basis of the ratio of the slope from the 50 % flow value to the origin to the slope from maximum flow to 50 % flow. Where this ratio is less than 1,5 we call the curve near-linear and where it is more than 4 we call it near-horizontal. On this basis, three elements (X6 OI, Z6OI and Y2) gave near-linear curves and five (Y6io, Y6OI, Z6io, X2 and Z2) gave near-horizontal curves. There were no intermediate cases. The same grouping can be derived from the slopes of log-log plots.

Apart from one outlier 6" element (Z6OI) that charged the fuel positively when all other elements charged it negatively, an obvious feature of Figure 18 is that the spread of charge densities is broadly similar for both 2" and 6" elements. For element brands Y and Z, the difference in charging between 6" elements with out-to-in (OI) and in-to-out (io) flow directions can be compared. For both brands the in-to-out flow charged more negatively, although the difference was relatively small for brand Y elements.

8.2.5 Electric field measurements: the influence of flow rate and differences between 2" and 6" elements

Figure 19 shows the variation of maximum measured electric field with flow rate. The field always increases with the flow rate but the form of the dependence is quite variable. Sometimes the increase is quadratic, sometimes near linear, sometimes it levels off: e.g. cases

Y6io and Y6OI. Although the maximum currents generated were similar between cases X2 and Y6io the fields are higher in case Y6io. The maximum field occurs at the end of the fill and is therefore related to the final charge in the tank. The final charge is given by equation (F.4). Evaluation of this equation for the two cases shows that the ratio of the final charges between Y6io and X2 is ~1,25 whereas the ratio of maximum fields is ~2,0. This suggests that other factors, e.g. non-uniform charge density with different distributions between cases, may also be influencing the potentials. The variation of the final field divided by the final charge density is considered in 8.3.

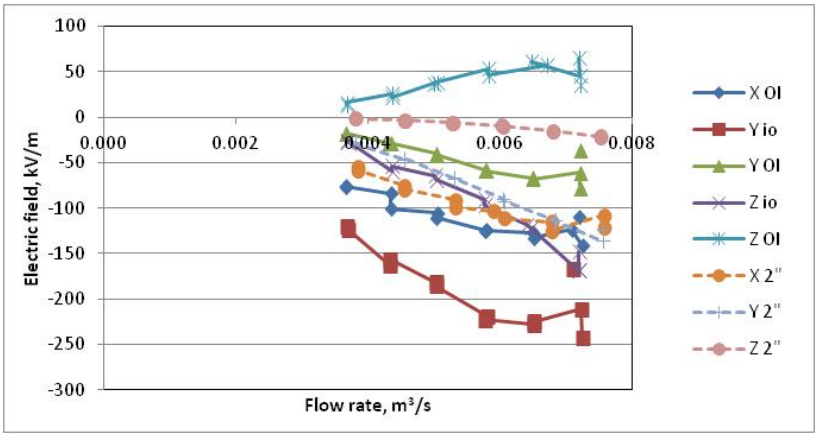

Figure 19: Maximum measured electric field versus flow rate

8.3 THE RATIO OF FINAL ELECTRIC FIELD TO ESTIMATED FINAL CHARGE (PHASE 1 AND PHASE 2 DATA)

Figure 20 shows the ratio of final flat-roof electric field to estimated final charge density.

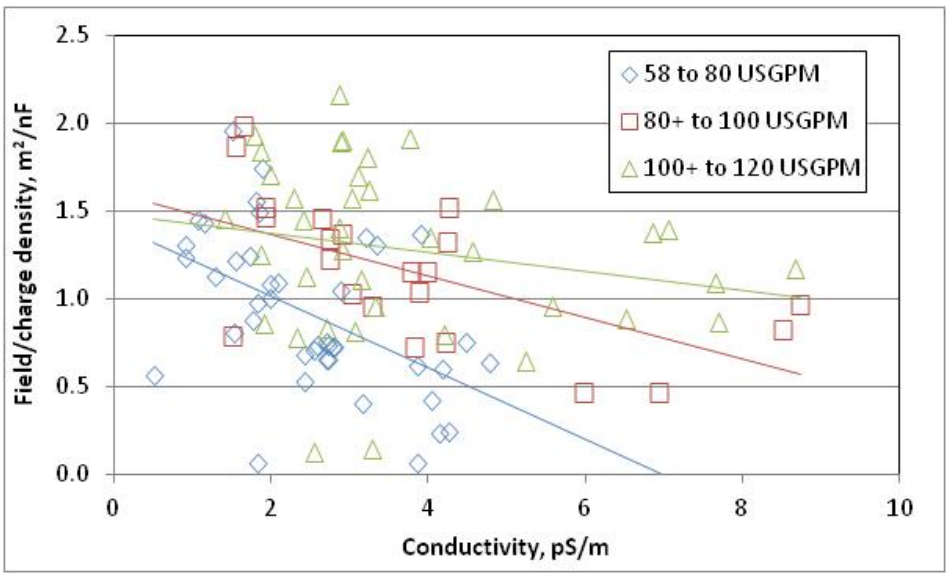

Figure 20: Final measured field/estimated final charge density

There is considerable scatter but the trend lines, which perhaps have doubtful significance given the scatter, suggest an average value of around 1,5 m^2/nC at low conductivity that tends to decline as the conductivity increases. The decline appears to be more marked at low flow rates. At the lowest conductivities there is the least dissipation during a fill so the charge is more nearly uniform, particularly for those fills with near constant streaming currents. At higher flow rates, there is more vigorous mixing, which also tends to make the charge more uniform. Non-uniform charge densities may be expected to be higher near the inlet so, as the filling is from the bottom, non-uniform charge density distributions may be expected to produce lower fields. The trends that are possibly apparent in Figure 20 may thus be linked to the effects of non-uniform charge density.

9 DISCUSSION

9.1 COMPARISON OF MAXIMUM CHARGE DENSITIES WITH OLDER DATA

The results of pre-2004 measurements of charging in 30" x 2" filter monitor elements at maximum rated flow were summarised in [2], which noted measured element-exit currents up to 5,4 μA per element (charge density ~2 870 μC m^{-3}) on a sustained basis[11] with transient peaks slightly greater than 16 μA (~8 500 μC m^{-3}). It was postulated that element exit currents could be rounded up to about 10 μA (charge density 5 300 μC m^{-3}) on a sustained basis with transient peaks up to about 20 μA (charge density 10 600 μC m^{-3}). The rounded values were generated to provide simple working current values for determining the element resistance needed to avoid discharge damage[12]; they are not measurements and should not be used when making comparisons with measured data. There has been no more openly-published work since [2] was published, so we take the [2] data as the best available summary of the behaviour of older systems. Whilst there is no reason to expect either [2] or the present measurements to reflect an ultimate worst case, the highest measured values reported in each work probably represent the best basis for comparison between present behaviour and historical behaviour.

We make the comparison with [2] using charge density, rather than current, because the charge density is independent of the number of elements in parallel. Our highest effective filter charge densities were measured at Flange 2 with an effective conductivity of around 2 pS/m for hose dissipation, which corresponds to an effective relaxation time of τ = 9,3 s. In conjunction with the residence time of T = 0,33 s given in Table 1, this gives the estimated proportion of filter element exit charge density reaching Flange 2 as $\exp(-T/\tau)$ = 0,97. The minimal loss of charge density between the element exit and Flange 2 allows our measured Flange 2 charge densities to be compared directly to the element exit charge densities in [2].

The maximum absolute effective charge densities obtained in the present work using Jet A with 4th and 6th edition 2" filter monitor elements at full rated flow (3 130 μC m^{-3} and 2 750 μC m^{-3} respectively) closely match the maximum sustained charge density reported in the older work (2 870 μC m^{-3}). The differences between the maxima in the present measurements and the older one are 260 μC m^{-3} or less whilst the standard deviation of our Phase 1 Jet A charge densities at conductivities between 2 pS/m and 5 pS/m is 1 500 μC m^3. Thus, based on the spread of our Jet fuel measurements, the difference between the highest old and new values is well within the scatter of the results.

We tested Green diesel as a potentially higher charging fuel than Jet A to compensate for being unable to test enough jet fuel samples to find a worst case. In keeping with this, our maximum absolute effective charge density of 4 640 μC m^{-3} (see Table 5) was obtained with Green diesel. This maximum Green diesel charge density is, however, only 1 770 μC m^3 more than the maximum absolute sustained charge density in the earlier jet fuel measurements (2 870 μC m^{-3}). Thus, to useful confidence levels, even the difference between the old Jet A data and the current Green diesel data is within the uncertainties associated with the scatter of charge densities.

We conclude that there is no evidence that charge generation in aviation fuel filter monitor systems has changed substantially since the older measurements.

11 The concept of effective current and charge density had not been introduced at that stage.
12 And partly because the older measurements were unlikely to include a global worst case.

9.2 DELAY BETWEEN END OF FLOW AND DECAY OF ELECTRIC FIELD

In the runs that were done at low enough conductivity to measure the electric field decay time there was usually a substantial (5 s to 10 s) delay after the tote inlet current stopped before the field began to decay. The reason for this is not known. It may be associated with the build-up of surface charge as the internal tank flows decay. This could be enhanced by the meter protrusion which would tend to attract extra surface charge below the meter. Other charge transport effects associated with inhomogeneous charge distributions may have a role.

9.3 MEASUREMENT LIMITATIONS: POSSIBLE FUTURE IMPROVEMENTS

9.3.1 Current measurements

For future tests the insulating flanges should ideally provide a higher resistance between isolated segments than in the present work, where it was adequate for measuring the main currents, but marginally adequate for obtaining an accurate current balance. This made the assessment of the inlet streaming current subject to a degree of doubt.

9.3.2 Field measurements

9.3.2.1 Alternative meter systems and mounting arrangements

The Boltek meter worked well and was sufficiently sensitive but is rather large and cumbersome. It may offer more flexibility and easier mounting to explore the use of some of the smaller field sensors that have been mentioned. Although sensitivity was not generally an issue, increased sensitivity (lower noise levels) would enable in-tank field and field decay measurements up to higher liquid conductivity.

If a faster flow stop can be engineered it may be also useful to explore the use of a faster response field meter.

The delays before charge decay and the 'wobbly' nature of some field decays are not understood. To explore these issues, it would be useful to enable multiple methods of meter mounting to verify they are not an artefact of a specific meter-mounting configuration: flush mounted, protruding and voltage probe meter configurations all have different advantages and drawbacks and it could be useful to switch between them.

Fitting the field meter flush with the roof, rather than letting it protrude into the tank, would have reduced the recorded electric field for a given surface potential. This would reduce the maximum conductivity at which electric field and field decay time measurements could be made. However, in compensation, flush-mounting the meter would have avoided possible perturbations arising from hanging the meter in the tank and thereby attracting extra induced charge whenever mixing processes were weak. Hence it could improve the quality of those measurements for which the sensitivity is adequate.

9.3.2.2 Field meter calibration

There was little time allowed in the present work plan for field meter calibration. The outstanding work falls into the following categories:

– Verification of the manufacturer's electric field calibration for a meter flush-mounted on a plane surface and exploration of the conditions (e.g. electrode size and spacing)

under which this calibration is valid. Previous work using this model of meter did verify the manufacturer's calibration and gave us confidence this time. However, the limits to the validity of the verification were not explored and the conditions that gave the verification were not recorded in detail because the earlier work focused mainly on voltage probe calibration.

– A more careful experimental check on the enhancement of field readings when a meter projects from a surface as it did in the present work to check the validity of the calculated protrusion correction factor.

– Voltage probe calibrations if this type of measurement is planned.

9.3.3 Insulating flanges

The insulating flanges were able to maintain a high enough level of insulation to permit the main measurements to be made, but the residual leakage errors may have affected the upstream current balance. I have been involved with similar measurements in which the insulating flanges could reliably maintain a resistance in excess of 1 Gohm. In any follow-up it is recommended that higher quality insulating flanges be used.

9.3.4 Conductivity measurements

The clay treatment appeared, from the decay time data, to reduce jet fuel conductivities to ~0,1 pS/m. Significant changes in fuel charging and dissipation behaviour occur below ~1 pS/m but in this range a dip cell conductivity meter reads '0' pS/m. To obtain more systematic data comparisons in this low conductivity region it would be better, in any future testing, to replace the dip cell with a conductivity meter such as a concentric electrode cell capable of measuring below 0,1 pS/m in jet fuel.

9.3.5 Decay times and effective conductivities

9.3.5.1 Flow start/stop time

The flow into the receiving vessel did not start and stop instantly. The flow meter had a response time of about 1 s so we do not know exactly how fast the flow could be stopped but in some cases the current took a few seconds to fall to zero. Thus, decay times of less than a few seconds could not be reliably measured and in-tank effective conductivities could only be observed by electric field decay time measurements for liquids with effective conductivities below about 10 pS/m (relaxation time ≥2 s). If the flow stop time into the receiving tank could be made very rapid (e.g. by a rapid acting valve diverting the flow to a bypass?) perhaps faster decay time measurements could be made. This would also require faster data logging. The delay before the onset of field decay would, however, need to be understood before this was worthwhile.

9.3.5.2 Interrupted fills

Unpublished work using interrupted fills has shown that decay times can vary with liquid depth. To map out appropriate decay times for different stages of filling it could be useful to do interrupted fills. That is, tests in which single fills are paused at regular intervals with a charge decay measurement being made at each pause.

10 CONCLUSIONS

We have carried out tests to measure charge generation in commercial filter monitor elements. The test rig was designed to produce similar charge densities, residence times and fill times as full-scale fuel handling facilities. Streaming currents, charge densities, in-tank electric fields and charge and field dissipation times were measured. All brands of element known to have been qualified to EI 1583 6th edition were tested in 2" and 6" diameter forms and each 2" element was tested in both an as-received (dry) state and water-wetted. Tests were done with two fuels (Jet A delivered without SDA, and a hydrocarbon-based Green diesel). They were tested, as received, after clay filtration, after adding varying amounts of static dissipater additive (SDA) and after adding a fixed amount of a candidate pro-static agent. Test flow rates varied from 50 % to 100 % of rated flow. A range of fuel charging behaviours is present globally in aviation fuel distribution systems and it was not practicable to test every potential situation. The conditions chosen for testing seek to provide the industry with a fair insight into the expected behaviour within the limitations of a feasible test programme. The conclusions drawn from the results obtained under the chosen test conditions are as follows:

1. The maximum magnitude of effective charge-density at the filter vessel exit measured with Jet A at the rated flow per element was 3 130 μC/m^3. The corresponding streaming current at a flow rate of 90 USGPM/340 litre per min (rated flow for the three 2" x 30" elements) is 17,5 μA[13]. The maximum magnitude of filter vessel exit charge-density measured with Green diesel was 4 640 μC/m^3, corresponding to a current 25,4 μA at 90 USGPM. Charge densities in the test rig are expected to be directly comparable to real-world values; currents at rated flow should scale with the number of elements.
2. The highest charge density measured with Jet A in the present work (3 130 μC/m^3) is close to the highest charge density reported in earlier measurements which was ~2 870 μC m^{-3} on a sustained basis [2]. The maximum magnitude of Green diesel charge density was about 50 % higher than with Jet A and hence was close to the postulated round-number steady value of 5 300 μC m^{-3} suggested as a useful representative high value for Jet A in the earlier work.
3. Neither the presence of the candidate pro-static agent nor water-wetting of the elements had a significant influence on the maximum charge density in the test system.
4. Comparative tests between 4th and 6th edition elements did not produce a significant difference in charge density (a measured 11 % decrease from 4th to 6th edition).
5. At rated flow there was no significant difference in charge density between 2" elements and 6" elements of either flow format (differences between formats were less than the scatter between brands).
6. At face value, Conclusions 2, 3 and 5 suggest that the changes to fuels and filter monitor element design that have taken place in recent years have made little difference to electrostatic charge densities. It should, however, be noted that, although the influence of filter monitor element design has been well covered, the evidence on fuels is much more limited. The present charge densities fall within the spread of the older data and because of the sparse fuel sampling we cannot distinguish long-term trends in maximum charging from batch-to-batch variations. As only one batch of Jet A was tested it is unlikely to represent a worst case. Similar limitations apply to each of the individual earlier tests, but as there are more of them there is more chance of a closer approach to a worst case. Consequently, it

13 For similar residence times.

is probably only safe to say that maximum charge densities are similar to what they were and that there is no evidence they have increased. The results confirm the safety advice provided in existing industry literature, such as IEC TS 60079-32-1, which emphasises that high filter monitor outlet charge densities can be observed with low (~1 pS/m) fuel. Although the maximum charge densities do not appear to have increased, the results confirm the importance of following existing industry guidance to ensure adequate charge relaxation time between refueling filtration equipment and aircraft.

7. The streaming current or charge density delivered to the receiving tank tended to increase with effective conductivity up to about 1 pS/m. High values were observed between 1 pS/m and 4 pS/m with a trend from positive to negative at around 2 pS/m. Above 4 pS/m there was a steady decline.
8. When SDA (STADIS® 450) was added to give measured conductivities of approximately 15 pS/m, 200 pS/m and 600 pS/m the measured currents delivered to the receiving vessel were substantially lower than in the unadditised fuels.
9. The highest in-tank electric fields were recorded at conductivities below 4 pS/m. All the enhanced conductivity levels (15 pS/m and above) produced by adding SDA gave a substantial reduction in the maximum electric field measured at the centre of the roof during a fill. Specifically, the maximum measured roof-centre electric field was 195 kV/m at low conductivity but only 2,9 kV/m between 15 pS/m and 23 pS/m: a factor of 67 reduction. At 200 pS/m and above, the measured roof centre field was at or below the noise threshold for field measurement, which was about 0,005 kV/m. This is a factor of $3{,}74 \times 10^4$ lower than the maximum field.
10. The electric field magnitudes decline faster than the currents with increasing conductivity because of the additional effects of in-tank dissipation and the tendency of the charge to cluster around the inlet at high conductivities.
11. Although the electric field decay times in the tank and the charge decay times in the hoses were correlated with the measured conductivity there was not close agreement between measured and effective conductivity. This is commonly observed [e.g. 8]. Competing factors that could possibly contribute to differences include hyperbolic relaxation (the enhancement of conductivity by the presence of charge at low conductivity [9–11]), the hindering of dissipation in the tank by the free surface, changes in the charge distribution and the hindering of dissipation in hoses by slow reaction rates at the walls [12].
12. Hyperbolic relaxation is evident in the data at low conductivities, which shows faster decay times in the parts of the system containing more highly charged liquid. Thus at 10 pS/m the decay time in the hoses was 1,4 times faster than the initial in-tank field decay time and at the lowest effective conductivities it was 4,9 times faster. Both are faster than the final electric field decay time.
13. In contrast, at the highest conductivities at which decays could be measured, the effective conductivity for field decay became lower than the measured conductivity. This may be evidence of hindered decay but the effect only happened where the electric field decay time became hard to measure because the relatively slow transition into decay merged into the decay itself. It may therefore represent a measurement problem rather than a real difference.
14. An electrostatic risk assessment involves factors outside the terms of reference of this study. Factors relevant to changing risks are changes to flammability arising from changes in fuel handling temperatures and volatility and changes to charging and dissipation arising from different operational flow rates, residence times and fill times. However, the maximum charge densities measured in this study were not found to be significantly different to those reported in earlier work on 2" filter monitor charging.

11 REFERENCES

[1] H.L. Walmsley, P. Rugen and S. Threadgold, *Electrostatic discharges in two inch aviation fuel filter monitors*, IP Research Report, October 2002.

[2] H.L. Walmsley, P.D. Rugen, S. Threadgold, *Electrostatic discharges in two inch aviation fuel filter monitors Phase 2: Properties needed to control discharges*, IP Research Report, Energy Institute, January 2004.

[3] CRC 590, *The effect of aviation fuels containing low amounts of static dissipater additive on electrostatic charge generation*, CRC, May 1994.

[4] G. Sprenger, Velcon Filters Inc, *Static charge mitigation*, Presentation to CRC, May 2001.

[5] H.L. Walmsley, J.S. Mills, *Electrostatic ignition hazards in road tanker loading: Part 1. Review and experimental measurements*, Journal of Electrostatics, Vol. 28, No. 1 (1991) pp. 61–87.

[6] L. G. Britton, H. L. Walmsley, *Static electricity: New guidance for storage tank loading rates*, Process Safety Progress, Vol 31, (2012), 219–229.

[7] L.G. Britton, T.J. Williams *Some characteristics of liquid-to-metal discharges involving a charged 'low risk' oil*, J. Electrostatics, 13, (1982), 185–207.

[8] L.G. Britton, *Avoiding static ignition hazards in chemical operations*, Wiley, 2010 ISBN 0470935391, 9780470935392.

[9] W M Bustin, I Koszman, I Tobye, *Hydrocarbon process*, 43, (1964), 209.

[10] H. Kramer, G Schon, *Dechema Monographien*, 72, Verlag Chemie, Weinheim, (1974), 361.

[11] K. Asano, H. Kramer, J. *Electrostatics*, 2, (1976/77), 269–276.

[12] H.L. Walmsley, *Charge relaxation in pipes*, Inst. Phys Conf Ser 66, (1983) 209–214.

[13] J. Denker, http://www.av8n.com/physics/laplace.htm.

[14] K. Asano, *Electrostatic potential and field in a cylindrical tank containing charged liquid*, Proc IEE, 124, (1977), 1277.

[15] J. Carruthers and K. Wigley, *The estimation of electrostatic potentials, fields and energies in a rectangular metal tank containing charged fuel*, J. Inst. Petroleum, 48, (1962), 180–195.

ANNEX A: OPERATIONAL CONDITIONS AND THE SELECTION OF RIG PARAMETERS

A.1 GENERAL BASIS FOR SELECTING RIG PARAMETERS

We aimed to set up a rig to test charge generation on commercial filter monitor elements whilst providing a degree of charge dissipation representative of commercial jet fuel handling practices. This Annex sets out requirements that are designed to ensure the same charge densities in real and test systems. If, at all conductivities, the charge densities are the same in the test rig as in a real system then the ratios of surface potentials at different conductivities and the decay times should also be similar in the test rig and full scale equipment, subject to relatively minor differences arising from possible differences in charge distribution.

With exponential charge dissipation the charge density, ρ, in a tank during filling is given by :

$$\rho = \rho_0 \frac{\tau}{\delta T}\left[1-\exp\left(-\delta t_{fill}/\tau\right)\right] \tag{A.1}$$

where ρ_0 is the inlet charge density, τ is the effective charge dissipation time, δ is the fill fraction and t_{fill} is the time taken to fill the tank completely at the specified flow rate. At a particular value of δ that depends on tank shape, fill time and liquid conductivity, the surface voltage, Φ, goes through a maximum that can be written as:

$$\Phi = (K/\varepsilon_0)\rho C^{2/3} \tag{A.2}$$

where K is a dimensionless constant that depends on the shape of the tank and the distribution of charge within the tank (it can be calculated in some circumstances), ε_0 is the permittivity of free space (a fixed constant), ρ is the charge density and C is the tank capacity.

If the factors ρ_0, τ and t_{fill}, can be made to have values that are typical of full-scale systems, ρ should be representative. If the tank shape and inlet arrangement are reasonably typical, K should also be representative then the remaining factor, $C^{2/3}$, is the only systematic difference between the test system voltages and full scale system voltages apart from detailed differences comparable to those that might occur between different full-scale systems. Electric fields[14] are related to voltages by dividing by the tank length scale, $C^{1/3}$, so electric fields scale as $C^{1/3}$. Thus representative equivalent full scale voltages may be estimated by multiplying measured voltages by $(C_f/C_t)^{2/3}$ and many representative fields may be estimated by multiplying measured fields by $(C_f/C_t)^{1/3}$.

The factors governing and ρ_0, τ, t_{fill} and K are as follows:

– The inlet charge density, ρ_0, is determined by the charging and dissipation processes that occur upstream of the tank. In the real systems of relevance here, the main charging occurs in a filter monitor and partial dissipation of the filter monitor charge occurs as the liquid passes along the pipes and hoses from the filter monitor to the storage vessel (e.g. road tanker compartment or aircraft tank). A smaller amount of 'pipe' charging occurs in the interconnecting pipes and hoses. To ensure a representative filter monitor element outlet charge density, ρ_e, we use a commercial

14 This applies to the fields that are determined by the overall tank shape (e.g. radial field at the wall of a cylinder, vertical field at the roof). Localised fields around protrusions scale as the local potential divided by the protrusion size and so may vary, for example, as the tank voltage if the protrusion does not scale with tank size.

filter monitor element run up to its maximum rated flow. To ensure typical near-worst-case dissipation, the residence time in the downstream filter chamber, t_f, and the residence time, t_{res}, in the interconnecting pipe and hose need to be comparable with the shortest times found in practice. Although pipe charging is much smaller than the filter monitor charging, if we want the rig to get conductivity dependences right, it is necessary to scale it correctly, because it may dominate the delivered charge density at high conductivity when the filter monitor charge is virtually all dissipated before reaching the tank. Pipe charge densities are now thought to be best represented as proportional to *v/d* [5,6] so, for the pipe charging contribution to be properly represented, the ratio of *v/d* in the pipe and hose should be similar to that in a real system.

– The decay time, τ, is determined by the liquid.
– The fill time, t_{fill}, can be made representative by choosing a suitable test tank size for the flow rate.
– The shape factor, *K*, depends on the gross tank proportions (i.e. on the ratios of length and width to height), to some extent on the distribution of charge within the tank and, to a much lesser extent, on the detailed tank shape (e.g. cylindrical or rectangular). As long as the inlet arrangement is reasonably representative, the charge distribution will be similar for a given conductivity. Medium-sized tanks or compartments are often either roughly equal in length, width and height, e.g. a road tanker compartment, or taller than they are wide, e.g. vertical axis tanks on a small-scale congested tank farm.

If all this matching is done we should end up with charge densities that are relevant to real world cases and, as all the relevant parameters are controlled and known, any residual differences can be allowed for as necessary. This is in contrast to many older measurements in which, for example, filter vessel outlet charge densities were recorded without any information being provided about the residence time between element outlet and vessel outlet.

A.2 SPECIFICS: MATCHING RIG PARAMETERS TO 'REAL' SYSTEMS

To translate the principles in A.1 into a rig design we select a 'representative' real world scenario and make the factors ρ_e, t_{res}, *v/d*, *T* and *K* in the rig match the scenario as closely as we can. The closeness of the match is limited by the need to use standard pipe and hose diameters and integer numbers of filter monitor elements. The real scenario we chose is filling a 5 m^3 truck compartment at 2 400 l/min in a 4" line (vd = 0,5 m^2/s) via a filter monitor unit 20 m upstream of the tank[15]. The data for this scenario and the equivalent data for the ideal test rig are shown in Table A.1

15 The truck filling scenario was used because of the potential complexity of on-board aircraft fuel systems (line residence times, line branching, tank fill times, liquid overflows to other tanks) and the lack of sufficient information to enable a representative worst case to be picked out.

Table A.1: Rig design data compared to a real world scenario

System	Pipe dia, in	Pipe dia, m	Flow rate, USGPM	Flow rate, l/min	Flow speed, m/s	v/d, s^{-1}	Relative pipe current	Pipe+ hose length, m	Pipe+hose residence time, s	Tank capacity, m^3	Fill time, s
Real	4	0,102	633	2 400	4,87	**47,6**	1	20	4,1	5	125
Phase 1, 2"	2	0,0525	**90**	**341**	2,62	**49,9**	1,05	6,6	**2,52**	1,35	238
Phase 2, 2"	2	0,0525	**120**	**454**	3,50	**66,6**	1,40	6,6	**1,90**	1,35	178
Phase 2, 6"	2	0,0525	**115**	**435**	3,35	**63,8**	1,34	6,6	**1,97**	1,35	186

The key points of comparison are picked out in bold in Table A.1. From left to right:

– The flow rate is the maximum for the elements.
– *v/d* is similar to the real scenario value for the Phase 1 rig flow rate so the expected pipe charge density should also be similar. In Phase 2 the *v/d* values are up to 1,4 times the real values so the charge densities produced by pipe flow would be expected to be higher by this factor in these tests.
– In all tests the hose residence times are rather short so a higher proportion of the filter monitor charge will reach the tank than in the real system. The measured tote inlet charge densities should therefore be higher than the corresponding real behaviour. The shortest real-world residence time is not known so this may provide a useful margin.
– The fill times are longer than the real-world case; this provides more time for dissipation and reduces the charge density in the tank.

The compromised fill time was adopted because it was required to keep the system to tote scale and some key sponsors specifically wished to ensure a minimum test duration of 120 s, even though the tote could not be completely filled in a test (to avoid immersion of the field meter). The lower flow rate associated with the longer fill time also helped to minimise the number of elements needed for testing at maximum rated flow. As the main focus of the work was to establish charging behaviour rather than to match in-tank fields and potentials, the loss of tank fill time similarity was judged to be an acceptable compromise.

In addition to these points we do not know the shortest residence time between filter monitor element and vessel outlet that could occur in practice but we record the value in the test rig so allowance can be made for it. It was 0,57 s at 115 l/min.

ANNEX B: CALIBRATION AND ANALYSIS PROCEDURES FOR CURRENTS, ELECTRIC FIELDS AND DECAY TIMES

B.1 CURRENT

B.1.1 Ammeter details

The currents were measured with three Keithley type 6 514 multimeters and a Keithley type 6 485 picoammeter. All have ±2 V full scale analogue outputs and scales that increase or decrease in decades either side of ±2 μA. The rated meter accuracy is 0,1 % or 0,2 % over a one-year period for the ranges that were used. The 6 485 was within a year of purchase at the commencement of testing and thus covered by the manufacturer's calibration but at least two of the three type 6 514 meters were outside the one-year calibration period. Furthermore, the rated accuracy applies to the front panel readings and digital outputs, not to the analogue output. The rated accuracy for the 6 485 analogue output is given as 3 %. I could not find a rated analogue output accuracy in the specification for the 6 514 meters but expect it to be similar. There are further possible calibration differences in the logged results arising from the gains in the data acquisition system.

The logged values of the meter analogue outputs were therefore checked against the (in calibration) 6 845 front panel readings by the method described as follows, which includes calibration of the data acquisition system gains.

B.1.2 Range setting

The range setting was noted manually in the header for each run of logged data. The logged analogue outputs were scaled with this range setting.

B.1.3 Zero offsets

The residual zero offsets obtained from the pre-flow data were subtracted from the in-flow readings to ensure a good baseline, although this correction was only important at the highest conductivities where currents were small. At these conductivities noise on the signals typically varied from 1 nA to 5 nA.

B.1.4 The relationship between measured currents and streaming currents

During each test we measured the current from the receiving tote to earth, I_{mt}, the current from the second hose section to earth, I_{mh2}, the current from the first hose section to earth, I_{mh1}, and the current, I_{mf}, from the filter housing to earth. The relevant electrostatic streaming currents flowing in the system are the current from the pump and inlet piping into the filter housing, I_{sin}, the current from the filter housing into the hose, I_{sf}, the current from hose 1 into hose 2, I_{sh1}, and the current from the hose into the receiving drum, I_{sd}. Applying current balance (Kirchoff's current law) to the receiving drum, hoses and filter housing section we get:

$$I_{sd} = I_{mt} \tag{B.1}$$

$$I_{sh1} = I_{sd} + I_{mh2} \tag{B.2}$$

$$I_{sf} = I_{sh1} + I_{mh1} \quad \text{(B.3)}$$

$$I_{sin} = I_{sf} + I_{mf} \quad \text{(B.4)}$$

At low conductivities the inlet streaming current, I_{sin}, is usually much smaller than the filter outlet streaming current, I_{sf}, hence the measured filter current is approximately the same magnitude as the filter exit streaming current but with reversed polarity and the sum of the measured hose and drum currents should be approximately equal and opposite to the measured filter current. At very low conductivities there is little dissipation in the hoses and then $I_{sf} = I_{st}$ and $I_{mf} = -I_{mt}$.

B.1.5 Estimating the upstream inlet streaming current by current balance

With low-noise and high leakage resistance both to ground and between isolated sections the streaming current entering the measurement sections from the pump and upstream piping is given by the balance of the four measured readings (see B.1.4). Unfortunately, the balance is usually a small difference between relatively large readings and consequently is highly susceptible to noise, leakage currents and small differences in meter calibration. In the present work, the current measurements were not seriously affected by noise and meter calibrations were corrected as discussed in B.1.6 but flange leakage resistances were only just at an acceptable level. Only the leakage across Flange 4 affects the current balance used to obtain the upstream current but this was often marginally adequate for measuring currents at the level of small differences. Hence our estimates of the inlet streaming current may not be of high accuracy.

B.1.6 Calibration procedures

A current source was used to inject currents of approximately 10 nA, 100 nA, 1 μA and 10 μA into each meter in turn. The meters were set to the corresponding ranges, the front panel readings were recorded and the analogue output values were logged on the data acquisition system.

The front panel readings of the meters were first compared to check if the uncalibrated 6 514 s were still operating within the manufacturer's specification. The differences were within the expected range except on the 20 μA range of the filter electrometer, which was reading high by about 1,1 %. We adopted the average of all the in-specification values as the 'true' reading for each range and then, for each meter and each current range, formed the ratio of the logged analogue output value (averaged over 30 + readings) to the true value. These ratios are given in Table B.1. The logged currents need to be divided by these the calibrated values to obtain calibrated values.

Table B.1: Ratio of logged current values to 'true' value

Range	Filter	Hose 1	Hose 2	Tote
20 nA	1,011	1,003	0,9943	1,000
200 nA	0,9993	1,001	0,9807	0,9997
2 μA	1,003	1,051	1,048	1,047
20 μA	1,005	1,051	1,037	1,058

Figure B.1 shows a plot of the maximum effective streaming currents calculated over all Phase 2 tests using both raw (uncalibrated) and calibrated ammeter readings. In the raw readings the different meter calibrations clearly affect the current balances required to calculate the upstream current, leading to some unexpected variations in upstream streaming current that are eliminated or greatly reduced by using the calibrated currents. For example, in the second group of data from the left in Figure B.1 a) the filter charge is high even at low flow rates and the upstream inlet charge is also high, whereas it would be expected to be unaffected by the change of filter element. There are still residual differences between runs in Figure B.1.b). These may arise from leakage currents across Insulating Flange 1 but it is also noted that the Phase 2) tests showed relatively large degrees of conductivity variation and it is possible that these arise from rig and fuel conditioning/contamination issues that affected the upstream current.

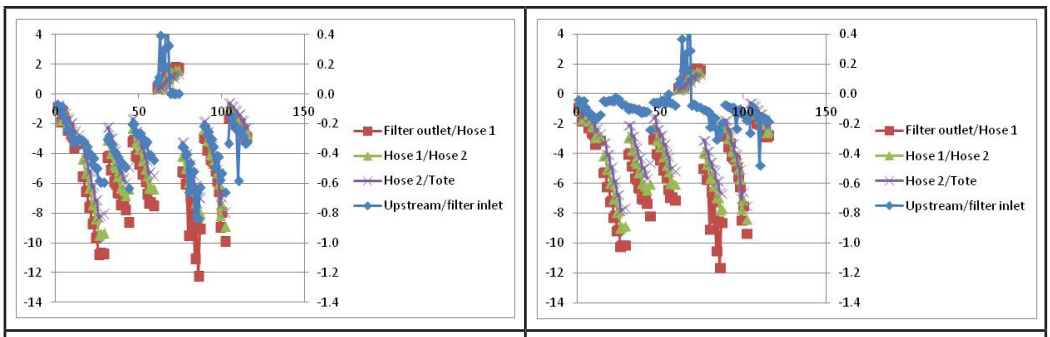

a) Uncalibrated currents | b) Calibrated currents

Figure B.1: The effect of current calibration

B.1.7 Insulation resistance and measurement lead integrity checks

The accuracy of the current measurements depends on the quality of the insulation separating the isolated sections. If the insulation resistance is too low, leakage currents lead to measurement errors. In particular leakage across Insulating Flange 1 will affect the overall current balance. The adequacy of the insulation resistance was directly checked daily by connecting the measuring meters in turn to a current source of the appropriate range. The current source was first connected directly to the meter without the meter being connected to the rig to obtain a baseline current reading. The current source was then connected to the rig component under test, the meter was also connected to the rig and a repeat reading was taken. With good insulation there should be no significant leakage and the baseline and the two test readings should be equal.

By making the connection from the current source to the rig for the leakage measurement via a separate current source lead the test was also able to verify the integrity of the signal lead to the meter; if this had become disconnected or broken it would show zero current in the leakage test.

B.1.8 Correction to measured tote current

In a few measurements at low conductivity (<5 pS/m) it appears as if the tote current measurement is subject to a small but distinct error starting about half to three quarters of the way through the fill. This causes a corresponding dip in all the derived streaming currents. At the end of filling, the upstream streaming current actually changes polarity and continues

after the end of the fill for a short time before settling to zero. An example is shown in Figure B.2 which shows both uncorrected streaming current signals containing this error and streaming currents corrected by the procedure described in this section.

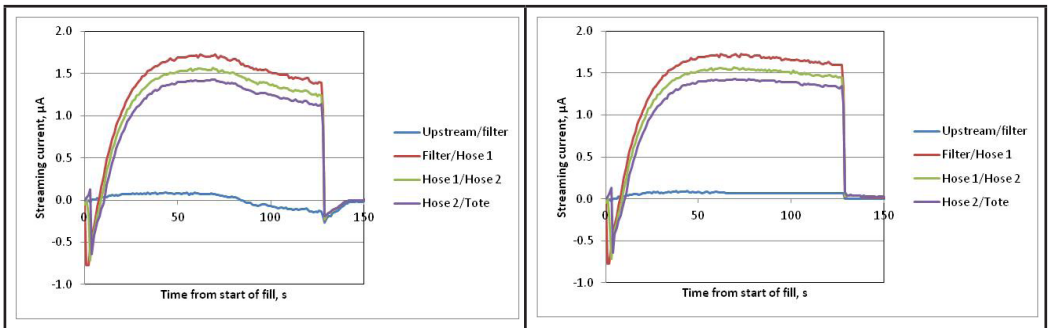

a) Streaming currents with uncorrected tote current	b) Streaming currents with corrected tote current

Figure B.2: Tote current correction

The error is thought to arise because the (rather large) field meter could not be isolated from earth whilst logging data and so had to be isolated from the tote. Hence the internal tote charge that linked to the field meter went unrecorded[16]. During filling this results in a current signal that gets progressively reduced as the coupling to the meter increases with rising liquid level. After the completion of filling no new charge is introduced into the tote but the proportion of the remaining charge that couples to the meter increases due to the reduction in flow-related mixing resulting in the period of apparent reverse polarity current.

At higher conductivities (above 5 pS/m) and even in many low conductivity runs the effect was absent. In these cases it would appear that the charge was stratified and concentrated lower in the tote so that the linkage to the field meter was always small and the error was too trivial to observe.

The streaming currents introduced by the filter elements often varied in complex ways during the fills but the upstream entry streaming current typically shows simple behaviour (more or less constant or slowly declining after an initial transient) and the tote current error often showed itself as an obvious departure from this (the analysis in B.1.4 shows that an error in the tote current would propagate through to all the streaming current estimates). A tote current correction was therefore obtained by assuming that the errors in the upstream current all arise from the tote current error and that until the end of the fill the actual upstream streaming current was fixed at a constant value taken from the point where the error became apparent whilst after the fill it was zero. Applying this correction to the tote current produced a satisfactory elimination, or at worst a major reduction, of the apparent tote current errors.

B.1.9 The 'Effective current': exponential averaging

Hazards are determined by the accumulation of charge in the receiving tank. This is governed by a time integral of the current so a short-lived transient has little effect. Consequently we

16 The field meter could not be isolated from ground because the connection between the analogue output and the data logging system introduced a ground leakage path. The meter has an optical link that would have avoided this issue but it was not planned to use it and there was no time to implement the change of output method by the time the issue became apparent.

do not wish to measure the highest recorded transient current irrespective of duration as it may make no significant contribution to a hazard. A consideration of the process of charge accumulation in a tank (see Annex F) leads to the conclusion that the best approach is to use exponentially weighted averaging of the current with a time scale based on the measured relaxation time. During the fill it would seem reasonable to assume that the relaxation time measured as early in the decay period as possible would give the best estimate of the relaxation time. We call the weighted exponential average obtained using this relaxation time the effective current, I_{eff}:

$$I_{eff}(t) = \int_0^t I(t')\exp\left(-(t-t')/\tau_0\right)dt' \Big/ \left\{\tau\left[1-\exp\left(-t/\tau_0\right)\right]\right\} \qquad \text{(B.5a)}$$

where $I(t')$ is the measured current at a time t' after the start of filling and τ_0 is the initial decay time. After the fill, if the relaxation time is variable it is given by:

$$I_{eff}(t) = I_{eff}(T)\exp\left[-\int_T^t \frac{dt'}{\tau(t')}\right] \qquad \text{(B.5b)}$$

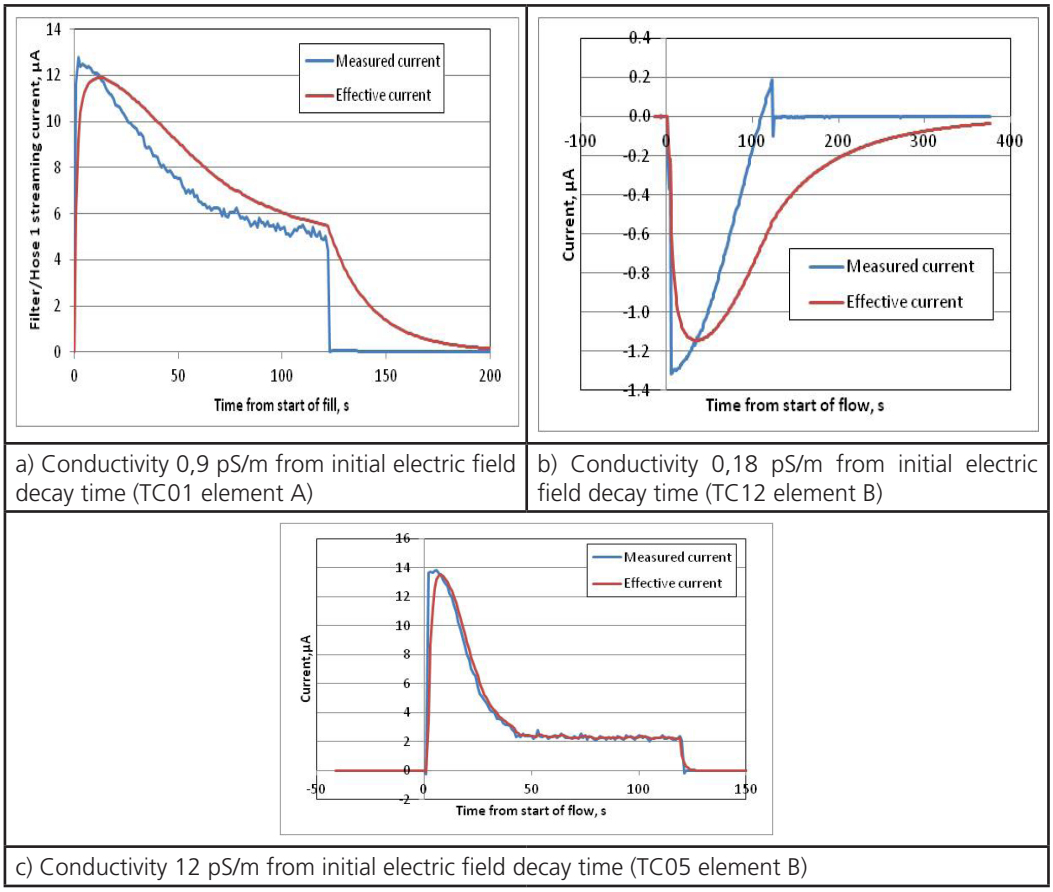

a) Conductivity 0,9 pS/m from initial electric field decay time (TC01 element A)

b) Conductivity 0,18 pS/m from initial electric field decay time (TC12 element B)

c) Conductivity 12 pS/m from initial electric field decay time (TC05 element B)

Figure B.3: Measured and effective currents

In our analysis we used a simple trapezium-rule method to evaluate the integral in equation (B.5) with the measured current data and hence determined values of I_{eff} throughout each fill.

Some representative I_{eff} vs time plots are given in Figure B.3, which compares the measured and effective streaming currents at the exit of the filter section (Insulating Flange 2) for representative low conductivity cases[17]. The effective current is a smoother curve than the measured current and has a slightly lower peak but higher currents at other times. As the conductivity increases it approaches the measured current. Above 12 pS/m we use only the measured current because the decay time needed to estimate the effective current cannot be determined accurately.

It was found in a few cases that when the relaxation time was not much longer than the digitisation interval, the maximum effective current was greater than the maximum measured current. This is a numerical error arising from the simple integration method. It was verified that the error disappears when the more accurate integration procedure outlined in Annex F is used, but in most cases at low conductivity the simple method is accurate enough and the results were not generally re-evaluated with the more accurate method.

At conductivities of more than about 15 pS/m we could not measure decay times accurately so the effective current could not be determined. However, there were relatively few data between 5 pS/m and 15 pS/m and at 15 pS/m the integration time for effective current is comparable to the sampling period, so for this conductivity and above there is little difference between the recorded and effective currents. Furthermore, at these conductivities the currents are low and the signals are noisy. For these conductivities we therefore only record the average current over the test run. This is useful mainly as confirmation of the low level of the currents. The fields and potentials are also low so a detailed analysis of the corresponding currents is not so important for hazard analysis.

B.1.10 Deriving the decay time or effective conductivity for charge dissipation in the hoses from the recorded currents

The effective exponential decay time for charge dissipation in a pipe or hose section may be written as:

$$\tau_{eff} = \frac{T}{\ln\left(\frac{I_{sin} - I_{s\infty}}{I_{sout} - I_{s\infty}}\right)} \tag{B.6}$$

where T is the residence time of the liquid in a section (e. g. Hose 1, Hose 2 or both), I_{sin} is the streaming current entering the section, I_{sout} is the streaming current exiting the section and $I_{s\infty}$ is the streaming current that would be reached in an infinitely long pipe or hose of the given type.

From equation (B.6) and the definition of relaxation time, the effective conductivity, κ_{eff}, for the dissipation of charge in a section of pipe or hose can be written as:

$$\kappa_{eff} = \frac{\varepsilon\varepsilon_0}{T}\ln\left(\frac{I_{sin} - I_{s\infty}}{I_{sout} - I_{s\infty}}\right) \tag{B.7}$$

where $\varepsilon\varepsilon_0$ is the dielectric constant of the liquid. We do not generally have a measure of $I_{s\infty}$ but the measurements of pipe current in the Phase 1 supplementary tests along with the inlet

17 These plots give the effective current calculated after the fill by using equation (B.5) with the initial decay time even after the end of the fill. After the fill the expressions in Annex F should really be used with the measured time-dependent decay time in place of τ_0.

streaming current estimates in the rest of the data suggest it is usually much smaller than the filter currents and so can be neglected. In this case κ_{eff} can be estimated from the current data using equation (B.7) with $I_{s\infty} = 0$.

B.1.11 Making allowance for dissipation within the filter section

The insulating flange forming the downstream boundary of the filter section was about 1 m downstream of the filter element exit and the corresponding residence time between the element and the insulating flange (~0,33 s) is thought to be reasonably typical of residence times in operational filter monitor housings so the measured exit charge densities are expected to be representative of filter monitor housing exit charge densities in real systems. However, if adjustments need to be made it may be useful to estimate the actual filter element exit current based on scaling the segment exit current. This has not been done in our analysis but can be done approximately by assuming an exponential decay of charge between the element exit and the insulating flange on a time scale equal to the measured charge dissipation time in the first hose (see 8.1.3.8).

B.2 ELECTRIC FIELD

B.2.1 Magnitude of the field

The electric field at the meter sensing surface was obtained directly from the logged analogue output voltage of the field meter (1 V out per kV/m of field with unattenuated sensitivity). The equivalent field that would exist at the tank roof without the protrusion of the meter was estimated from the recorded field using a calculated calibration factor of 0,31 (see Annex C). This value was roughly consistent with some practical calibration tests that gave a correction factor of 0,36. However the calibration tests were done with a rough and ready setup that did not have a well-defined geometry so the calculated results are felt to be more accurate[18].

The recorded data were logged as if the meter had full sensitivity. For some of the lower conductivity tests the meter sensitivity had to be reduced to avoid out-of-range signals. This was done with a plug-in attenuator resistance. When this was done, the attenuation resistance, R, in ohms was noted in the header of the logged data file. The meter manufacturer's literature then indicates that the sensitivity is reduced by an attenuation factor, α, of:

$$\alpha = \frac{R}{10^5 + R} \tag{B.8}$$

This factor was applied in the analysis spreadsheets.

B.2.2 Deriving the electric field decay time from post-fill field readings

A simple exponential decay is characterised by a single fixed value of the decay time [$\tau = -1/\mathrm{d}\ln(E)/\mathrm{d}t$] throughout the decay period. In some cases, this ideal behaviour was approached but usually the decay time varied throughout the decay. We tracked this in two ways.

18 It is recommended that follow-up work should be done to provide a more accurate measured estimate of the meter protrusion correction factor.

The simplest was to use the Excel Slope function to obtain d*E*/d*t* over a short moving segment of the measured field versus time curve and hence to directly determine −1/[dln(*E*)/d*t*] as a function of time. This was quick and easy but vulnerable to noise and not applicable to rapid decays. The second was to fit a second order polynomial curve to the plot of ln(*E*) against time (sometimes separate polynomials were needed at the start and end of the decay) and use the fit coefficients to obtain dln(*E*)/d*t*. This was generally found to be the more useful approach.

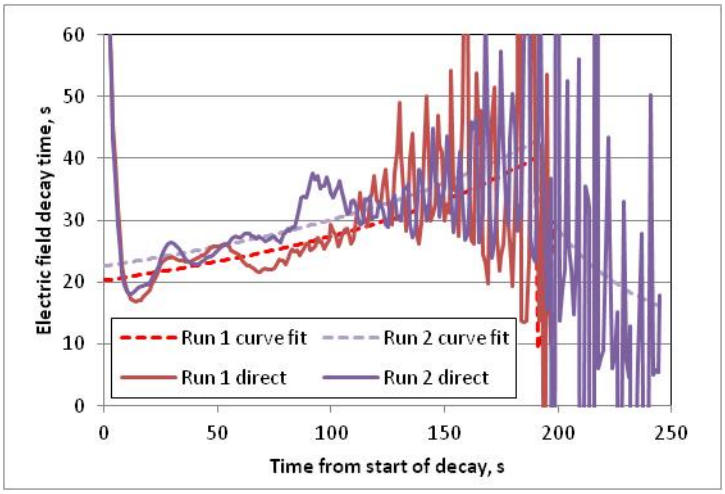

Figure B.4: Example of decay time measurements (TC01 A)

Figure B.4 shows example plots of decay time versus elapsed time from the end of fill obtained using both methods. It illustrates a common feature of the data: the initial delay of 5 s to 10 s between the end of flow and the commencement of the decay. This was nearly always observed. In the curve fit data we overcome this by fitting the curve from the end of the delay period onward and then extrapolating the fitted curve to the end-of-flow time.

The direct measurements commonly show the wavy features seen up to about 100 s in Figure B.4. It is speculated that these are caused by the movement of stratified layers of different charge density. If that is the case, extrapolation of the curve fits probably provides the best estimate of the average underlying decay time.

ANNEX C: CALIBRATION FOR METER PROTRUSION: CALCULATIONS AND TESTS

C.1 CALCULATIONS

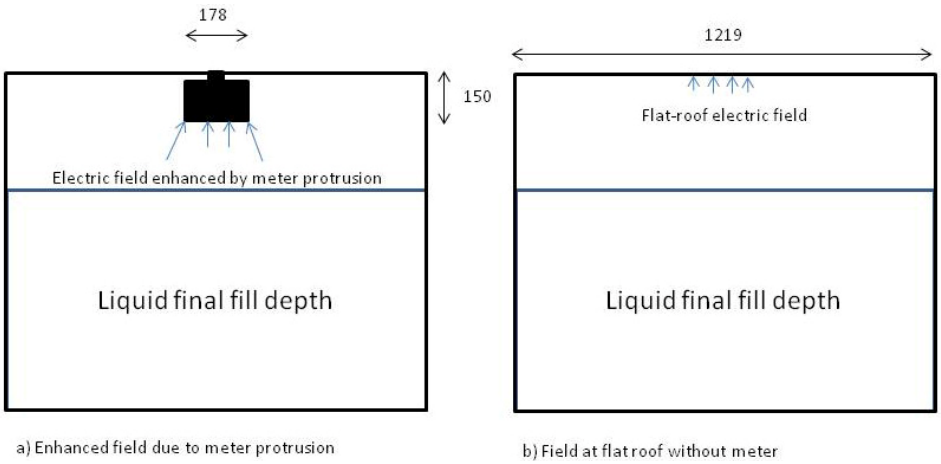

Figure C.1: Enhanced field due to meter protrusion

The protrusion of the meter from the tank roof raises the electric field at the meter sensing surface above that which would exist at a flat roof. Spreadsheet solutions for Laplace's equation with cylindrical symmetry are available using a relaxation method and we modified one of these [13] to solve a combination of Laplace's equation (vapour) and Poisson's equation (liquid). The overall dimensions were similar to the test tote geometry (1 m diameter, 1 m high) and comparisons of Asano solutions for cylindrical tanks [14] and Carruthers and Wigley solutions for rectangular tanks [15] have shown that for cubic and cylindrical tanks with the same height and cross-sectional area there is little difference in tank centre roof field. It is expected that the percentage distortion of roof fields by a protrusion, being essentially a local effect, would be insensitive to overall tank shape and so it was felt that the cylindrical solutions for an approximately equivalent geometry should give a reliable indication of the field enhancement.

The following modifications were needed to the original spreadsheet model to enable the calculations we required:

– Conversion to solving Poisson's equation in the liquid by adding a charge term into the relaxation expressions. This was set to zero in the vapour space and to the required charge density in the liquid.
– Alteration of the weightings in the uppermost layer of cells in the liquid to impose the normal-field boundary condition required by the liquid/vapour dielectric constant difference. The weighting of the potential of the lowest layer of vapour cells was changed from 1 to $2/(1 + \varepsilon_L)$ and that of potentials in the layer of liquid cells below the interface layer was changed from 1 to $2\varepsilon_L/(1 + \varepsilon_L)$.

Other changes were made for convenience. They included:

– Simplifying the outer boundary conditions. This was possible because we are dealing with the specific case of a system totally enclosed by an earthed conductor.

– Removing the calculation of information we do not need.
– Adding a means to set the liquid level and dielectric constant and to determine dimensional values for the electric fields and potentials.

With these modifications, the spreadsheet was set up on a 100 x 50 grid (making use of symmetry) to solve for the potentials and fields in a 1 m high 1 m diameter cylinder containing a variable depth of charged liquid (uniform charge was used but this is not essential). The earthed boundaries could be modified to make a meter-shaped protrusion at the centre of the tank roof. The fields at the meter surface with the protrusion and at the roof without the protrusion were then compared. The ratio was found to be 0,31. To this accuracy it was independent of fill depth.

C.2 CALIBRATION TESTS

An experimental check of the meter protrusion factor was made by mounting a meter a) flush with an earthed conductive surface and b) protruding below the surface as in the fill tests, then setting up a field by applying a voltage to a second conductive plate mounted below the meter assembly. The general layout is shown in Figure C.2.

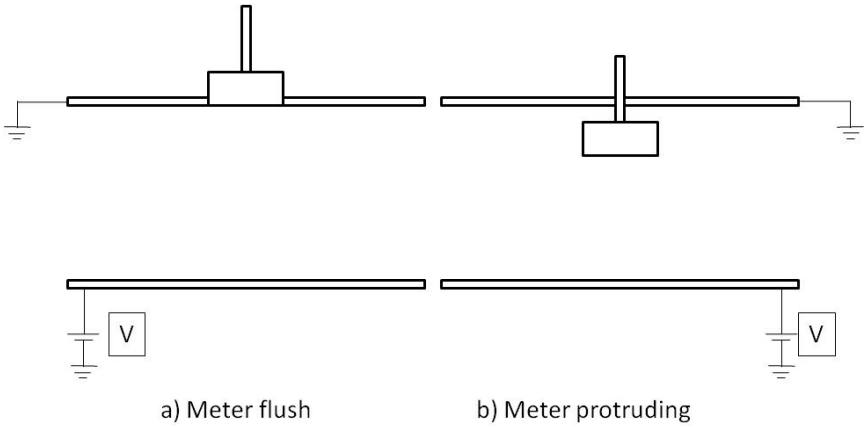

Figure C.2: Meter protrusion calibration test

In the actual tests we did not have a properly constructed calibration rig with those features. Instead a rough set up was jury-rigged with pieces of scrap metal that were lying around. With this set up, the bottom plate was rectangular and just over 1 m long and about 0,6 m across whilst the top plate, which was 0,57 m above the bottom plate, was made up of several separate rectangular sub plates supported on drums and fitting loosely round the meter with small gaps. The overall dimensions of this upper assembly were roughly 1 m square. When protruding, the rim of the meter shroud was 150 mm below the top plate (as in the test set up). The meter output with 100 V applied to the bottom plate was 180 mV when the meter was protruding and 65 mV when it was flush-mounted. This ratio is 0,36. Considering the rough and ready nature of the measured calibration set up, the agreement with the calculated factor is remarkably good. However, it is recommended that the calculated value should be used for interpreting the measurement data.

ANNEX D: FUEL PROPERTIES

Table D.1: Green diesel properties

Green diesel			
Method	**Test**	**Result**	**Units**
ASTM D5771	Cloud Point	–12	°C
ASTM D2709	Water and Sediment	<0,05	% Volume
ASTM D2624	Conductivity	0	pS/m
ASTM D4176	Appearance	Clear and Bright	
ASTM D4052	API gravity @ 60 °F	49,2	
ASTM D4052	Specific Gravity @ 60 °F	0,7823	
ASTM D93A	Flash Point	66	°C
ASTM D5453	Sulfur	<1	ppm (mg/kg)
ASTM D524	Ramsbottom Carbon	0,05	% Mass
ASTM D482	Ash	<0,001	% Mass
ASTM D445	Kinematic Viscosity @ 40 °C	3,0	mm^2/s
ASTM D130	Cu Corrosion (3 Hr @ 50 °C)	1a	
ASTM D86	Distillation Temperature, @ 90 %	301	°C
ASTM 4737 Pro. B	Cetane Index	83	

Table D.2: Jet A properties

Jet A			
Method	**Test**	**Result**	**Units**
ASTM D1176	Appearance	Clear and Bright	
ASTM D6045	Saybolt Color	25	
ASTM D3242	Acid Number	0,003	MgKOH/g
ASTM D6379	Mono-Aromatics	16,8	%(V/V)
	Di-Aromatics	1,9	%(V/V)
	Total Aromatics	18,7	%(V/V)
	Sulfur	0,0793	Wt %
	IBP	155,5	°C
	10 %	169,2	°C
	50 %	201,7	°C
	90 %	245,0	°C
	95 %	255,6	°C
	Final BP	270,3	°C

Table D.2: Jet A properties (continued)

Jet A			
Method	**Test**	**Result**	**Units**
	Residue	0,9	Vol %
	Corrected Loss	0,6	Vol %
	Corrected Recovery	95,8	Vol %
ASTM D93	Procedure Used	A	
	Corrected Flash Point	46,7	°C
ASTM D2386	Freezing Point	–44,0	°C
ASTM D445	Kin. Viscosity @ –4 °F	4,307	mm^2/s
ASTM D611	Method	B in F	
	Aniline Point	60,0	°C
ASTM 4529	Net Heat of Combustion	43,3	MJ/kg
ASTM D1322	Smoke Point (Manual)	29,0	mm
ASTM D1840	Naphthalenes	1,7	Mass %
	Naphthalenes	1,4	Vol %
ASTM D130	Cu Corrosion @ 212 °F	1a	
ASTM D3241	Temperature	260	°C
	Deposit Color	1,0	
	Max. Pressure Drop	0,0	mm Hg
	Spent Fuel Volume	450	ml
ASTM D381	Existent Gum	<1	mg/100ml
ASTM D1094	Change in Aq Layer	0,0	
	Interface	1	
	Degree of Separation	1	
ASTM D3942	MSEP Test A	98	
ASTM D4052	API Gravity @ 60 °F	44,5	°API
ASTM D2624	Temperature	70	°F
	Conductivity	0	

ANNEX E: FUEL HANDLING AND RIG PREPARATION PROCEDURES

E.1 RUNNING A TEST

The following test sequence was adopted:

- Set the required flow rate. This was usually done by adjusting a throttling valve located just downstream of the filter vessel between the vessel outlet and Insulating Flange 2, i.e. within the isolated filter section, but for the lowest flow rates required in Phase 2 it was necessary to use an additional throttling valve located just downstream of the pump (i.e. upstream of Insulating Flange 1).
- Return most of the fuel to the source tote, leaving 50 USG in the receiving tote as it was time-consuming to completely empty it[19].
- Start the pump and initiate logging. Open the stop/start valves after a short delay to log baseline data.
- After about 120 s manually close the start/stop valves and switch off the pump but continue logging data to capture the electric field decay.
- Stop logging once the field has decayed (this took several hundred seconds at the lowest conductivities).
- Return the fuel to the source tote, leaving 50 USG in the tank unless the fuel condition is to be changed.
- Save the logged data.

E.2 ADDITISATION

First the additive concentration increment required has to be determined. The pro-static agent was always added at a fixed concentration (5 g/m^3) that was expected to enhance charging whilst keeping the conductivity in the range where hazards would be expected (<~5 pS/m). For SDA, a conductivity response curve was measured for each fuel. From this and the existing conductivity the additional concentration needed to generate the next target conductivity was found.

The volume of fuel in the rig was known, hence the total weight of additive to be added was determined from the required concentration increment.

To facilitate accurate additisation and promote good mixing of the additive doses, an intermediate stock solution was made by mixing the total amount of additive for the addition step into 1 litre of test fuel. This stock solution was added gradually into the source tote whilst fuel was being circulated.

E.3 CLAY FILTRATION AND RIG CLEANING

Clay filtration and rig cleaning was done by circulating the fuel through the clay filter unit and the main part of the rig, then back to the source tote. Some fuel was then transferred to the test tote and the process was repeated with circulation through this.

19 A few tests were done with a completely empty receiving tote for comparison.

E.4 FLUSH (ADD FLUSHING FLUID TO RIG, CLEAN FLUID AND RIG, REMOVE FLUSHING FLUID)

1. Ensure both test totes are empty and filter vessel contains no elements. Activate system power. Set flow meter to read USG/minute.
2. Fill sending tote with minimum 200 USG of flush fuel.
3. Open valve 4.
4. Activate pump.
5. Direct flow through clay filter.
6. Continue recirculation for 30 minutes.
7. Shut off pump.
8. Flow 160 USG of fuel into receiving tote to clean tank base, pipes and hoses.
9. Activate pump and recirculate through clay filter for 30 minutes.
10. Close all valves and drain totes and filters.

E.5 CLAY TREAT/CLEAN (CLEAN UP RIG AND FUEL ALREADY IN RIG, FUEL TO BE RETAINED IN RIG)

1. Drain filter vessel and remove elements.
2. Ensure receiving tote is completely drained so all liquid is in sending tote.
3. Open valve 4.
4. Activate pump.
5. Direct flow through clay filter.
6. Continue recirculation for 30 minutes.
7. Shut off pump.
8. Flow 100 USG of fuel into receiving tote.
9. Activate pump and recirculate through the clay filter for 30 minutes.
10. Return all fuel to the sending tote.
11. Carry out a complete receiving tote fill followed by a conductivity check prior to testing.

E.6 ADD ADDITIVE

1. Drain filter vessel and remove elements.
2. Ensure receiving tote is completely drained so all liquid is in sending tote.
3. Open valve 4.
4. Activate pump.
5. Pour additive stock solution gradually into the sending tote.
6. Continue recirculation for 30 minutes.
7. Shut off pump.
8. Flow 100 USG of fuel into receiving tote.
9. Activate pump and recirculate through receiving tote for 30 minutes.
10. Close all valves and return all fuel to sending tote.

E.7 ADD WATER

1. With all fuel in sending tote begin recirculation.
2. Inject deionised water through water injection port using 60 ml syringe.

3. After each 60 ml injection, allow minimum 50 USG circulation and check differential pressure.
4. Once pressure differential reaches 8 psi, begin adding 30 ml per addition.
5. Discontinue addition when pressure differential reaches 10 psi. Continue flow for 150 USG, then commence testing.

E.8 CHANGE/INSERT ELEMENT

1. Close valves to isolate filter vessel.
2. Drain fuel from vessel.
3. Open vessel, extract any old elements that are present.
4. Remove new element from plastic sheeting and insert immediately.
5. Close vessel.
6. Close drain valves and refill filter vessel. Start pump and recirculate 300 USG through sending tote to bleed air and prime filters.
7. Open valves ready for next test flow.

Drained fluid is added back into the sending tote. Minimal fluid (~0,5 USG each set) is lost in the filter monitors themselves.

E.9 STANDARD TEST RUN

1. With a minimum of 230 USG fuel in sending tote and 50 USG fuel in receiving tote.
2. Simultaneously open valves 4 and 13 while activating pump.
3. Flow 180 ± 1 USG into the receiving tote.
4. Simultaneously close valves 4 and 13 while deactivating pump.
5. Monitor field meter until field has dissipated.
6. Fuel return.

E.10 EMPTY TOTE TEST RUN

1. With minimum 280 USG of fuel to be tested in sending tote.
2. Simultaneously open valves 4 and 13 while activating pump.
3. Flow 230 ± 1 USG into receiving tote.
4. Simultaneously close valves 4 and 13 while deactivating pump.
5. Monitor field meter until field has dissipated.
6. Fuel Return.

E.11 FUEL RETURN

1. After a run there is about 230 USG in receiving tote. The amount is known from the test flow data.
2. Open valve 4 and activate pump.
3. Return the volume required to leave 50 USG in receiving tote.
4. Shut off pump, close valves 4 and 14.

ANNEX F: EFFECTIVE CURRENT CALCULATIONS

F.1 ANALYTICAL INTEGRAL SOLUTIONS FOR IN-TANK CHARGE

I assume the charge in a tank is governed by (assumes charge transport only by conduction):

$$\frac{dq}{dt} = I(t) - \frac{q}{\tau(t)} \tag{F.1}$$

If we start from a time when there is no charge in the tank, the charge at a time t can be written:

$$q(t) = \tau_0 \int_0^{t/\tau_0} I(x\tau_0) \exp\left[-\int_x^{t/\tau_0} \frac{du}{\tau'(u\tau_0)} \right] dx \tag{F.2}$$

where u and x are dimensionless dummy time variables based on dividing real times by the initial relaxation time, τ_0, and corresponding to real dummy times $t' = x\tau_0$ and $t'' = u\tau_0$. Hence $I(x\tau_0)$ is the current at a time $t' = x\tau_0$ and $\tau'(u\tau_0) = \tau(t'')/\tau_0$ where $\tau(t'')$ is the observed relaxation time at a real time t''. This expression can be applied to the data as it stands because the experimental results give us I and τ'. However it is instructive to simplify. During the fill period we assume that $\tau = \tau_0$ and hence $\tau' = 1$. If the fill ends at time, T, we thus have for $t \geq T$:

$$q(t) = \tau_0 \int_0^{t/\tau_0} I(x\tau_0) \exp\left[-(t/\tau_0 - x) \right] dx = \tau_0 \exp\left[-(t/\tau_0) \right] \int_0^{t/\tau_0} I(x\tau_0) \exp(x)\, dx \tag{F.3}$$

This expression was evaluated numerically to obtain the in-flow charge[20] and hence the effective current using $I_{eff} = q/[\tau_0(1 - \exp(-t/\tau_0))]$. At the end of flow ($t = T$) we have:

$$q(T) = \exp\left[-(T/\tau_0) \right] \int_0^{T/\tau_0} I(x\tau_0) \exp[x]\, dx \tag{F.4}$$

For a time t greater than T the upper limit of the inner integral in equation (F.2) is t but the upper limit of the outer integral is fixed effectively at T because the current is zero for $t > T$. Thus for times after the flow period the only change to the outer integral is in the exponential relaxation term. To clarify this we look at the value of the outer integrand in equation (F.2) at a dimensionless dummy time x. For an integral extending just to the end of flow this value is:

$$I(x\tau_0) \exp\left[-\int_x^{T/\tau_0} \frac{du}{\tau'(u\tau_0)} \right] \tag{F.5}$$

For an integral extending to a time, t, which occurs after the flow it is:

$$I(x\tau_0) \exp\left[-\int_x^{t/\tau_0} \frac{du}{\tau'(u\tau_0)} \right] = I(x\tau_0) \exp\left[-\left\{ \int_x^{T/\tau_0} \frac{du}{\tau'(u\tau_0)} + \int_{T/\tau_0}^{t/\tau_0} \frac{du}{\tau'(u\tau_0)} \right\} \right] \tag{F.6}$$

20 These calculations were actually continued beyond the end of flow but have no real validity here as the decay time was then variable.

Thus the contribution of the current at time $x\tau_0$ to the remaining charge at time, t, is a factor $\exp\left[-\int_{T/\tau_0}^{t/\tau_0} \frac{du}{\tau'(u\tau_0)}\right]$ lower than its contribution to the charge at the time T (end of fill). This factor is independent of the current time, $x\tau_0$, hence when the integral extends to a time, t, that is beyond the end of flow time, T, the charge is given by:

$$q(t) = q(T)\exp\left[-\int_{T/\tau_0}^{t/\tau_0} \frac{du}{\tau'(u\tau_0)}\right] \qquad (F.7)$$

Equation (F.7) shows how to include the influence of variable decay time as was found experimentally after the end of the flow period. With a fixed time scale it reduces to an exponential decay (as it must). In fact, equation (F.7) has not been used in the analysis because the finite difference procedure described in Figure 4 was set up first.

F.2 EFFECTIVE CURRENT CALCULATIONS

From equation (F.3) the effective current can be written as:

$$I_{eff}(t) = \int_0^{t/\tau_0} I(x\tau_0)\exp(x)dx \Big/ \left[\exp(t/\tau_0) - 1\right] \qquad (F.8)$$

To evaluate this directly by trapezium rule integration we used the expression:

$$I_{eff,\,n+1} = \frac{I_{eff,\,n}\left[\exp(t_n/\tau_0) - 1\right] + 0{,}5\left[I_n \exp(t_n/\tau_0) + I_{n+1}\exp(t_{n+1}/\tau_0)\right]\delta t/\tau_0}{\left[\exp(t_{n+1}/\tau_0) - 1\right]} \qquad (F.9)$$

starting with $I_0 = 0$. Equations (F.8) and (F.9) apply during the fill. After the fill period we have:

$$I_{eff}(t) = I_{eff}(T)\exp\left[-\int_{T/\tau_0}^{t/\tau_0} \frac{du}{\tau'(u\tau_0)}\right] \qquad (F.10)$$

F.3 CORRECTIONS TO TRAPEZIUM RULE

Because of the exponential term in the integrand, the trapezium rule approximation sometimes gave large enough errors to give misleading results. The errors were never more than about 5 % but, for example, could sometimes lead to effective currents that were greater than the maximum of the current values from which they were derived. This is not a possible result as the effective current is just a weighted average and therefore cannot exceed the maximum raw current. Consequently, a correction was applied. It would probably have been better to integrate with Simpson's rule but applying the correction was easier.

The trapezium rule approximates the mean value of the integrand over an interval by the mean of the end values. As the currents are approximately equal this is approximately $\bar{I}\exp(t_n/\tau_0)\left[\exp(\delta t/\tau_0) + 1\right]/2$. Integrating the exponential term over the interval shows

that the actual mean value would be $\bar{I}\exp(t_n/\tau_0)\left[\exp(\delta t/\tau_0)-1\right]/(\delta t/\tau_0)$. Thus, with slowly varying current (generally observed except at the start and after the finish) a correction factor of $\dfrac{2\left[\exp(\delta t/\tau_0)-1\right]}{(\delta t/\tau_0)\left[\exp(\delta t/\tau_0)+1\right]}$ should be applied. This was found to eliminate the anomalies.

In lower conductivity cases (κ < 5 pS/m, τ_0 > 4 s) the correction factor is very close to 1 and was found to be unimportant but around the upper limit conductivity for decay time measurements (15 pS/m to 20 pS/m, τ_0 < 3 s) it was found to be useful.

F.4 FINITE DIFFERENCE SOLUTIONS

Instead of using the analytical integral solutions to equation (F.1), an alternative is to use a finite difference approach to integrate it directly. In setting this up it seemed best to average the rate of change rather than the time constant for charge decay. This gives:

$$\frac{q_{n+1}-q_n}{\delta t}=\frac{I_{n+1}+I_n}{2}-\frac{(q_{n+1}+q_n)}{2}\frac{(1/\tau_{n+1}+1/\tau_n)}{2} \tag{F.11}$$

Rearranging this expression to obtain q_{n+1} in terms of earlier values gives:

$$q_{n+1}=\left[\frac{(I_{n+1}+I_n)}{2}+q_n\left\{1-\frac{(\tau_{n+1}+\tau_n)\delta t}{4\tau_{n+1}\tau_n}\right\}\right]\Bigg/\left\{1+\frac{(\tau_{n+1}+\tau_n)\delta t}{4\tau_{n+1}\tau_n}\right\} \tag{F.12}$$

Where this was used the effective currents were then calculated as $I_{eff,\,n}=q_n/[\tau(1-\exp(-t_n/\tau_0)]$. These results have no validity outside the flow period although the charge data are valid to the extent that the model is applicable. In a couple of cases the I_{eff} obtained in this way from equation (F.12) during the flow time was compared with the analytical integrals evaluated using equation (F.9) with good agreement. After the flow time, the charge decays produced by the method were compared to the electric field decays used to determine the decay times after normalising both with the experimental end of flow values. Again agreement was good.

F.5 POSSIBLE ALTERNATIVES

Arguably it may have been better to use $\dfrac{q_{n+1}/\tau_{n+1}+q_n/\tau_n}{2}$ for the decay and Simpson's rule for the analytical integrations but these alternatives were not tried as relatively approximate solutions were considered good enough and seemed to work adequately after some corrections to the trapezium rule for the cases where the decay times were of the same order as the 1 s intervals between data points (conductivities 5 pS/m to 20 pS/m).

ANNEX G: STREAMING CURRENT VS TIME PLOTS

This Annex gives all the Phase 1 individual corrected streaming current vs time plots.

Table G.1: Streaming currents in main Phase 1 test sequence

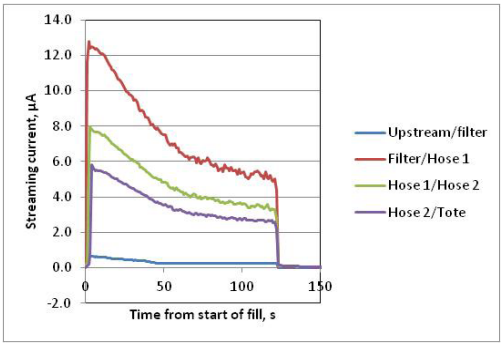

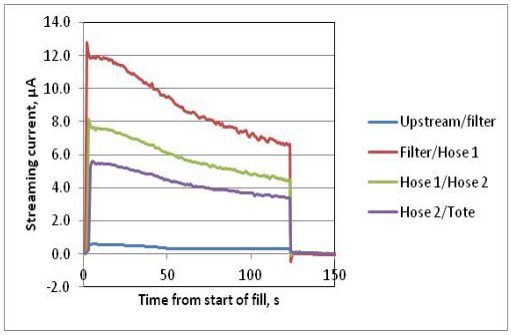

TC01 A

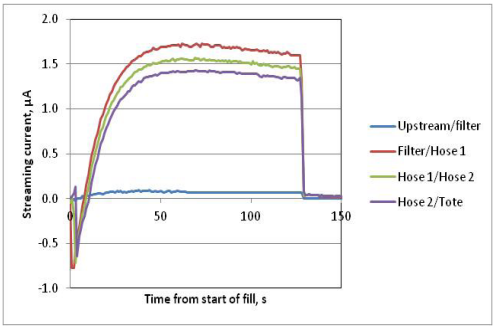

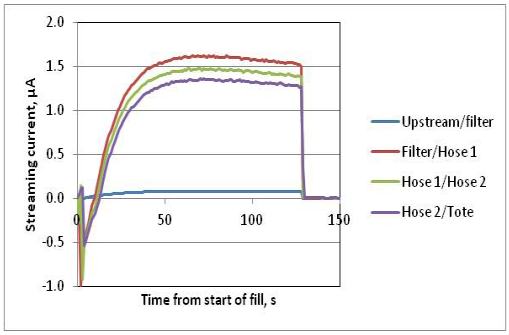

TC01 B

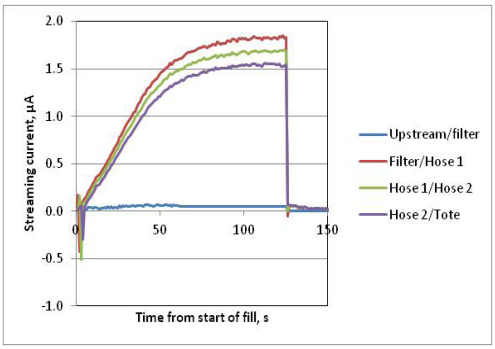

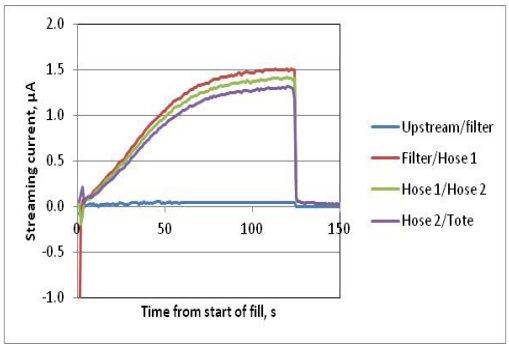

TC01 C

Table G.1: Streaming currents in main Phase 1 test sequence (continued)

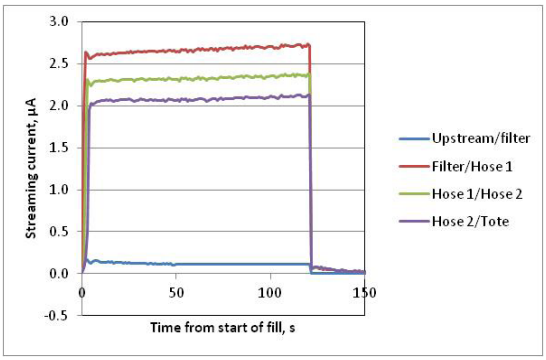

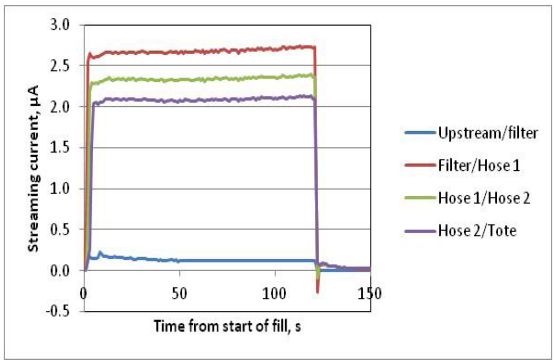

TC02 A

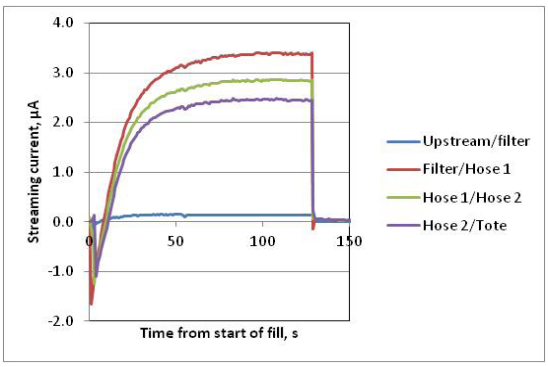

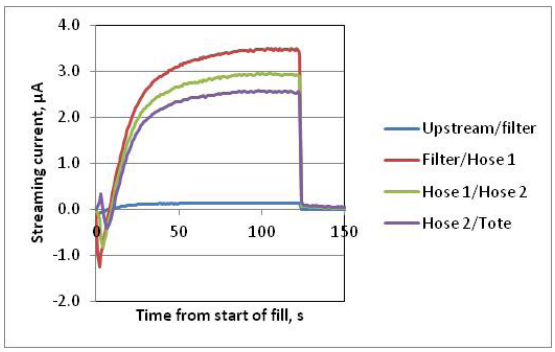

TC02 B

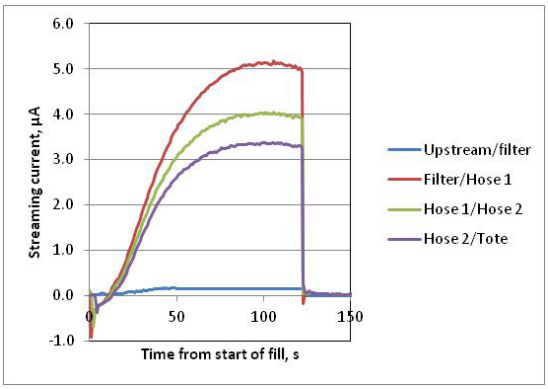

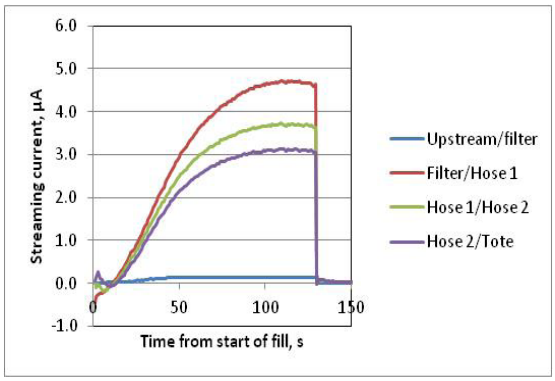

TC02 C

Table G.1: Streaming currents in main Phase 1 test sequence (continued)

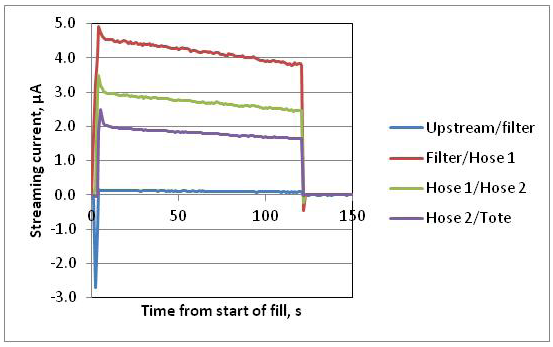

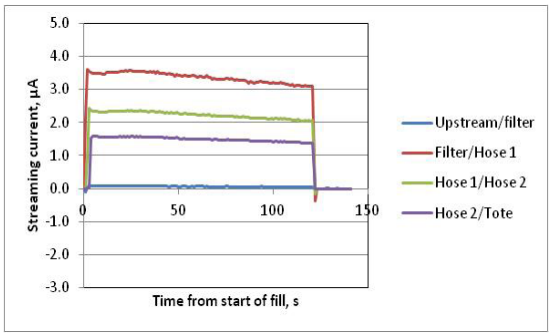

TC03 A

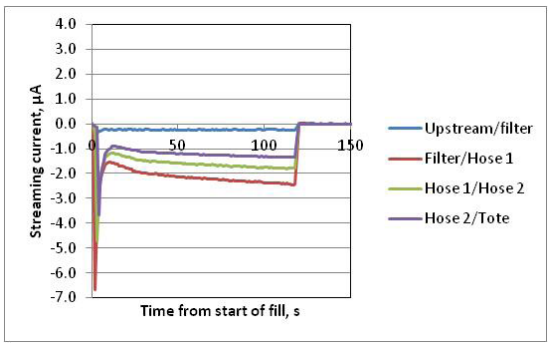

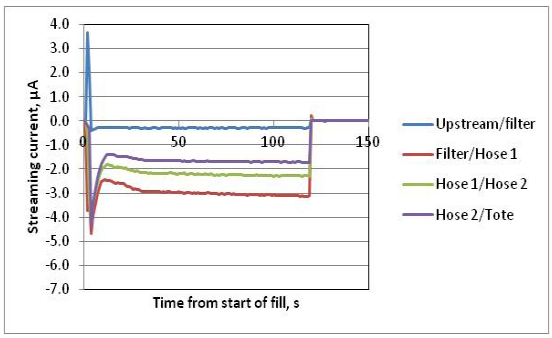

TC03 B

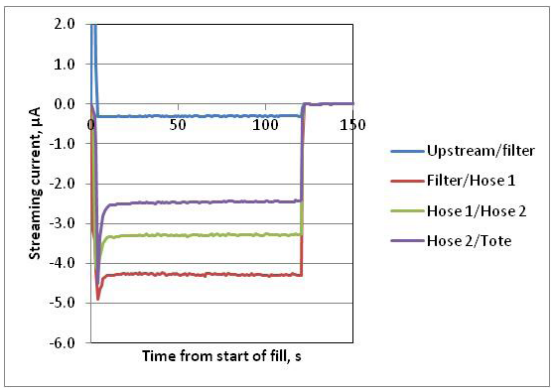

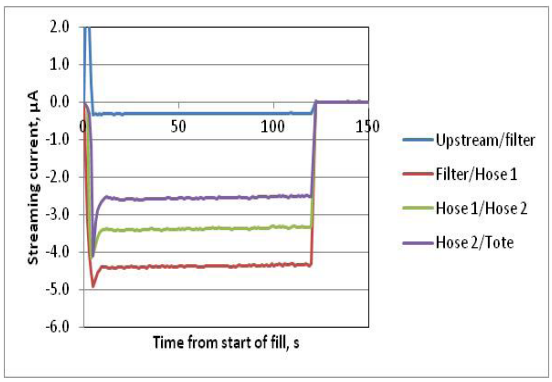

TC03 C

Table G.1: Streaming currents in main Phase 1 test sequence (continued)

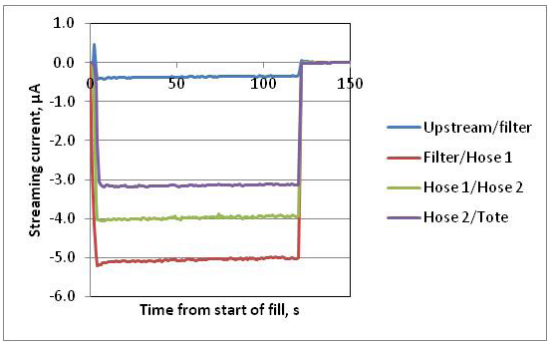

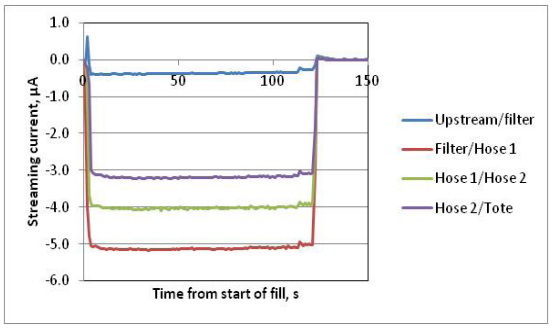

TC04 A

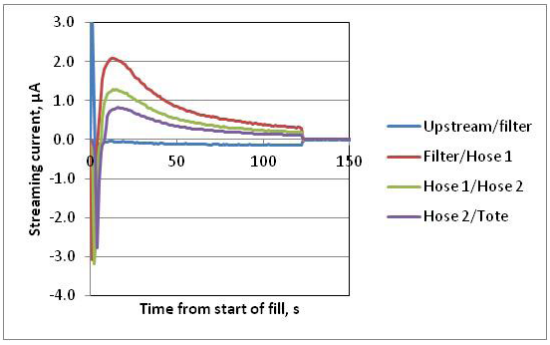

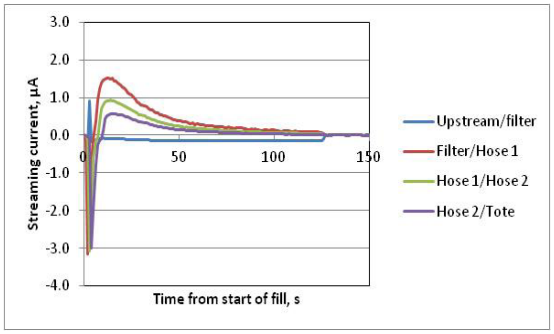

TC04 B

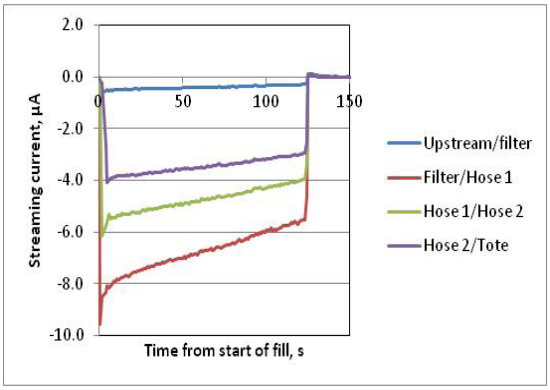

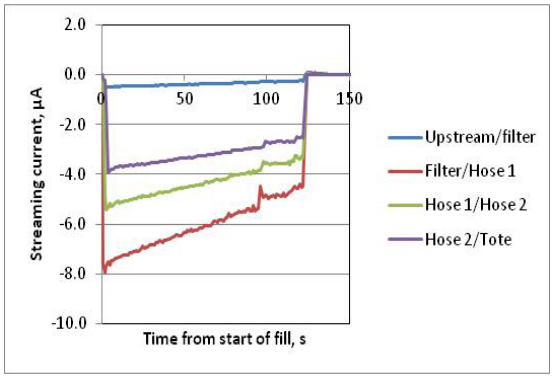

TC04 C

Table G.1: Streaming currents in main Phase 1 test sequence (continued)

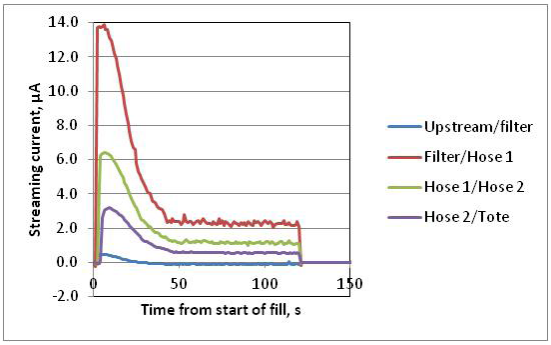

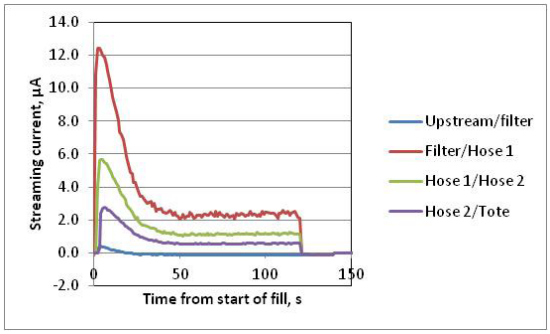

TC05 A

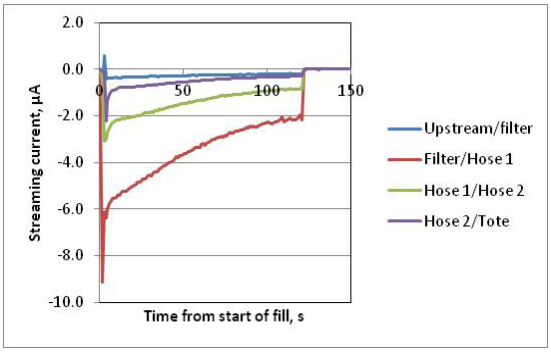

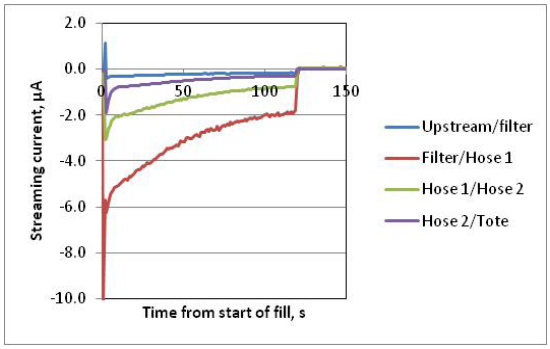

TC05 B

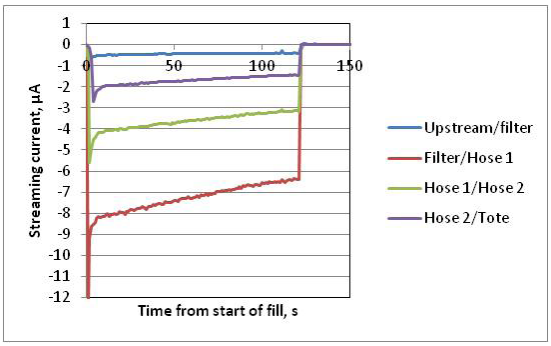

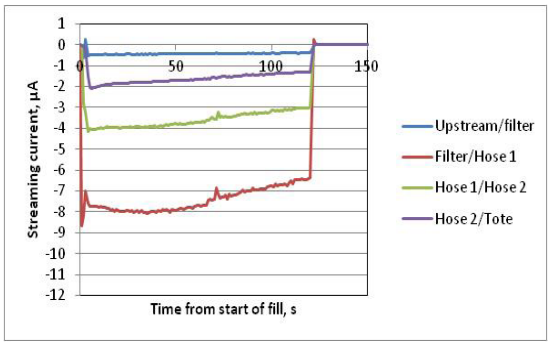

TC05 C

Table G.1: Streaming currents in main Phase 1 test sequence (continued)

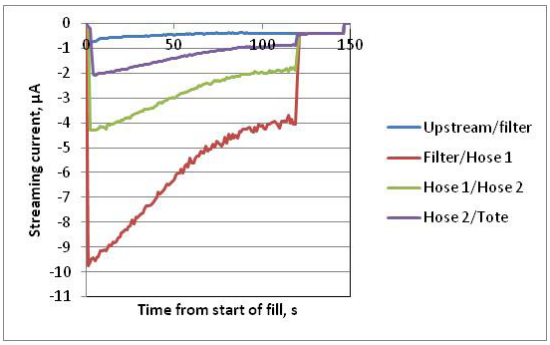

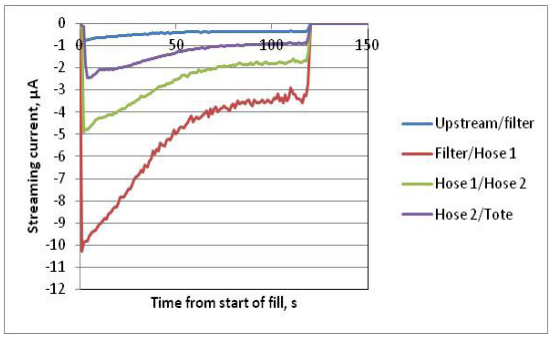

TC06 A

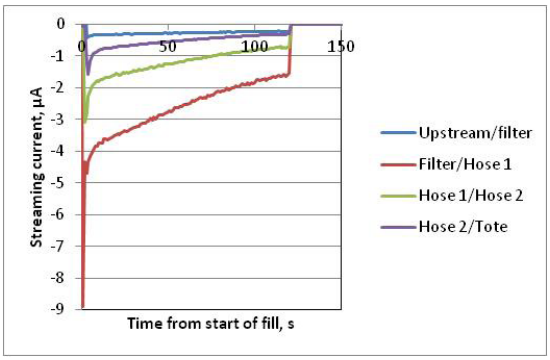

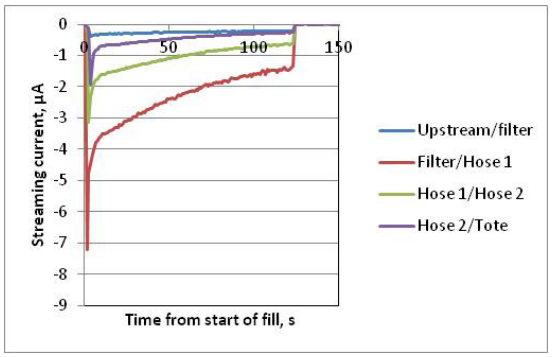

TC06 B

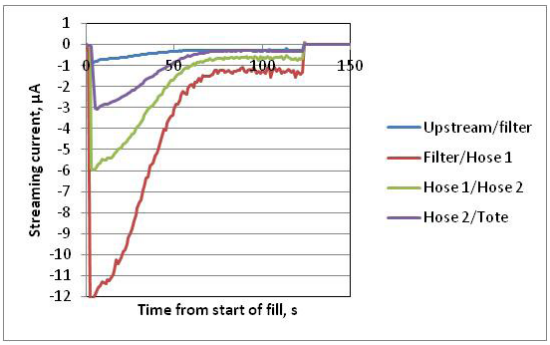

TC06 C

Table G.1: Streaming currents in main Phase 1 test sequence (continued)

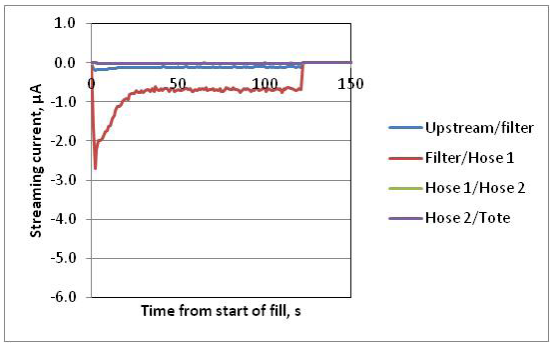

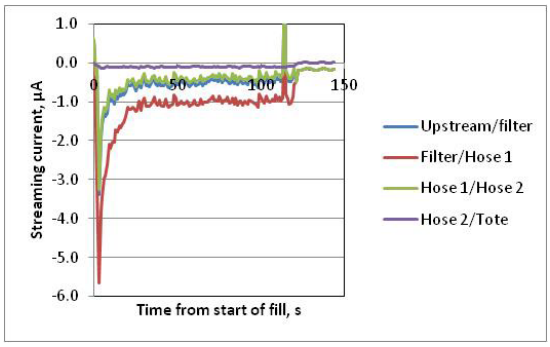

TC07 A

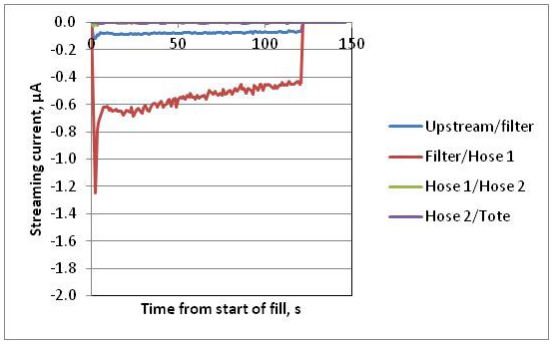

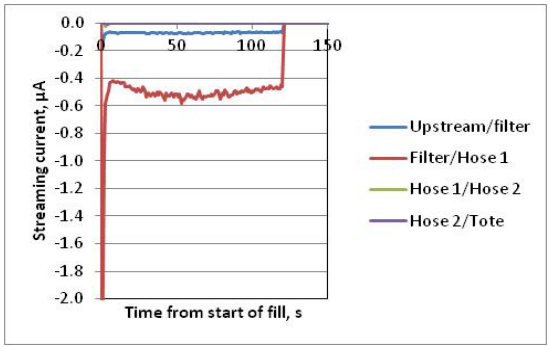

TC07 B

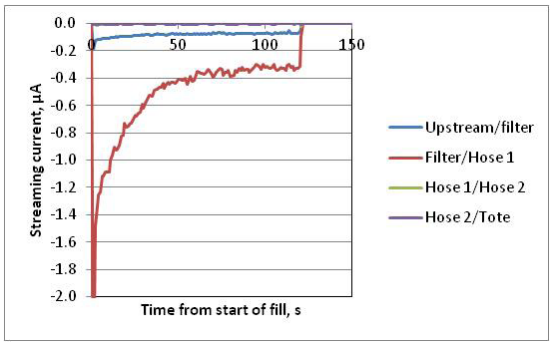

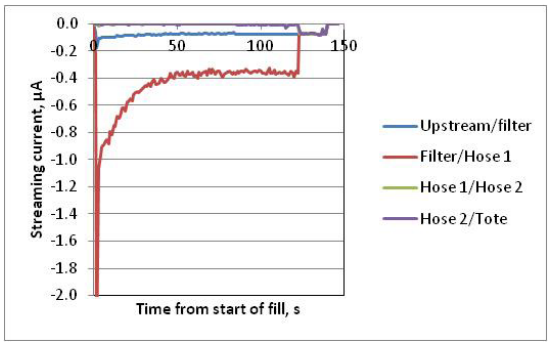

TC07 C

Table G.1: Streaming currents in main Phase 1 test sequence (continued)

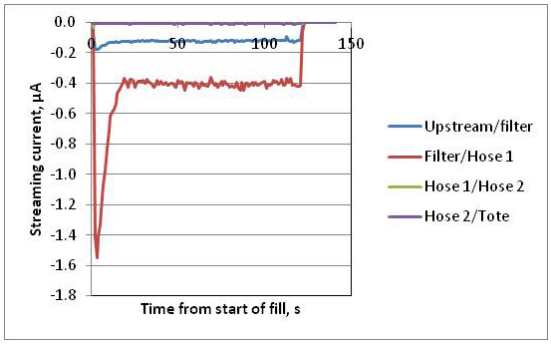

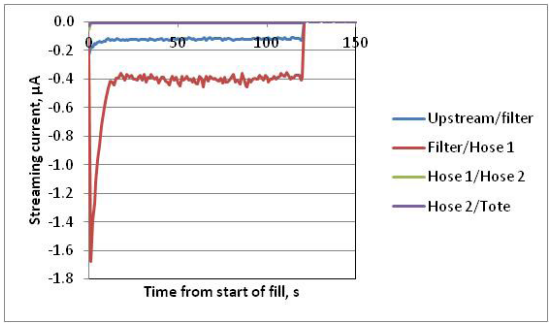

TC08 A

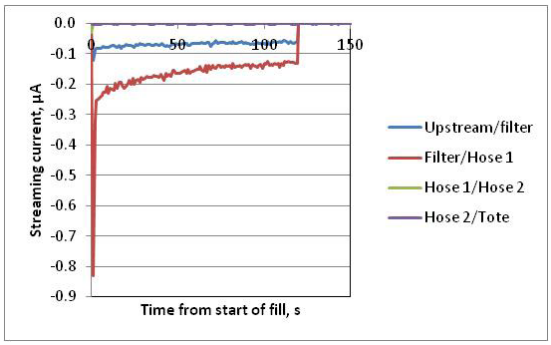

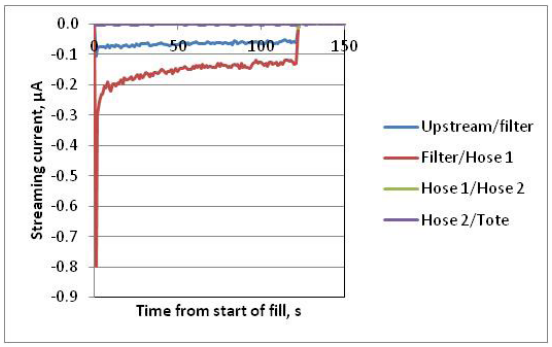

TC08 B

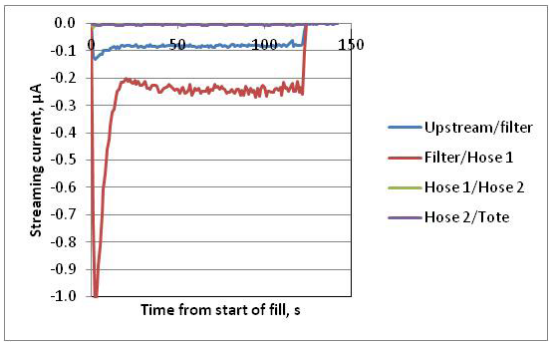

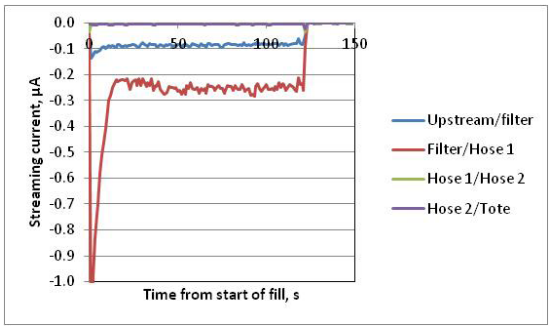

TC08 C

Table G.1: Streaming currents in main Phase 1 test sequence (continued)

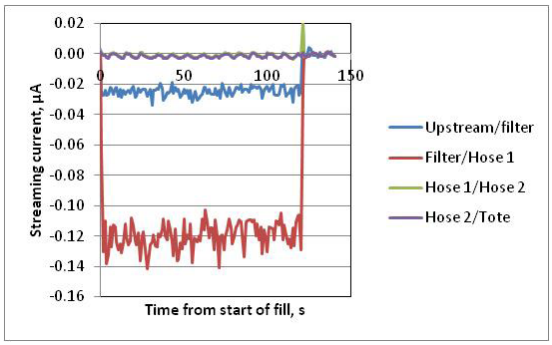

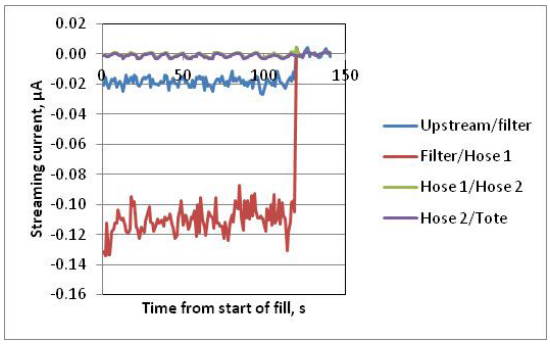

TC09 A

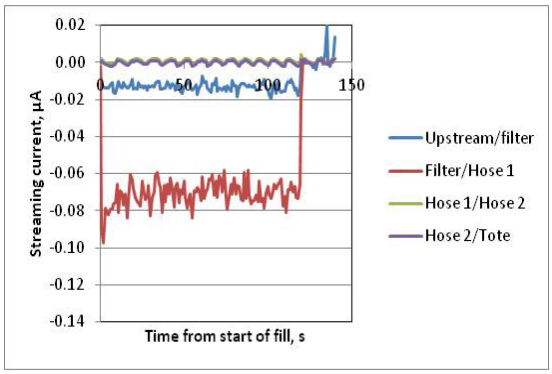

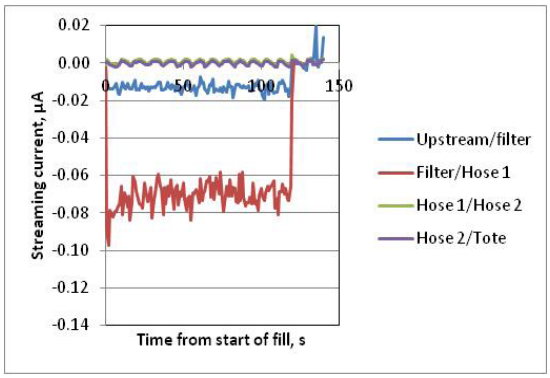

TC09 B

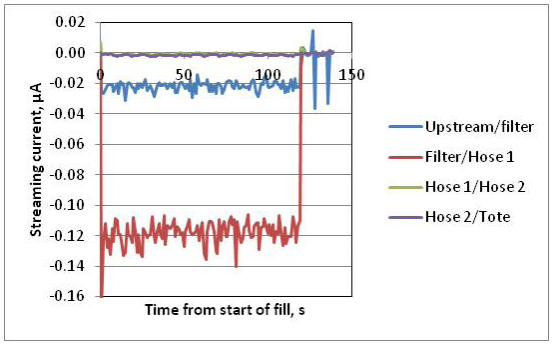

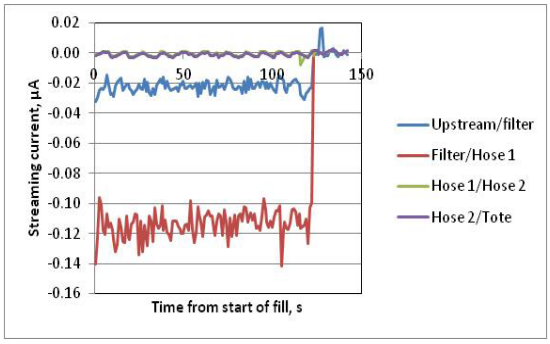

TC09 C

Table G.1: Streaming currents in main Phase 1 test sequence (continued)

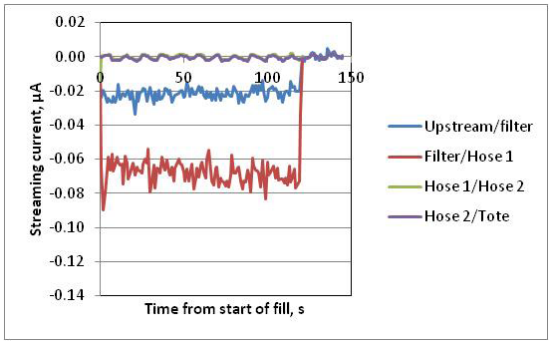

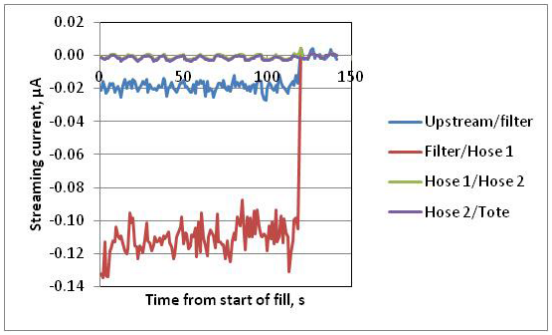

TC10 A

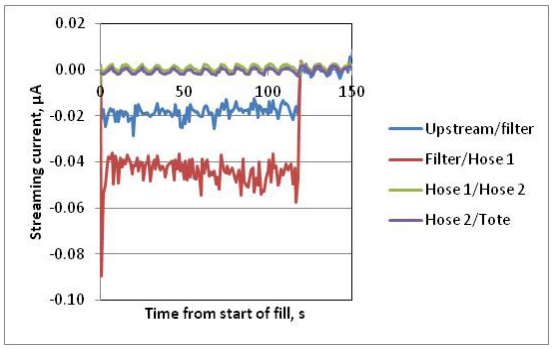

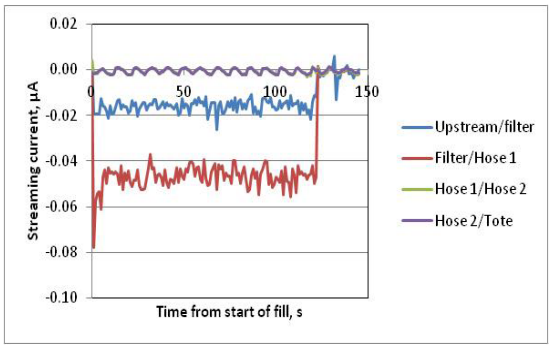

TC10 B

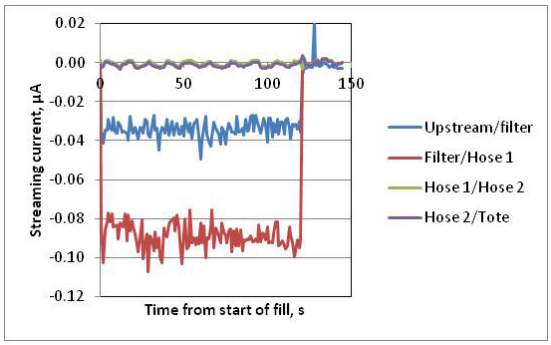

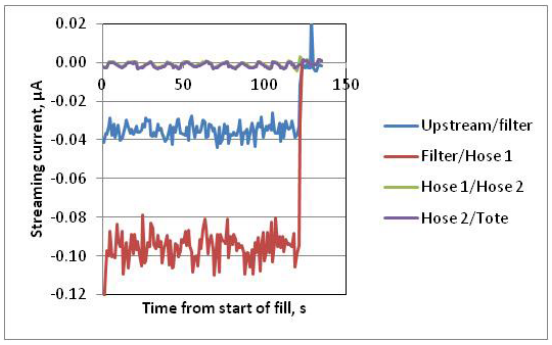

TC10 C

Table G.1: Streaming currents in main Phase 1 test sequence (continued)

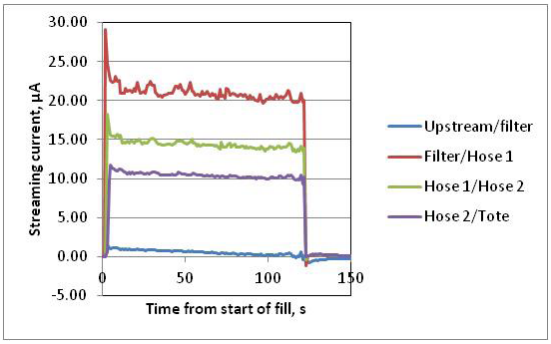

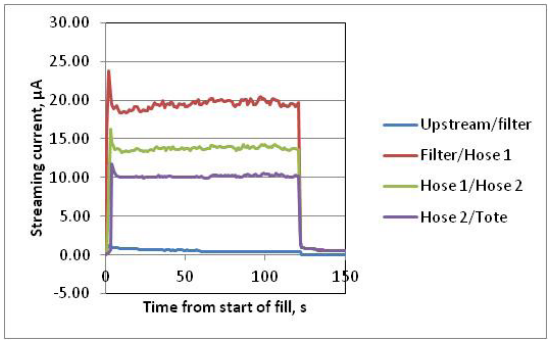

TC11 A

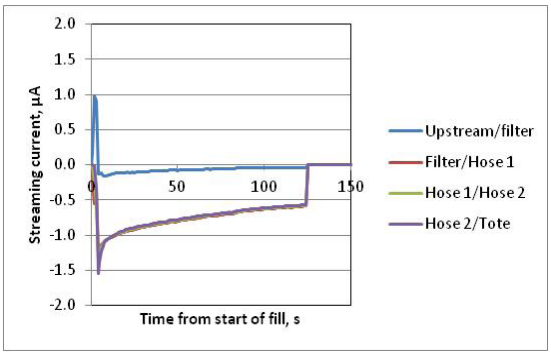

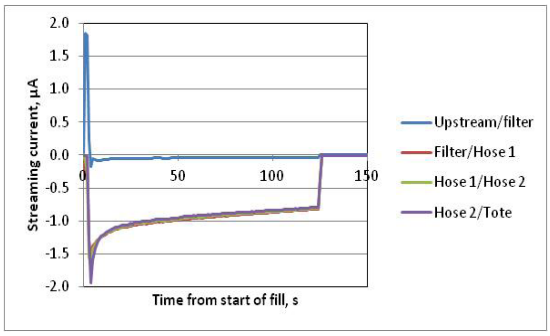

TC11 B

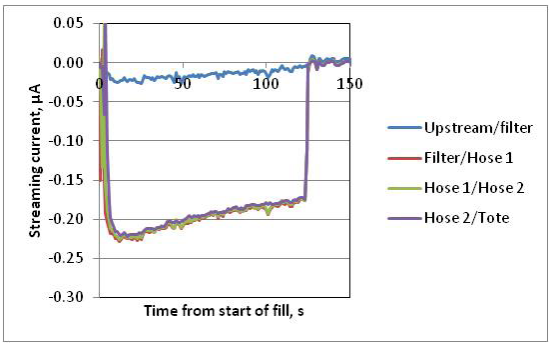

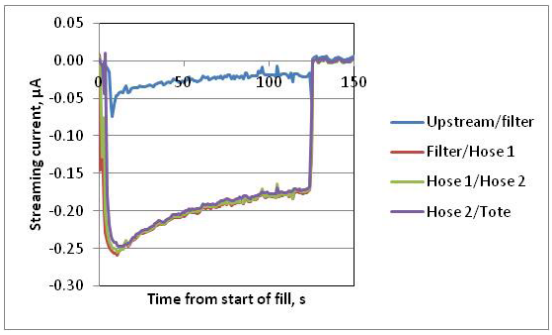

TC11 C

Table G.1: Streaming currents in main Phase 1 test sequence (continued)

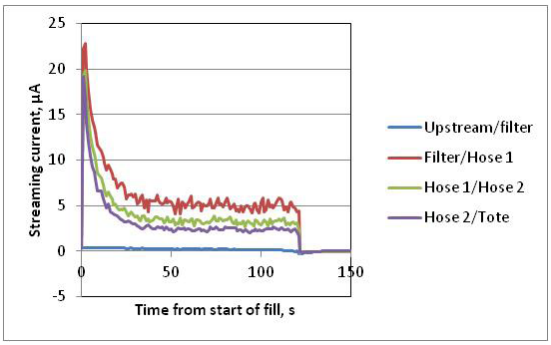

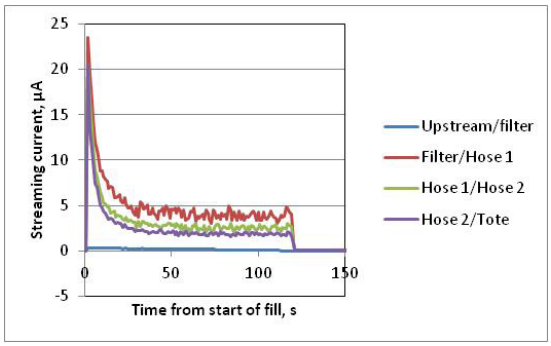

TC12 A

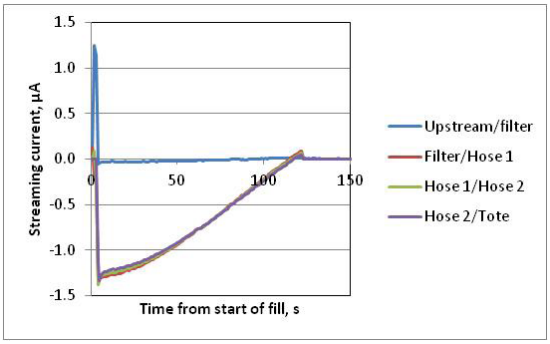

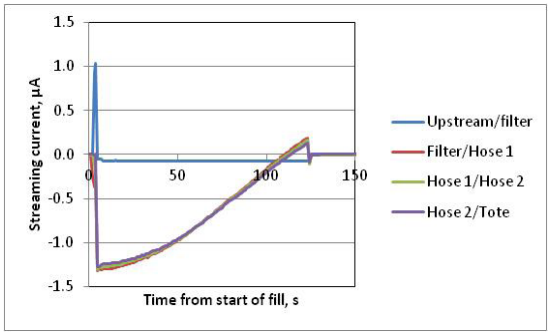

TC12 B

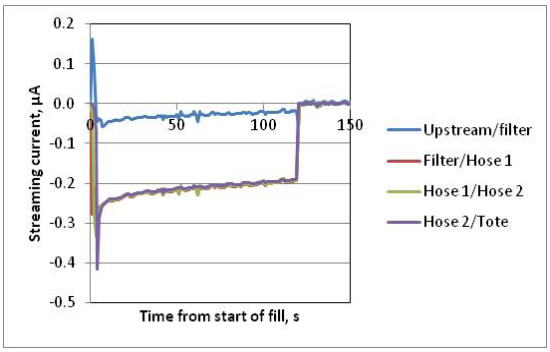

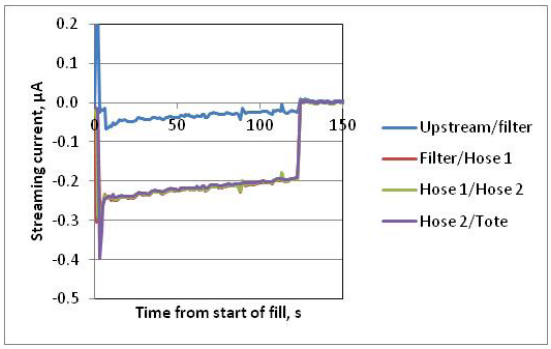

TC12 C

Table G.1: Streaming currents in main Phase 1 test sequence (continued)

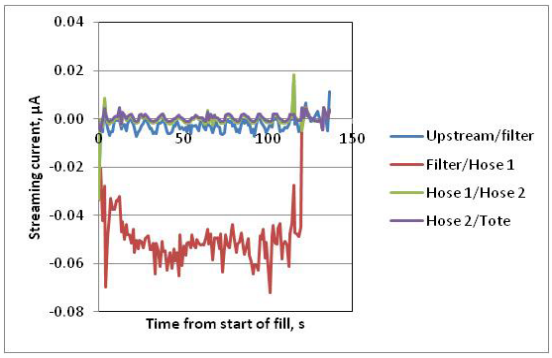

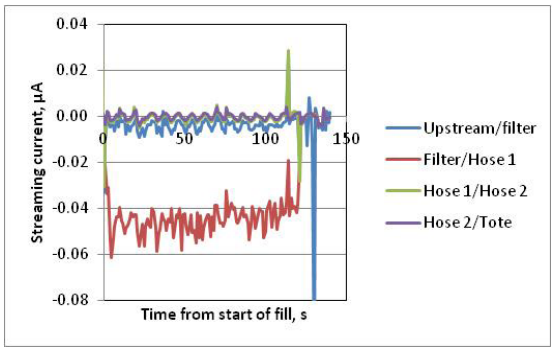

TC13 A

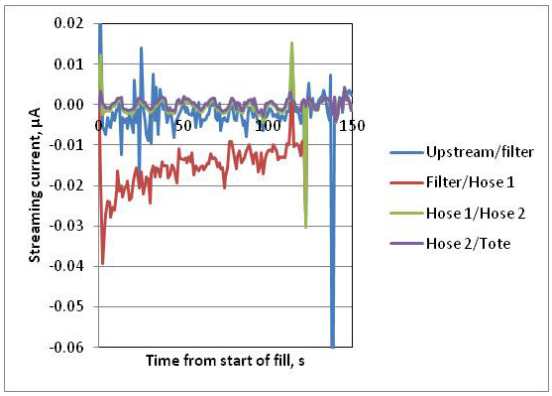

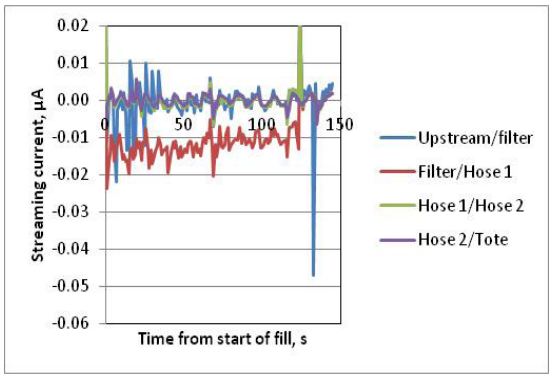

TC13 B

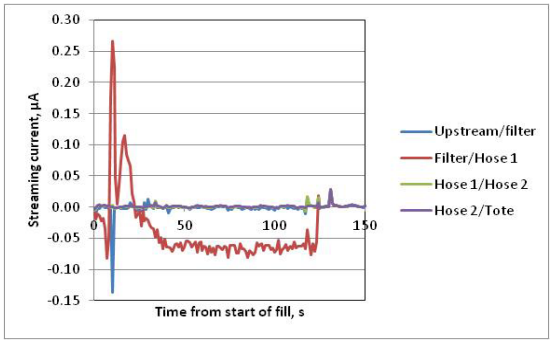

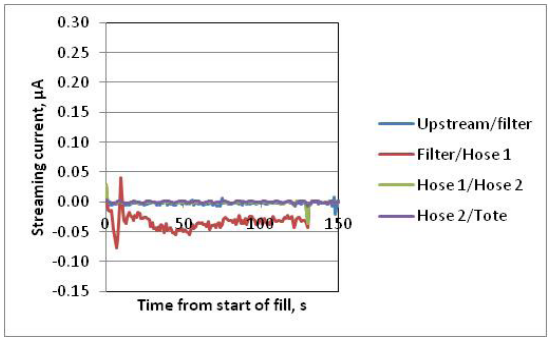

TC13 C

Table G.1: Streaming currents in main Phase 1 test sequence (continued)

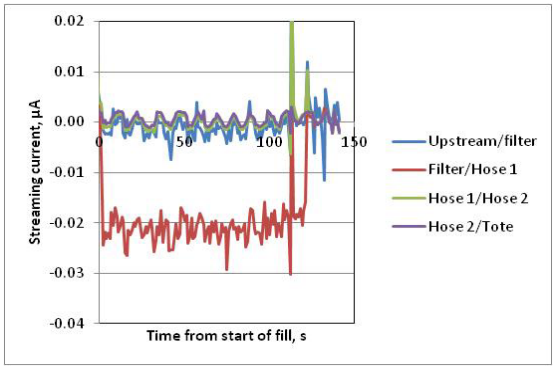

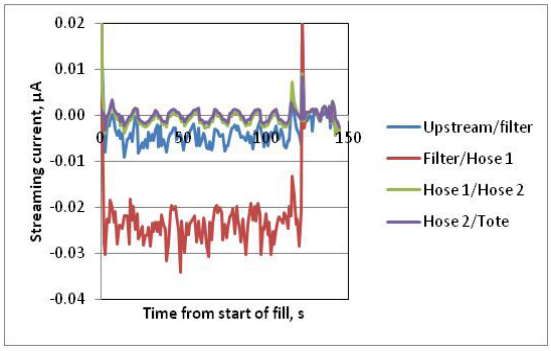

TC14 A

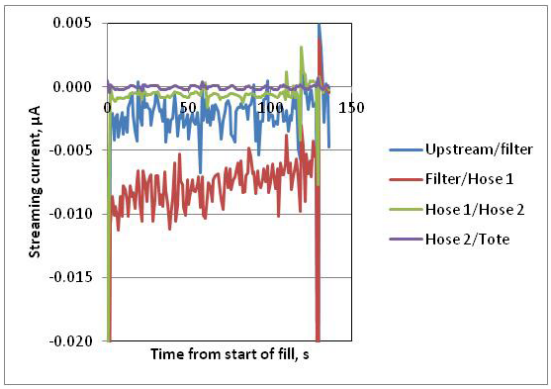

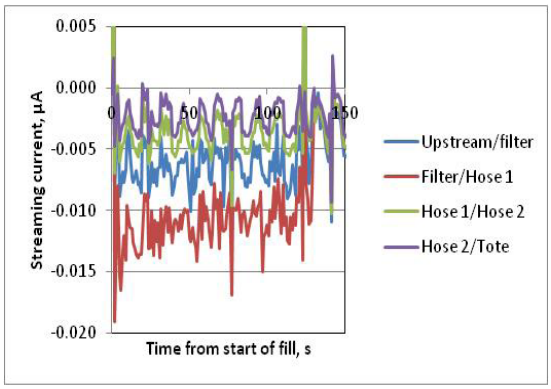

TC14 B

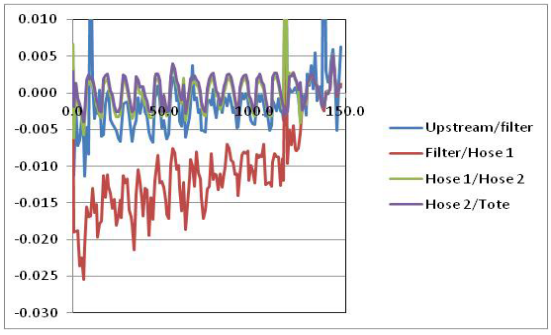

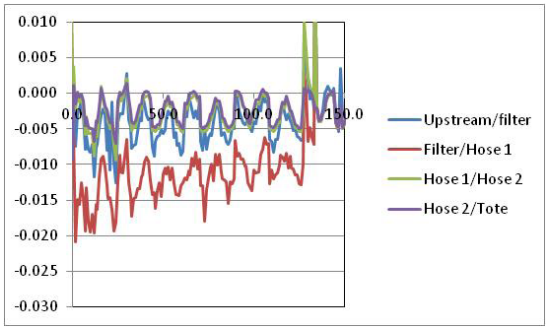

TC14 C

Table G.1: Streaming currents in main Phase 1 test sequence (continued)

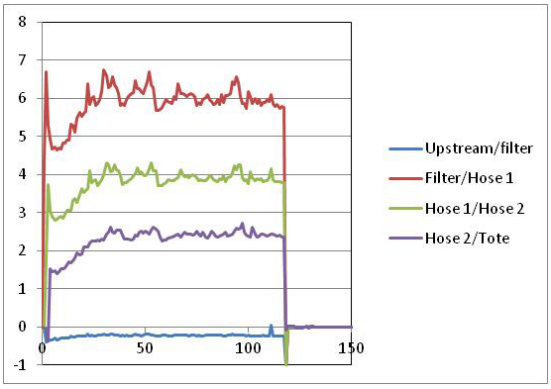

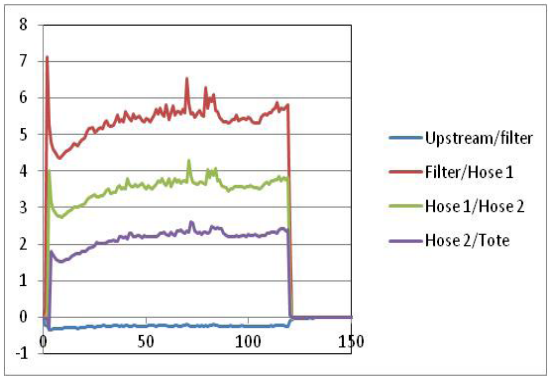

TC15 A

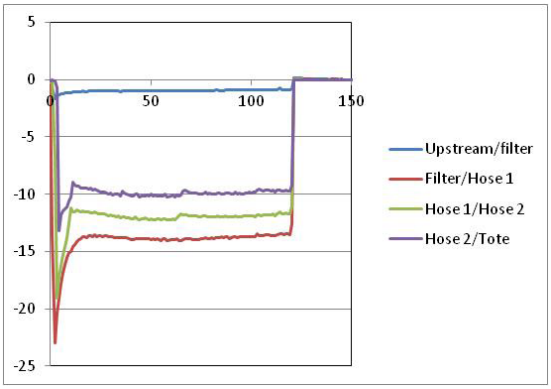

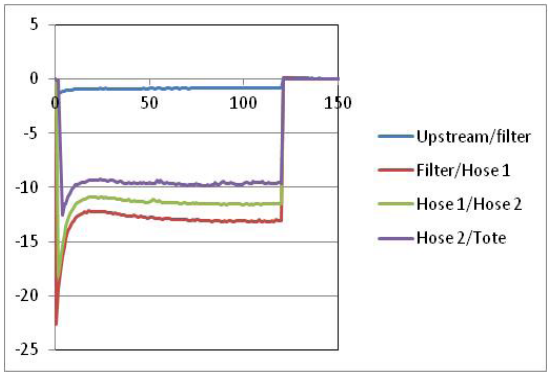

TC15 B

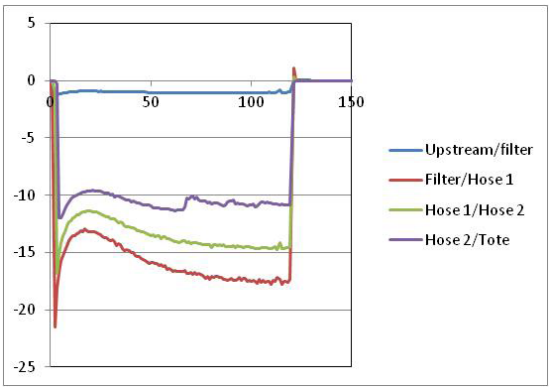

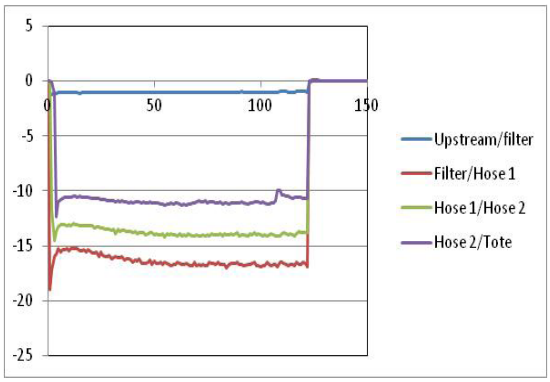

TC15 C

Table G.1: Streaming currents in main Phase 1 test sequence (continued)

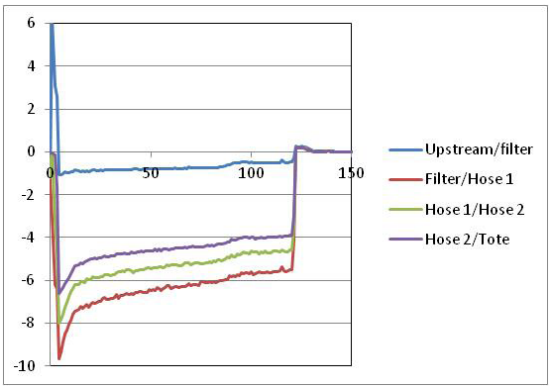

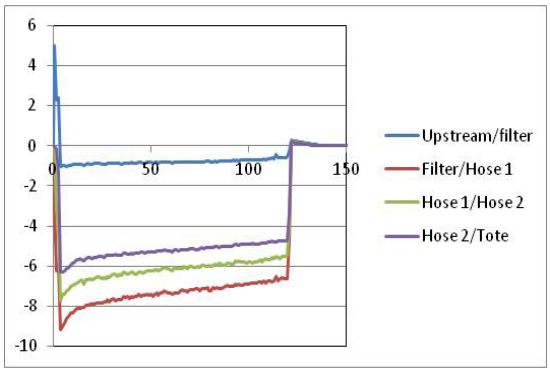

TC16 A

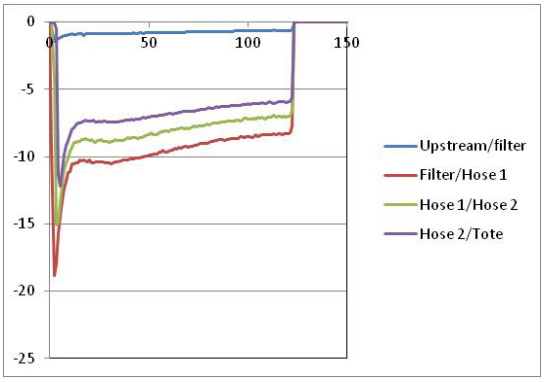

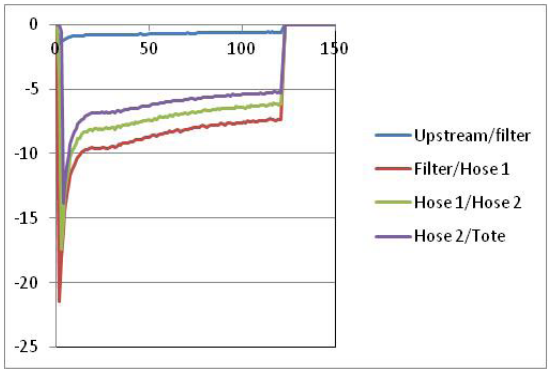

TC16 B

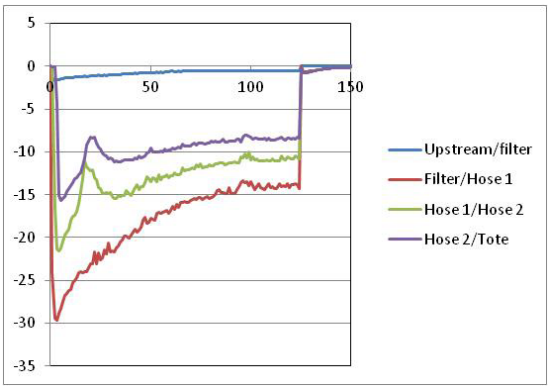

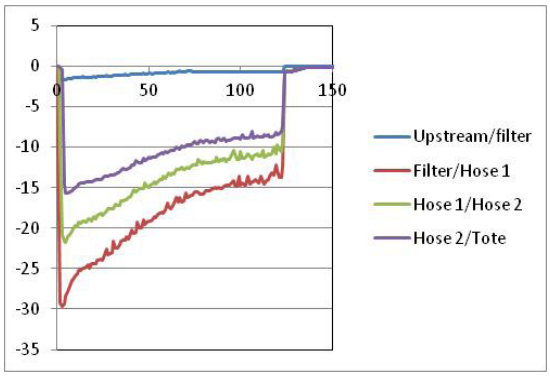

TC16 C

Table G.1: Streaming currents in main Phase 1 test sequence (continued)

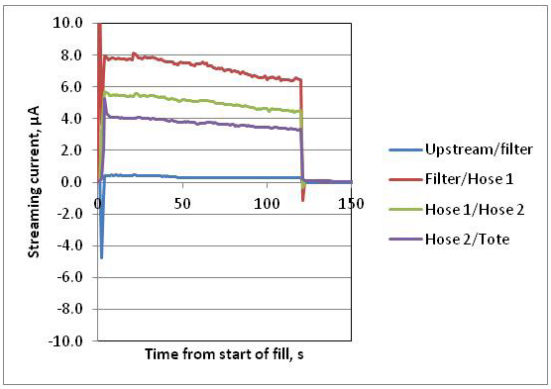

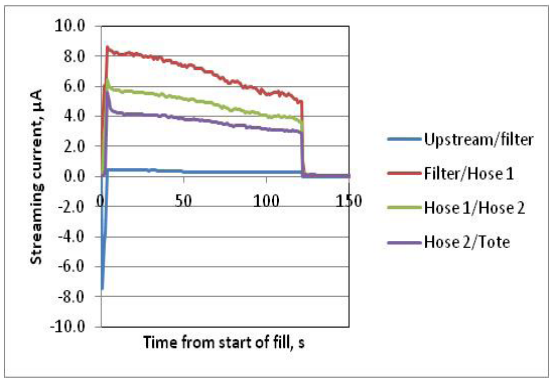

TC17 A

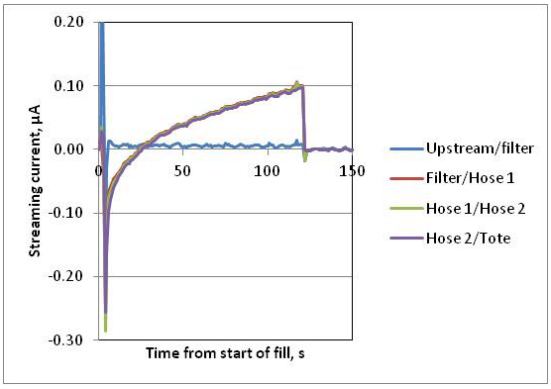

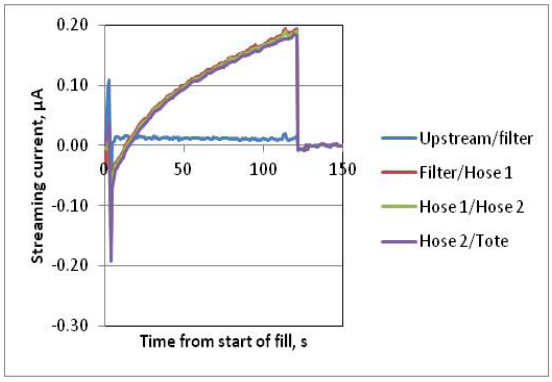

TC17 B

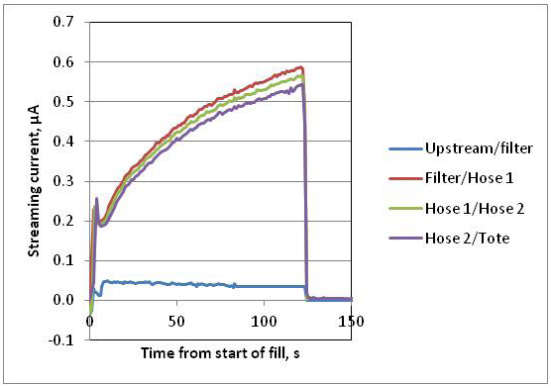

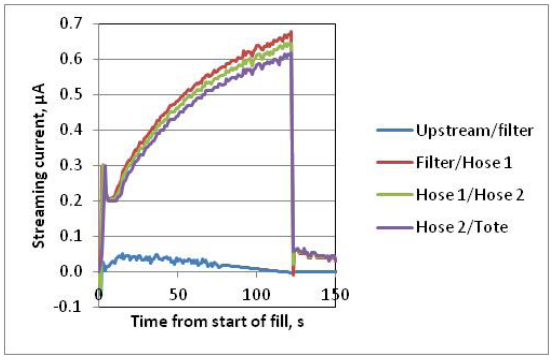

TC17 C

Table G.1: Streaming currents in main Phase 1 test sequence (continued)

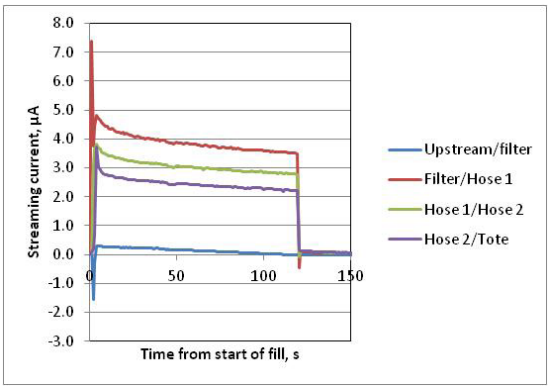

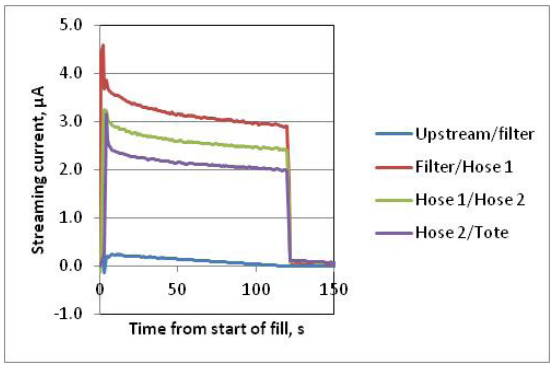

TC18 A

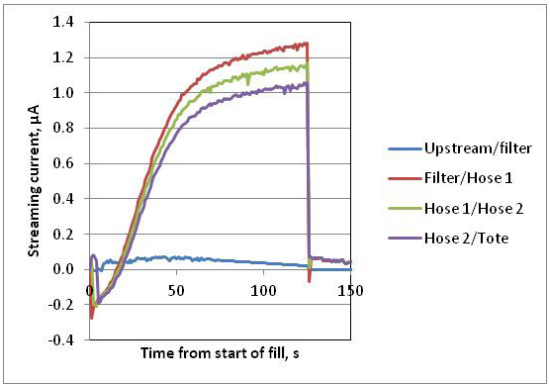

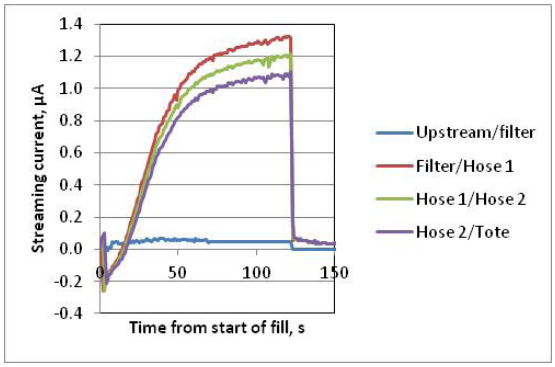

TC18 B

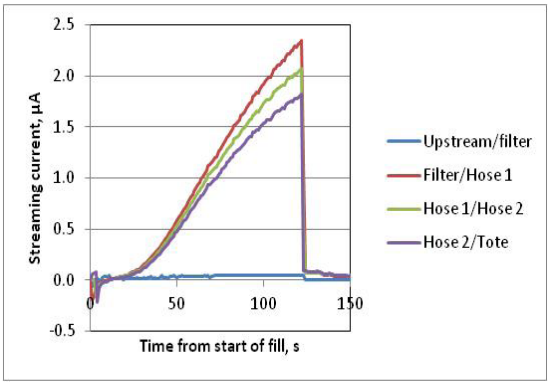

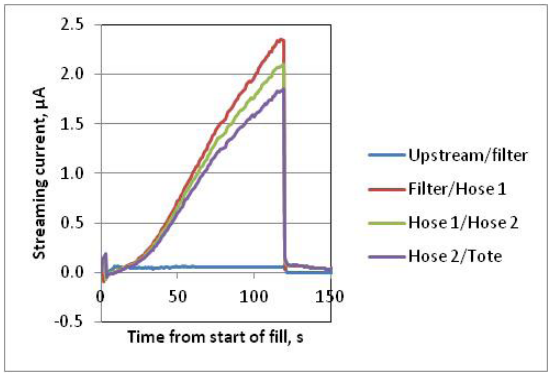

TC18 C

Table G.1: Streaming currents in main Phase 1 test sequence (continued)

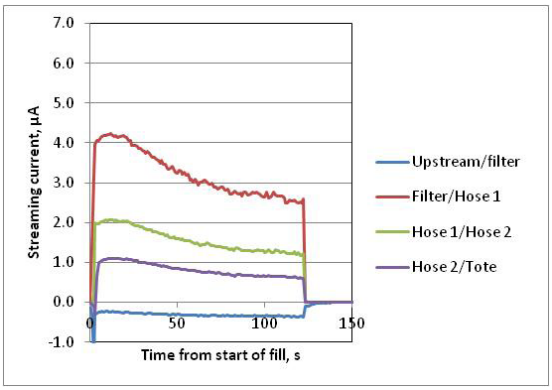

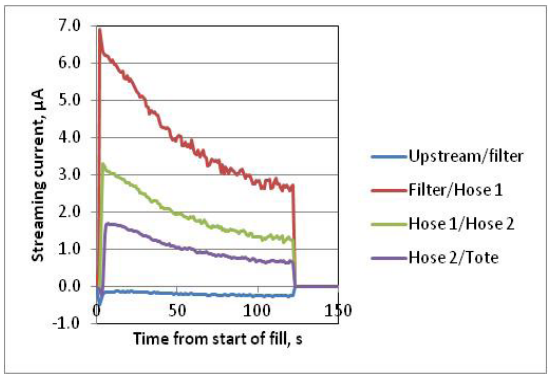

TC19 A

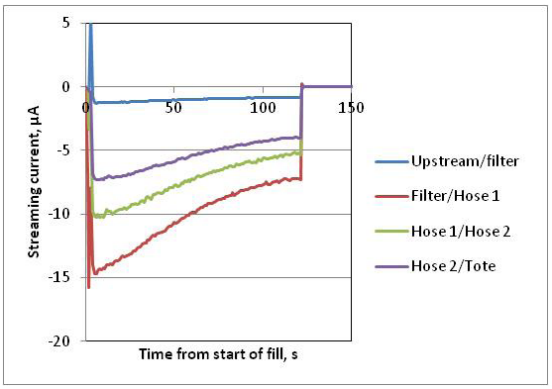

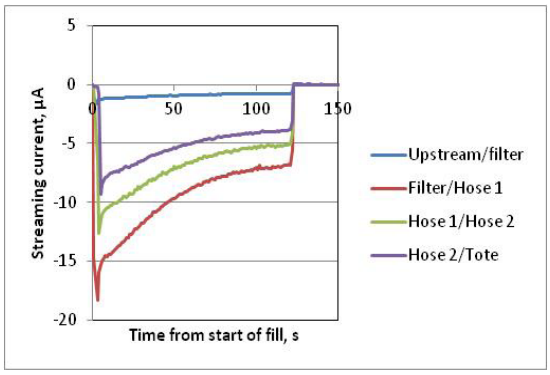

TC19 B

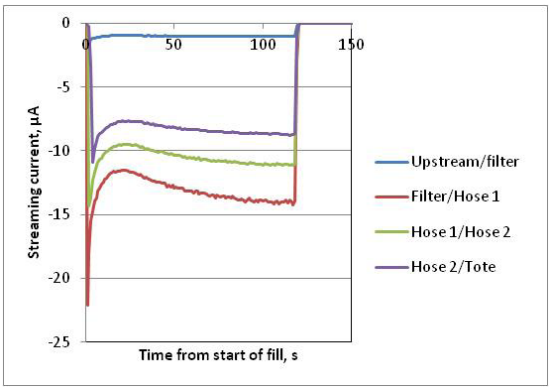

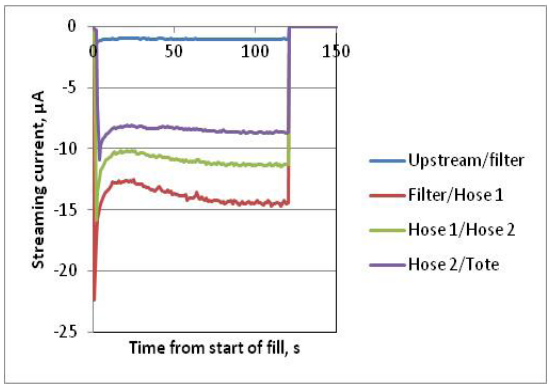

TC19 C

Table G.1: Streaming currents in main Phase 1 test sequence (continued)

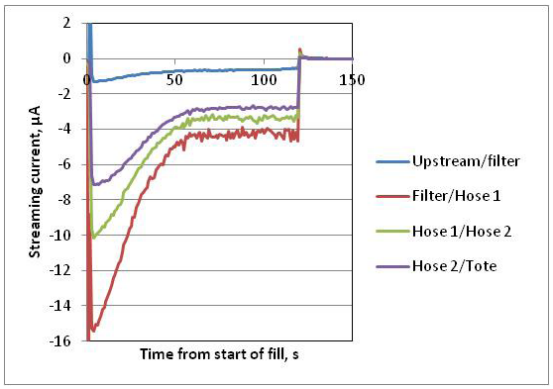

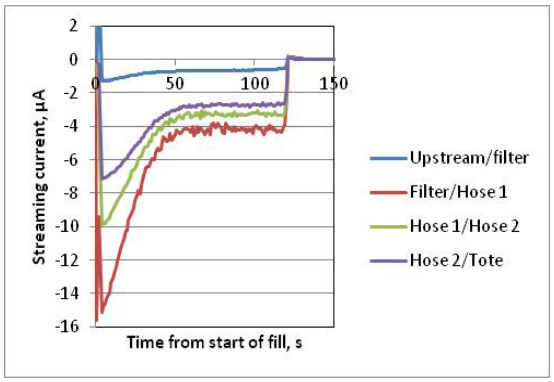

TC20 A

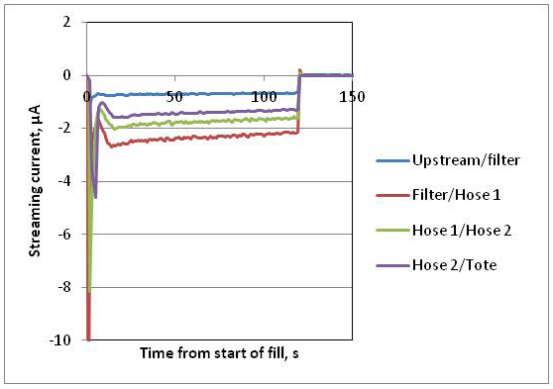

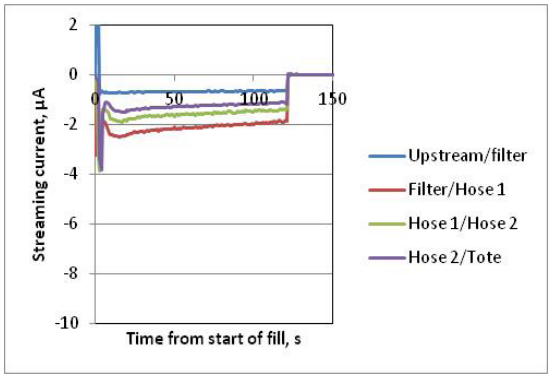

TC20 B

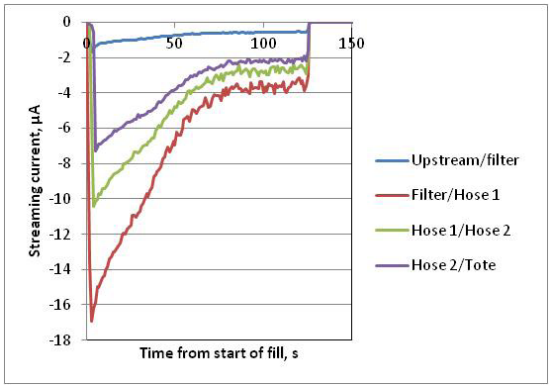

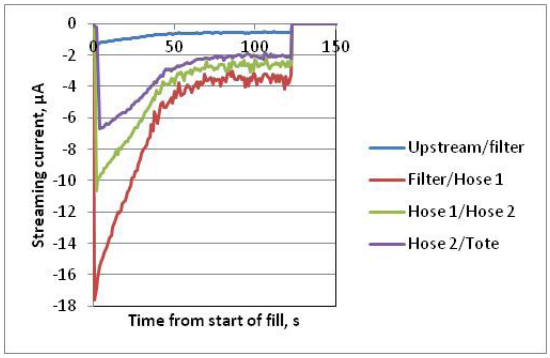

TC20 C

Table G.2: Streaming currents in Phase 1 supplementary tests

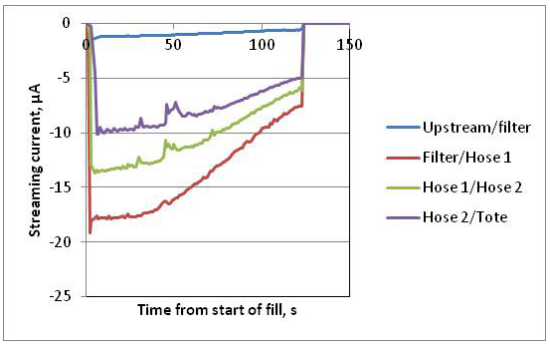

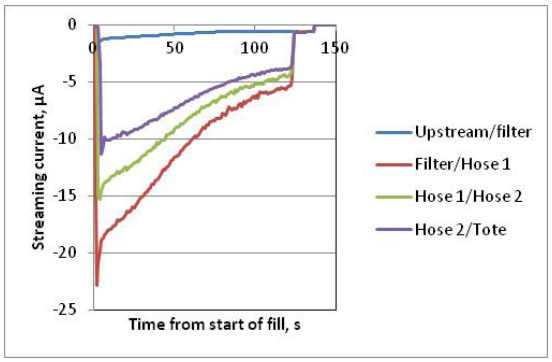

TC19 Generation 4 B element, dry

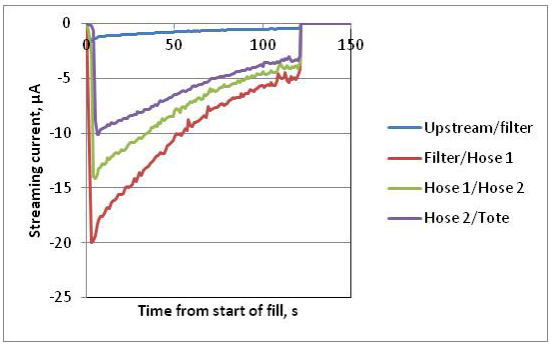

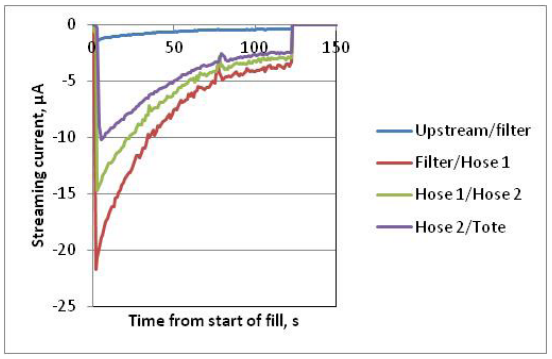

TC19 Generation 4 B element, wet

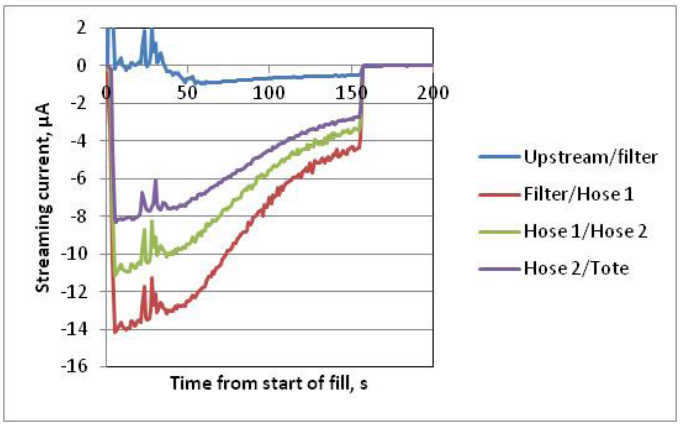

TC19 Generation 4 B element, wet, empty tote at start of run

Table G.2: Streaming currents in Phase 1 supplementary tests (continued)

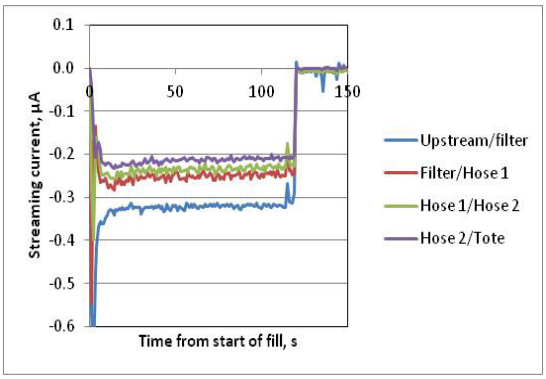	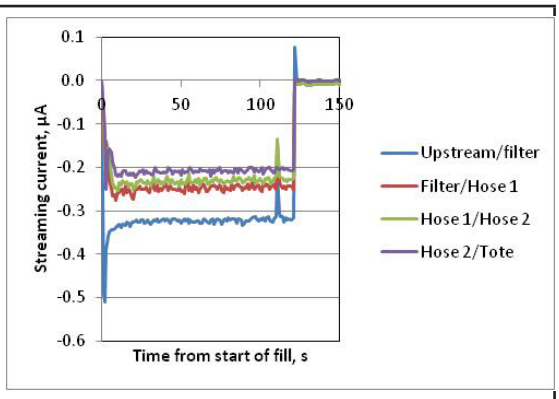
TC19 Pipe currents with no element	

Table G.3: Streaming currents in Phase 2 tests: 6" elements

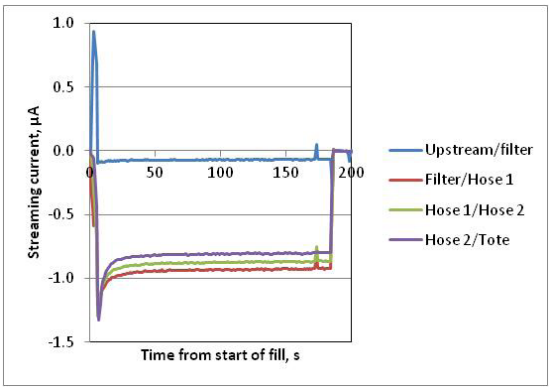

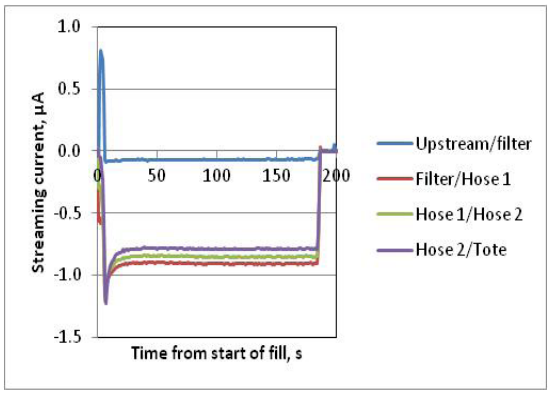

Element A/OI, 58 USGPM

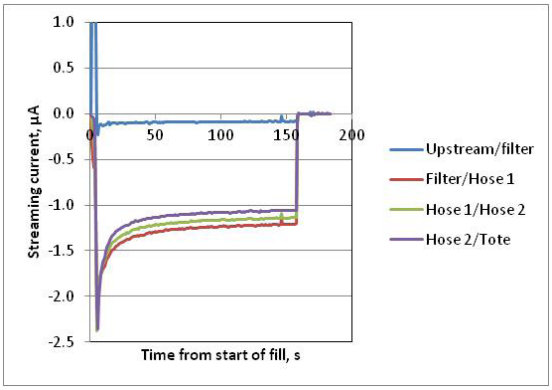

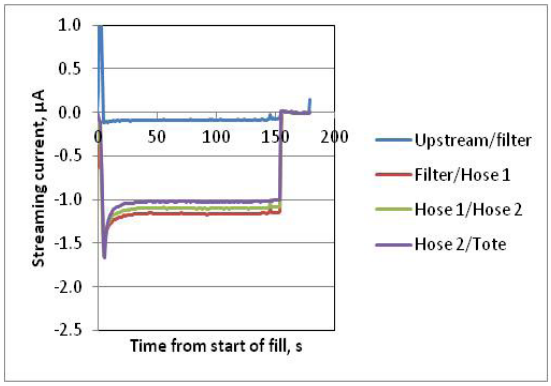

Element A/OI, 69 USGPM

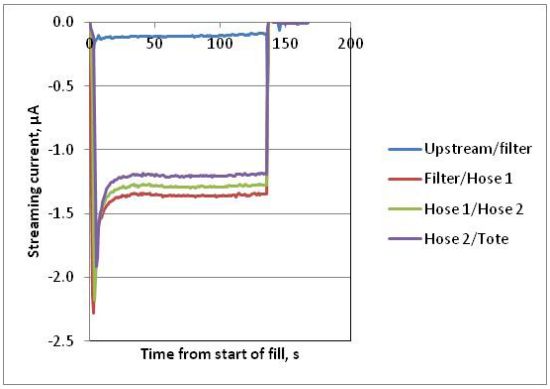

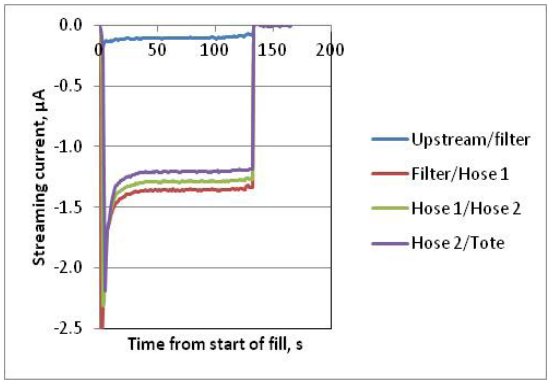

Element A/OI, 81 USGPM

Table G.3: Streaming currents in Phase 2 tests: 6" elements (continued)

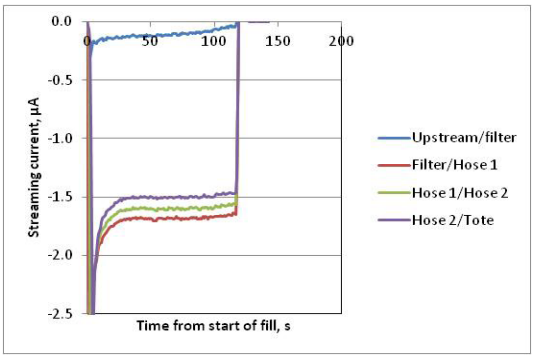

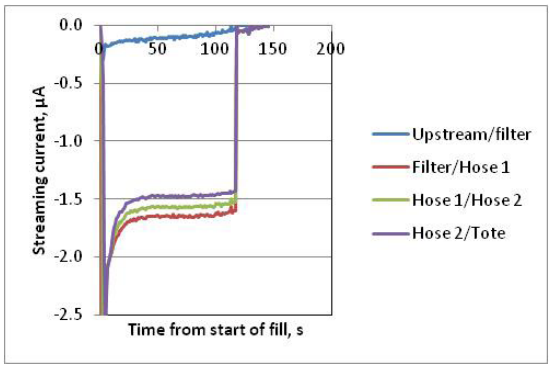

Element A/OI, 92 USGPM

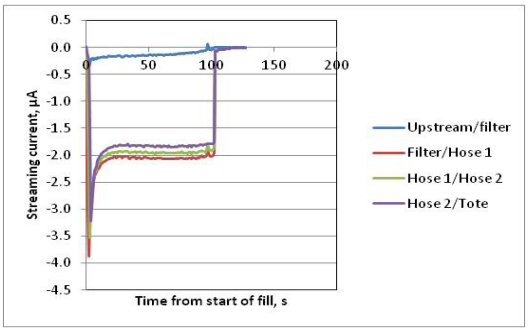

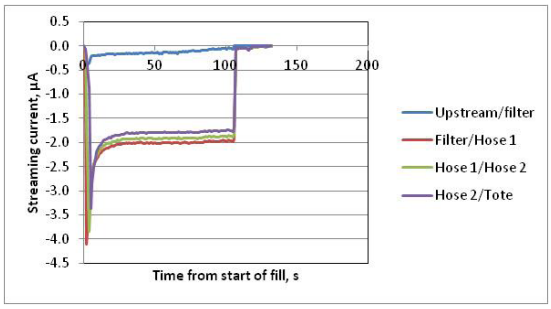

Element A/OI, 103 USGPM

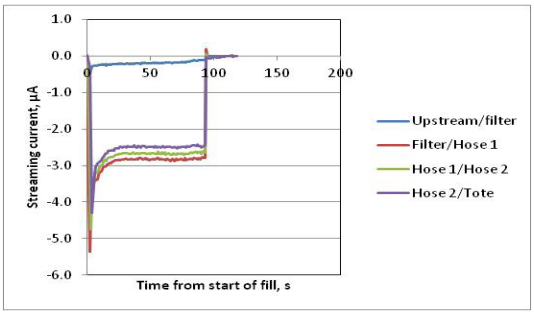

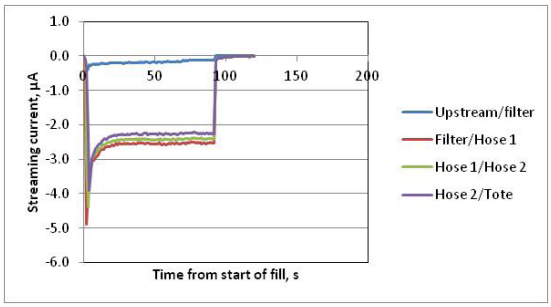

Element A/OI, 115 USGPM

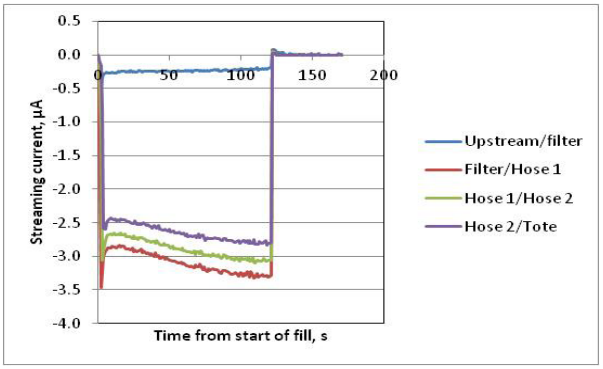

Element A/OI, 115 USGPM, empty tote

Table G.3: Streaming currents in Phase 2 tests: 6" elements (continued)

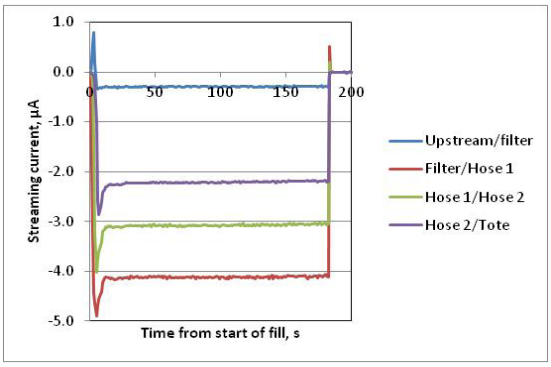

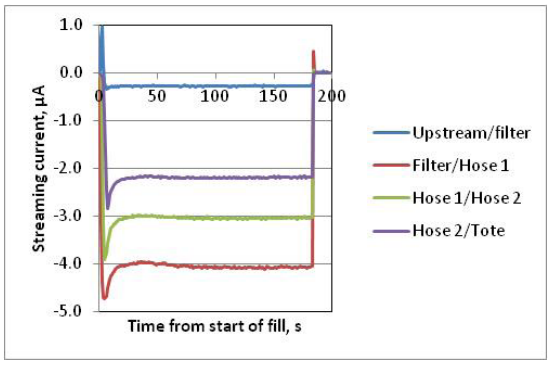

Element B/OI, 58 USGPM

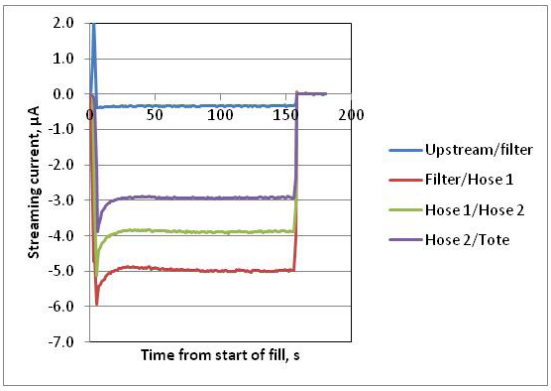

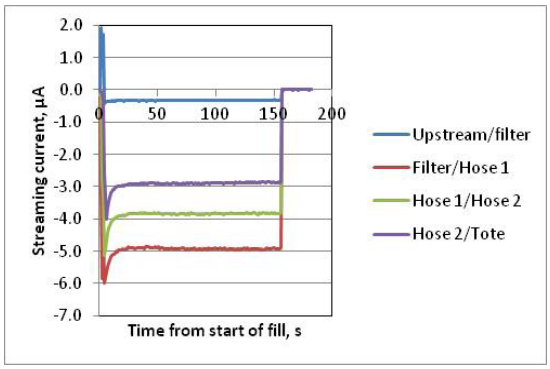

Element B/OI, 69 USGPM

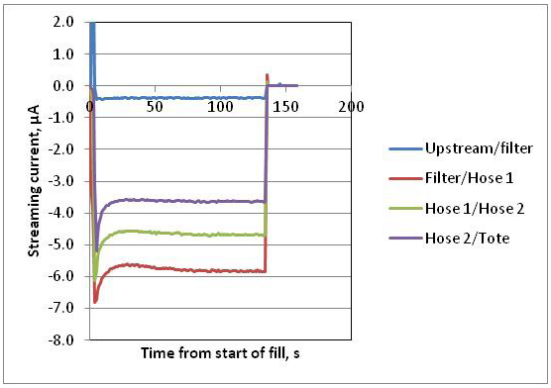

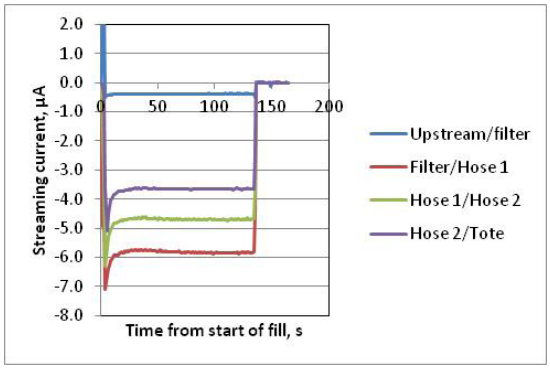

Element B/OI, 80 USGPM

Table G.3: Streaming currents in Phase 2 tests: 6" elements (continued)

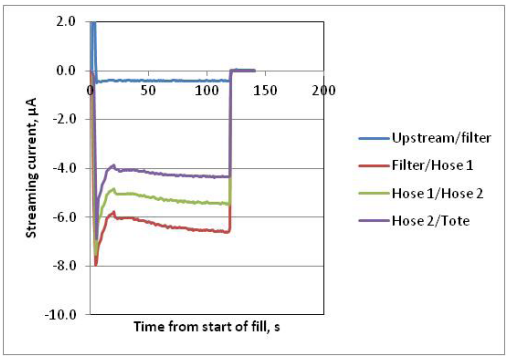

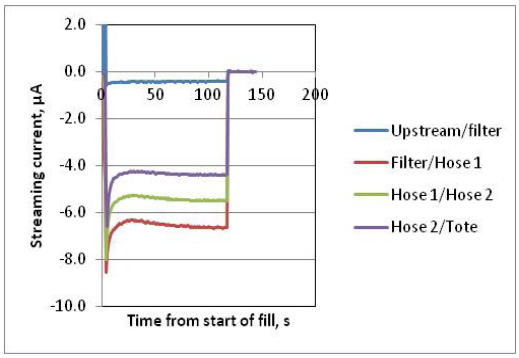

Element B/OI, 92 USGPM

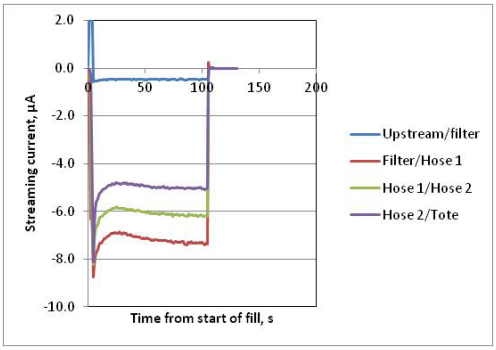

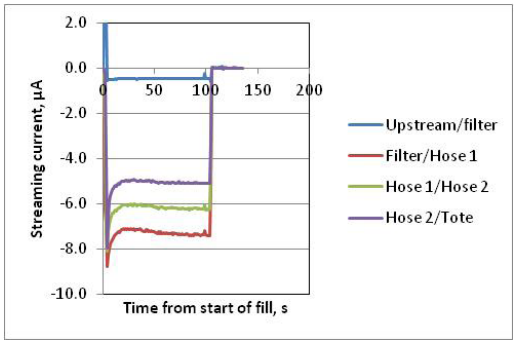

Element B/OI, 103 USGPM

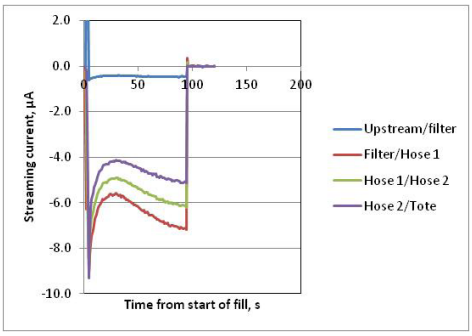

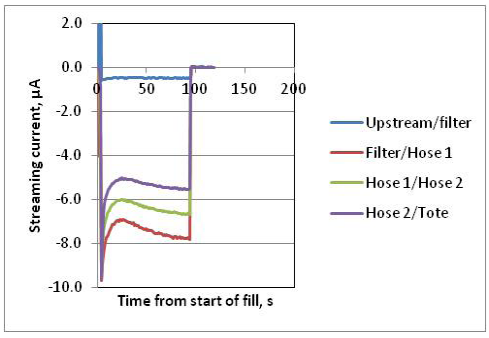

Element B/OI, 115 USGPM

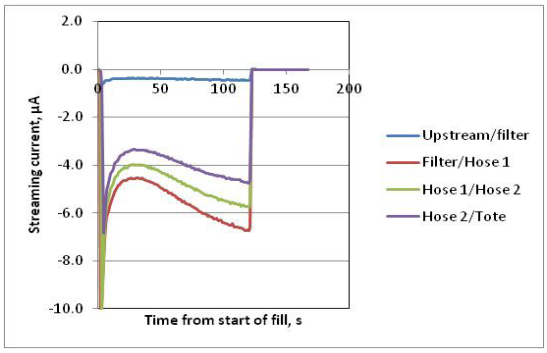

Element B/OI, 115 USGPM, empty tote

Table G.3: Streaming currents in Phase 2 tests: 6" elements (continued)

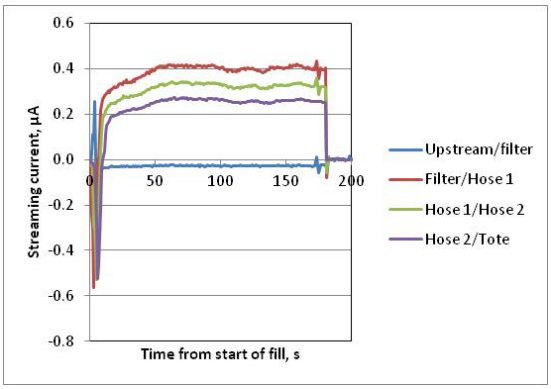

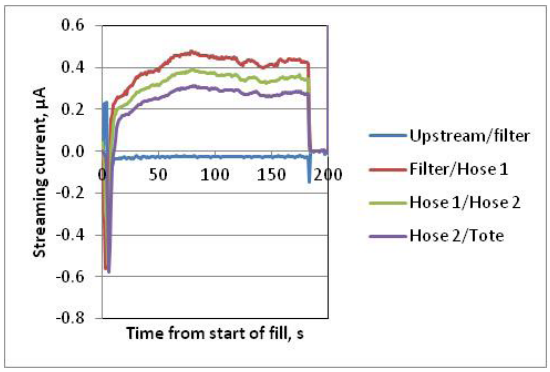

Element C/OI, 58 USGPM

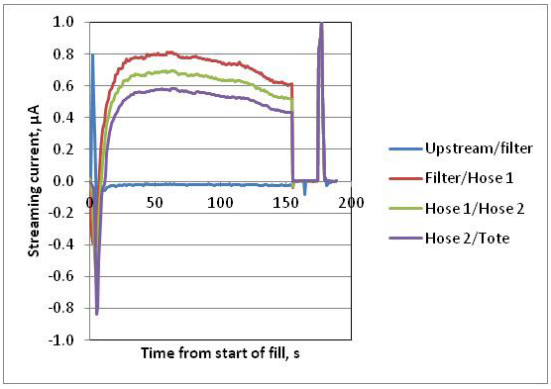

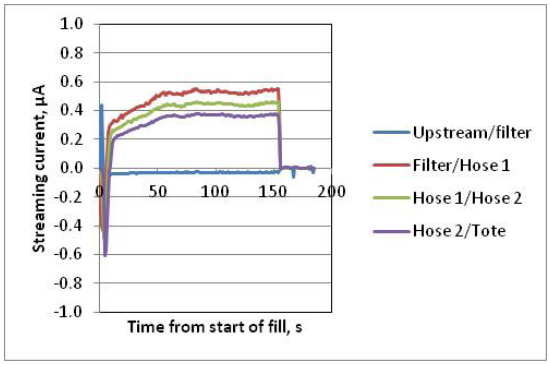

Element C/OI, 69 USGPM

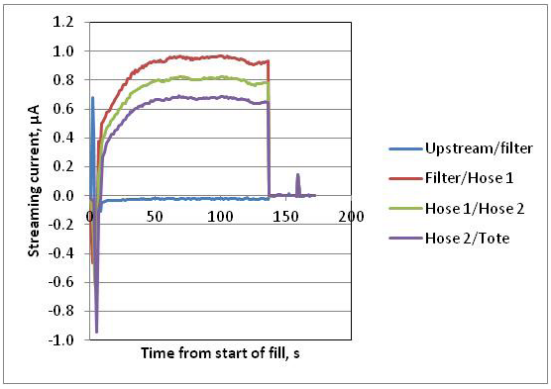

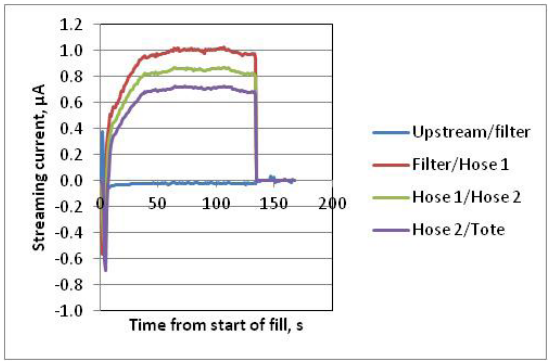

Element C/OI, 81 USGPM

Table G.3: Streaming currents in Phase 2 tests: 6" elements (continued)

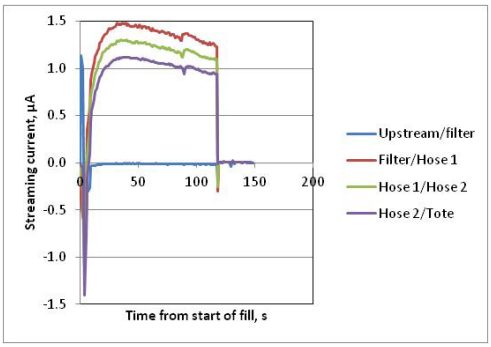

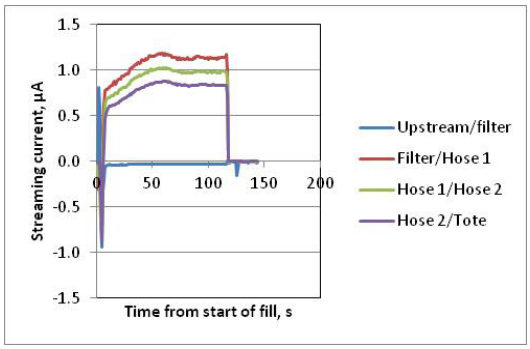

Element C/OI, 92 USGPM

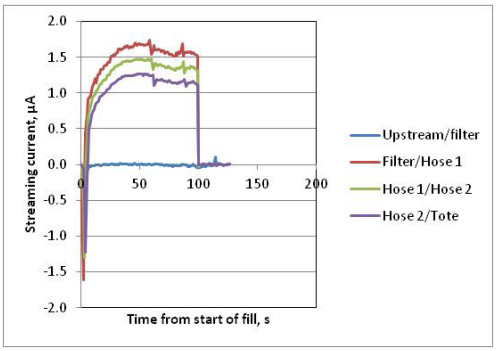

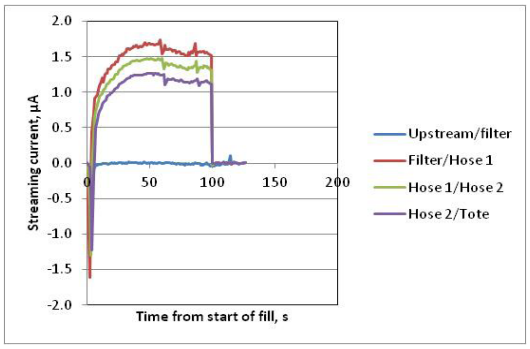

Element C/OI, 108 USGPM

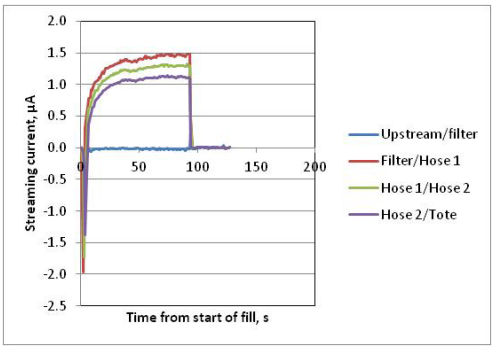

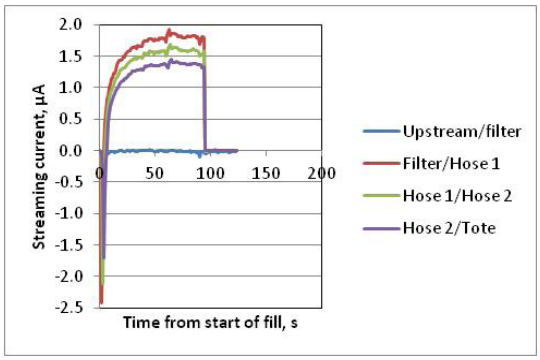

Element C/OI, 115 USGPM

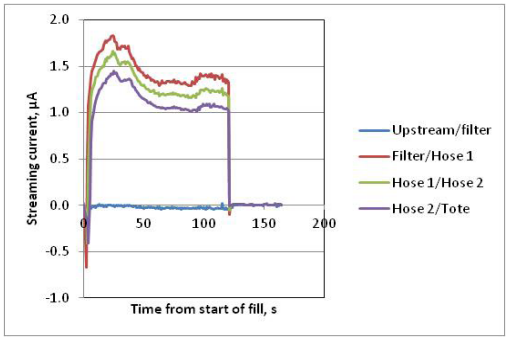

Element C/OI, 115 USGPM, empty tote

Table G.3: Streaming currents in Phase 2 tests: 6" elements (continued)

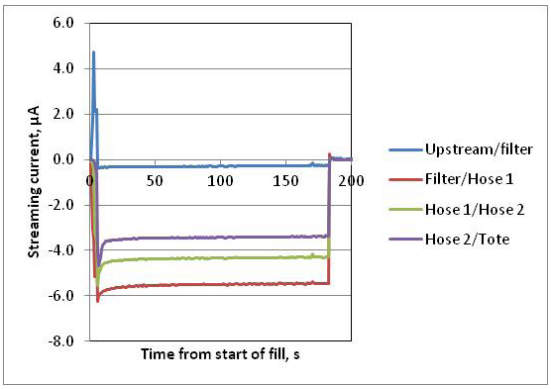

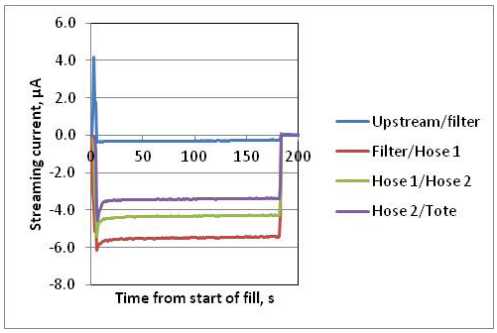

Element B/io, 58 USGPM

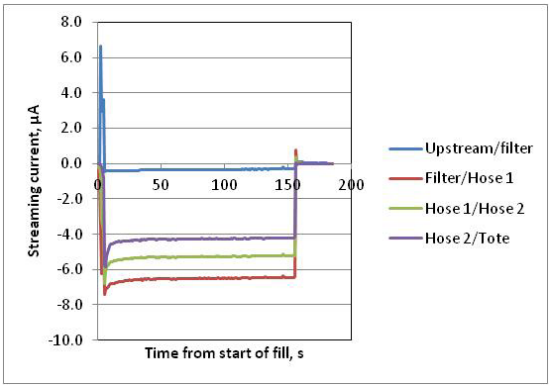

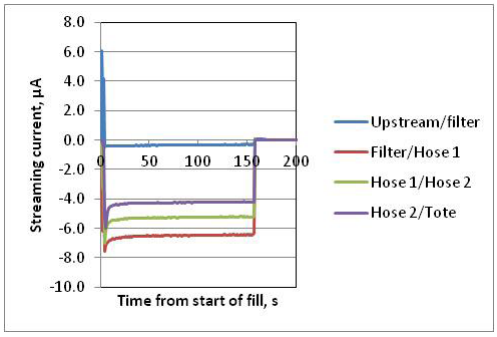

Element B/io, 69 USGPM

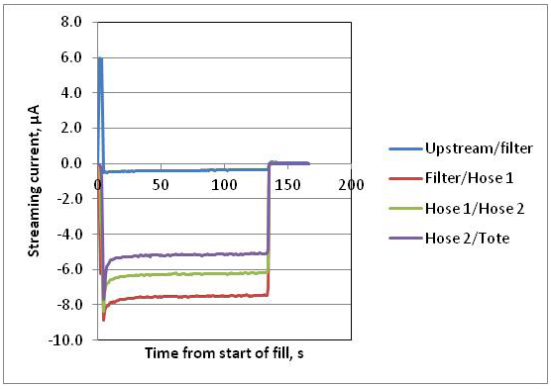

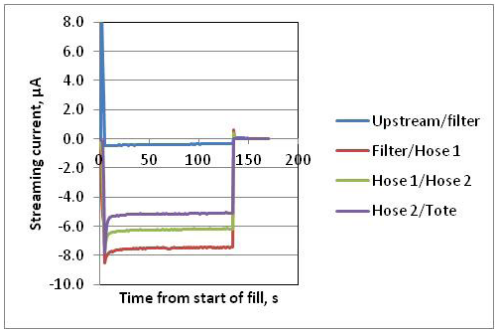

Element B/io, 80 USGPM

Table G.3: Streaming currents in Phase 2 tests: 6" elements (continued)

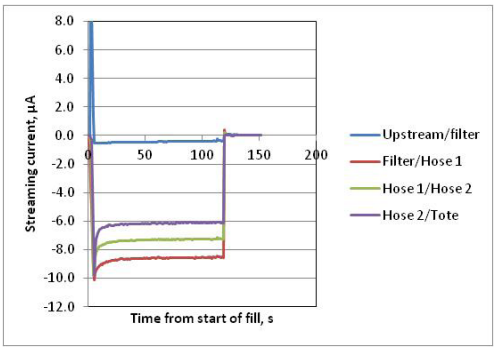

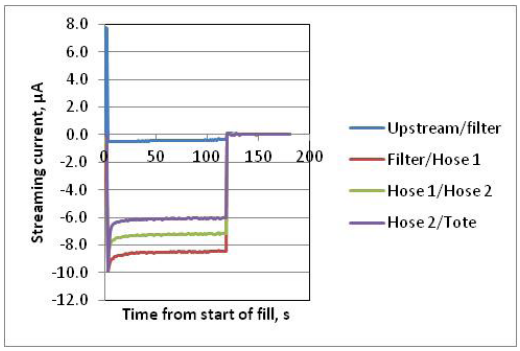

Element B/io, 92 USGPM

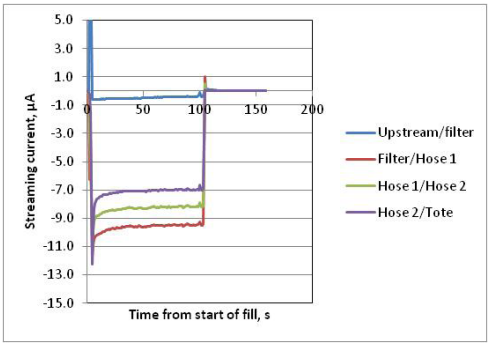

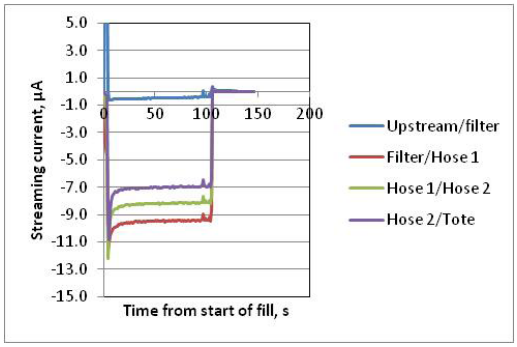

Element B/io, 103 USGPM

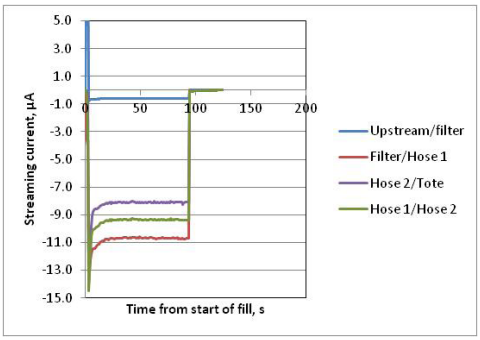

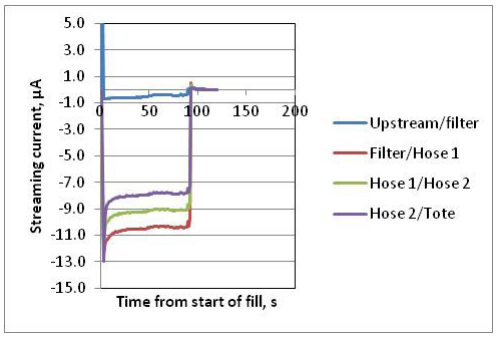

Element B/io, 115 USGPM

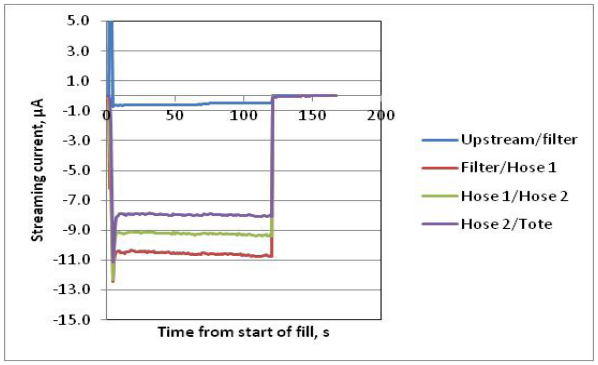

Element B/io, 115 USGPM, empty tote

Table G.3: Streaming currents in Phase 2 tests: 6" elements (continued)

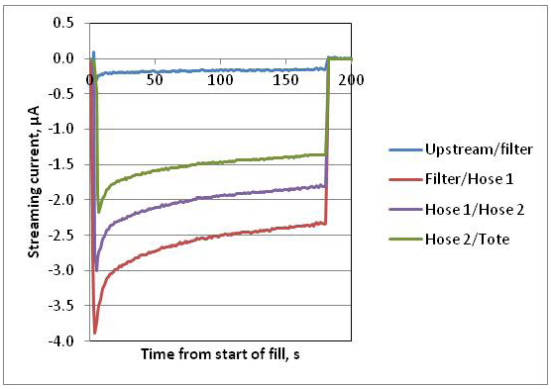

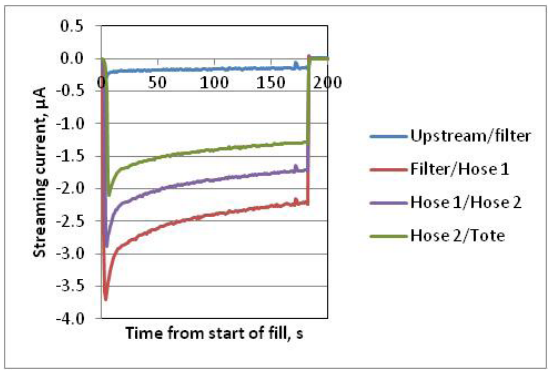

Element C/io, 58 USGPM

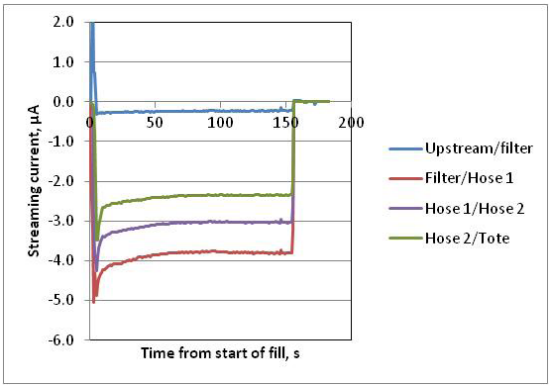

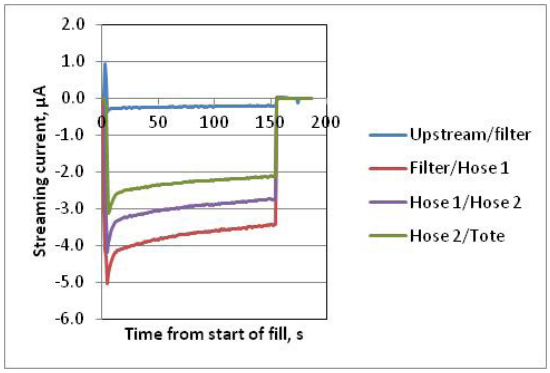

Element C/io, 69 USGPM

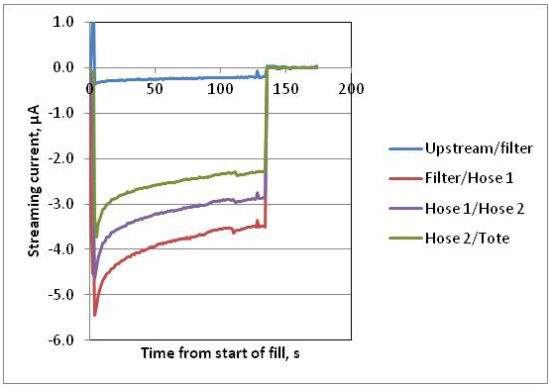

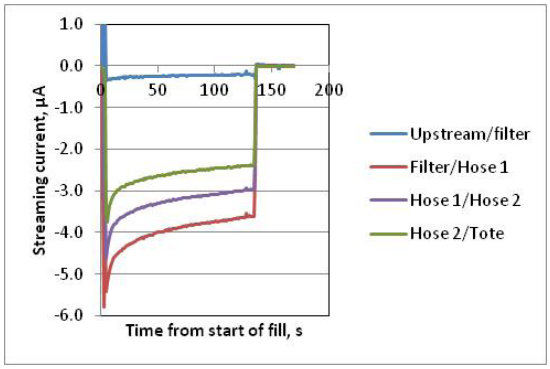

Element C/io, 80 USGPM

Table G.3: Streaming currents in Phase 2 tests: 6" elements (continued)

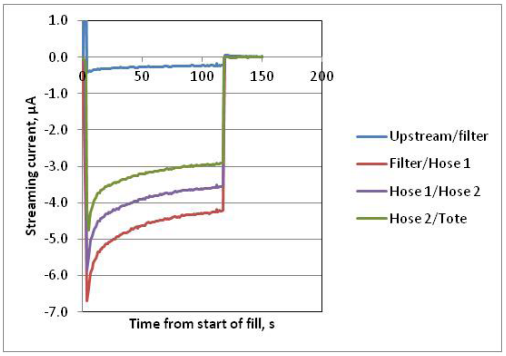

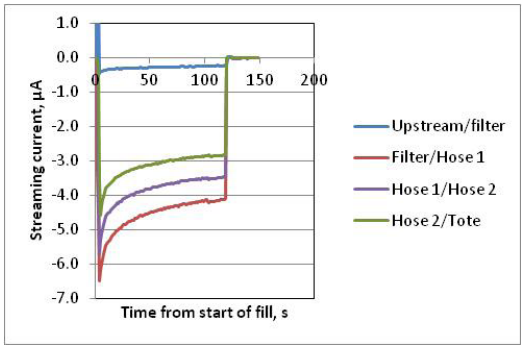

Element C/io, 92 USGPM

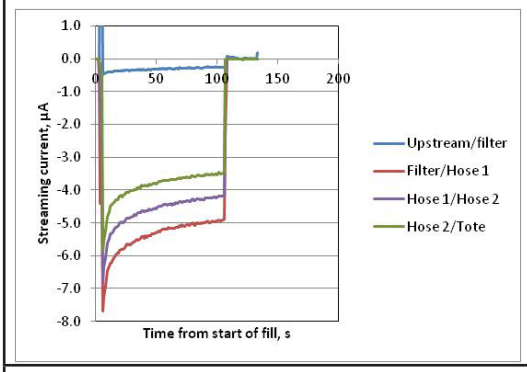

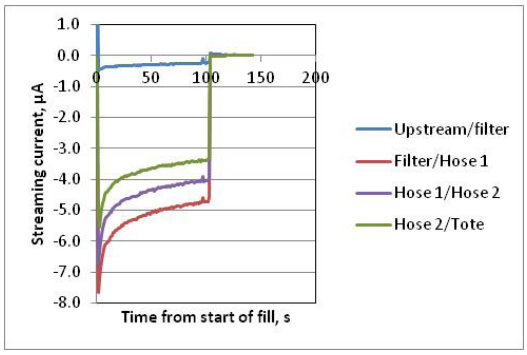

Element C/io, 103 USGPM

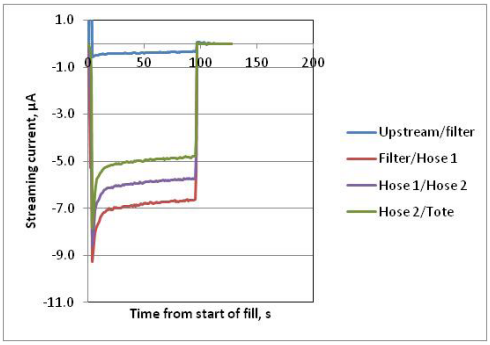

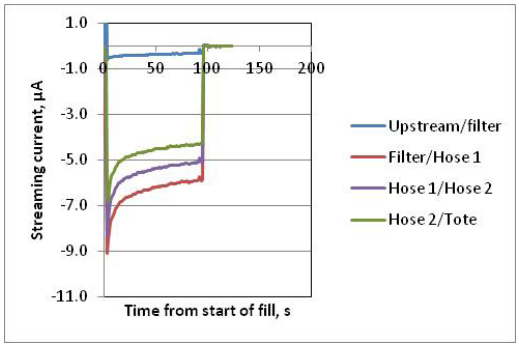

Element C/io, 115 USGPM

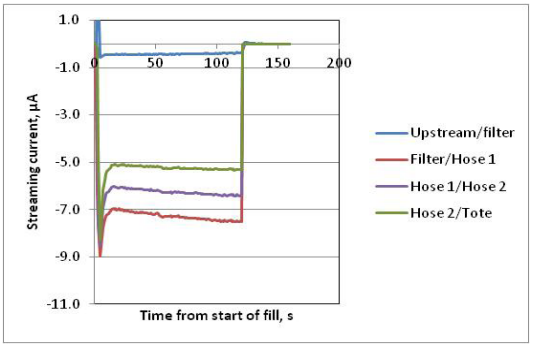

Element C/io, 115 USGPM, empty tote

Table G.4: Streaming currents in Phase 2 tests: 2" elements

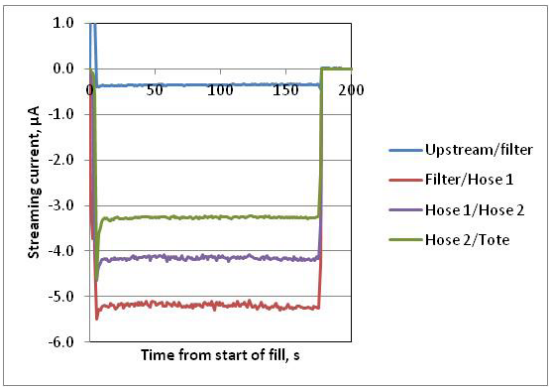

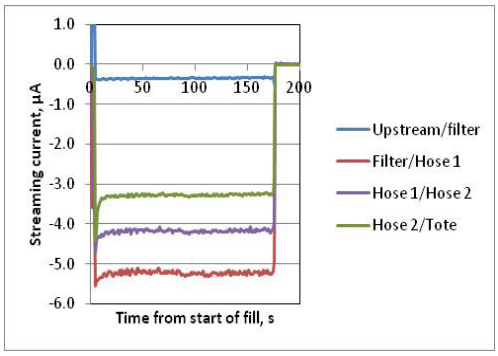

Element A, 60 USGPM

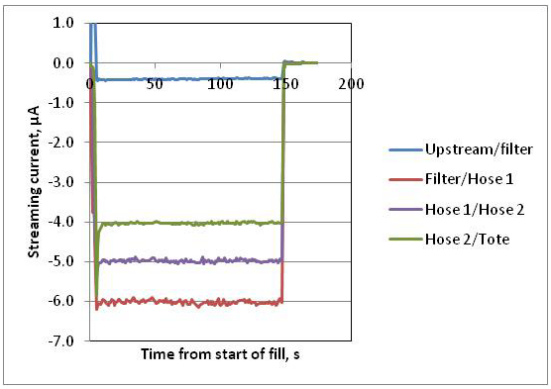

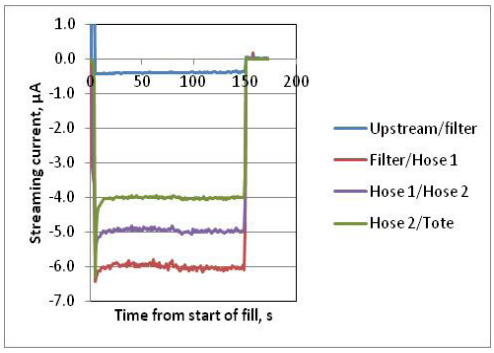

Element A, 72 USGPM

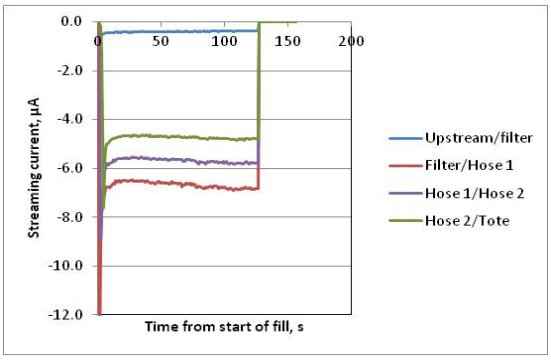

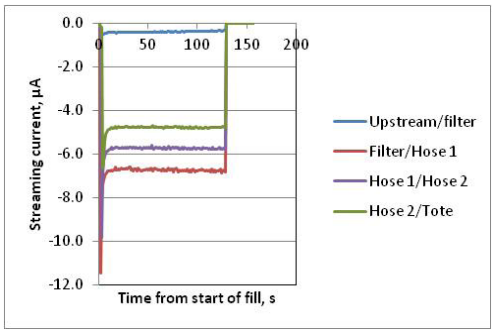

Element A, 84 USGPM

Table G.4: Streaming currents in Phase 2 tests: 2" elements (continued)

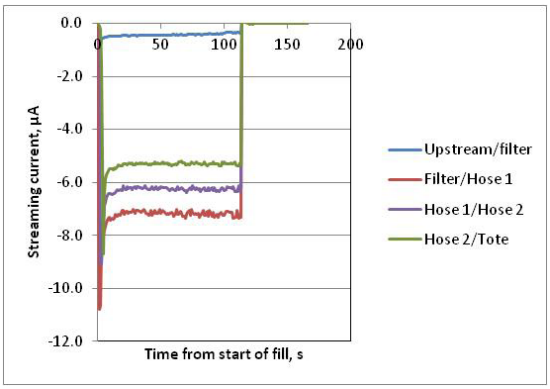

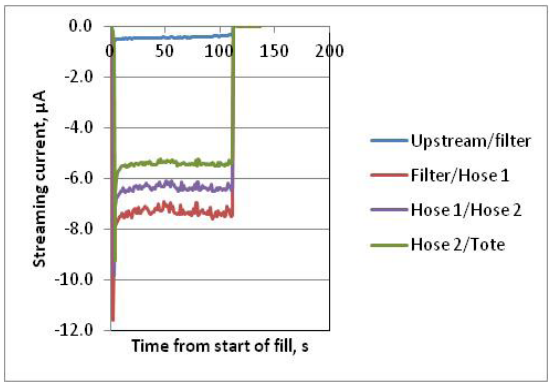

Element A, 96 USGPM

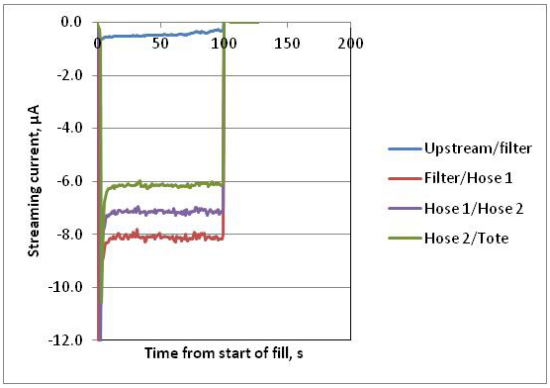

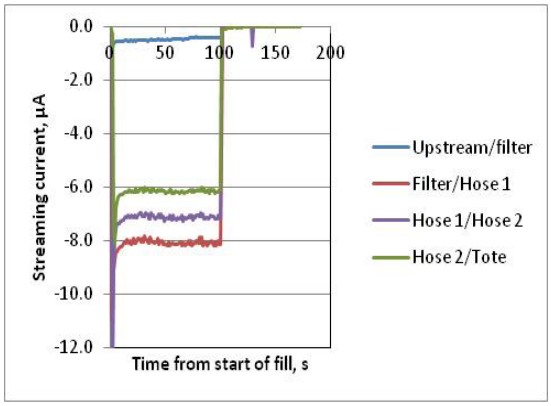

Element A, 108 USGPM

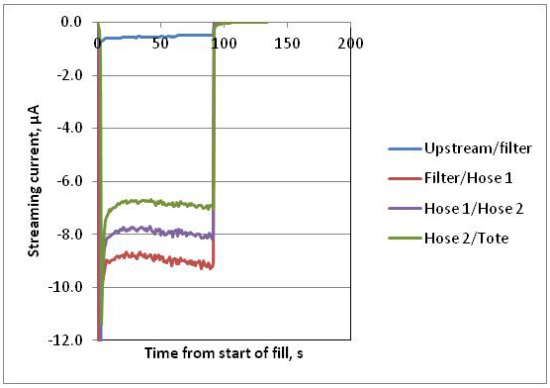

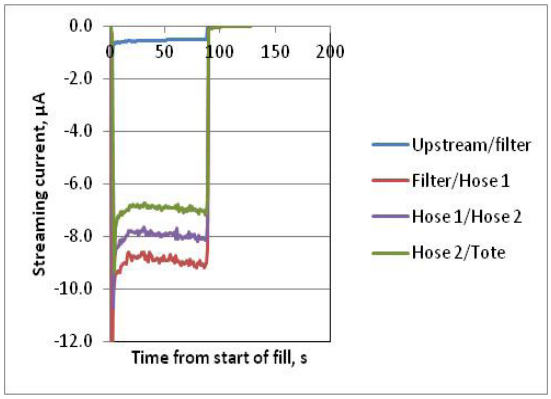

Element A, 120 USGPM

Table G.4: Streaming currents in Phase 2 tests: 2" elements (continued)

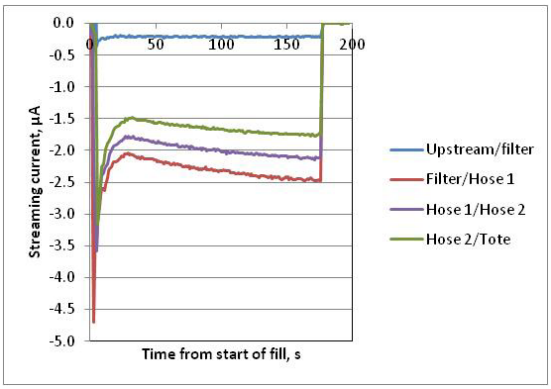

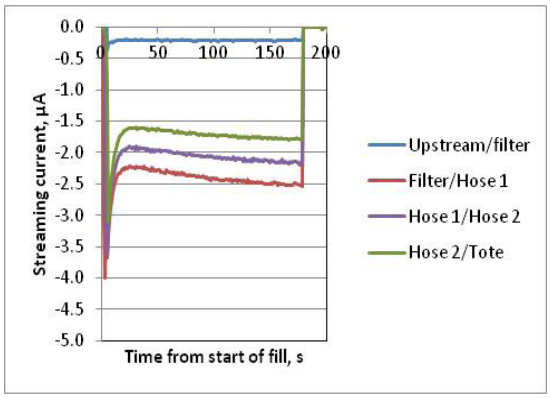

Element B, 60 USGPM

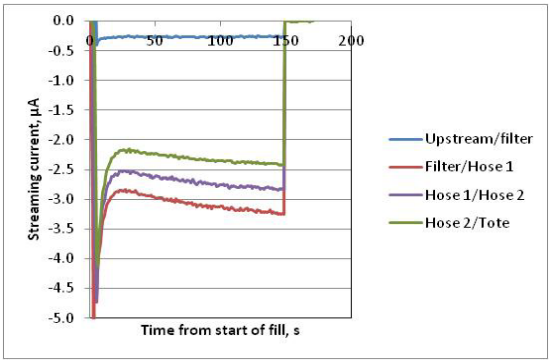

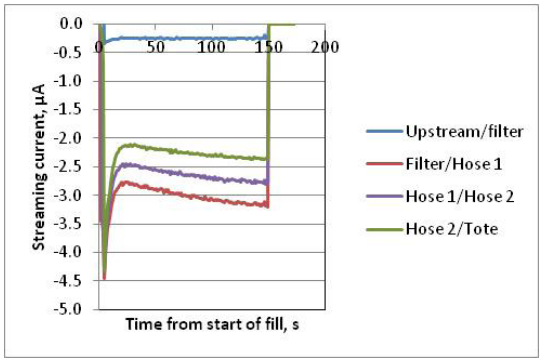

Element B, 72 USGPM

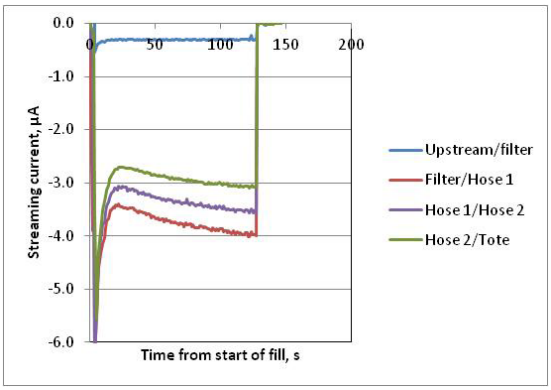

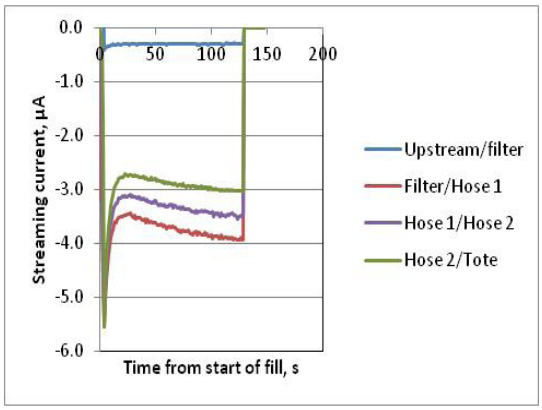

Element B, 84 USGPM

Table G.4: Streaming currents in Phase 2 tests: 2" elements (continued)

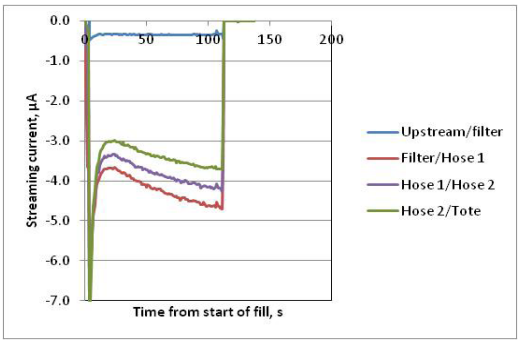

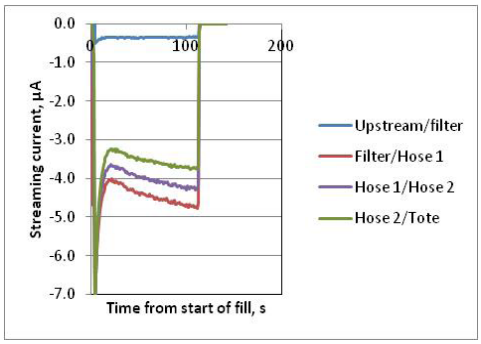

Element B, 96 USGPM

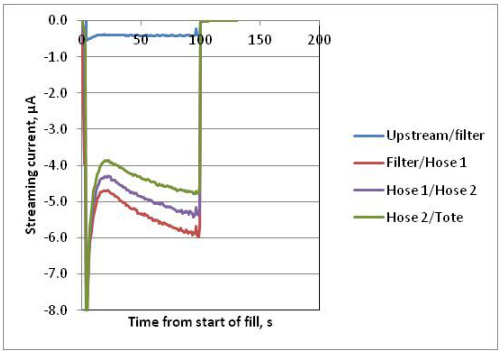

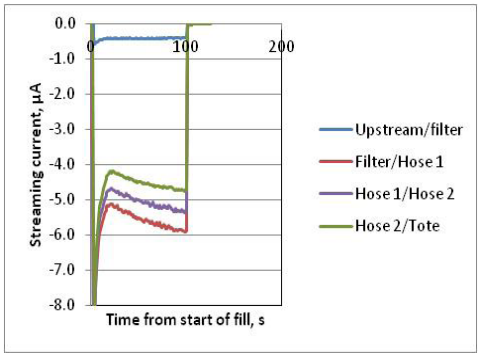

Element B, 108 USGPM

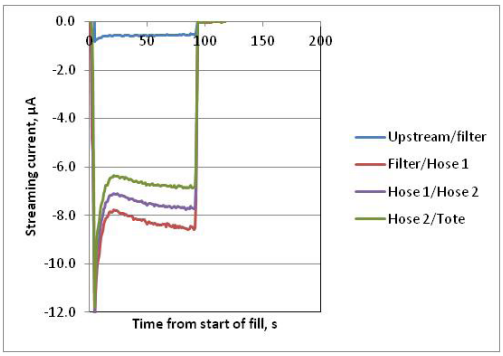

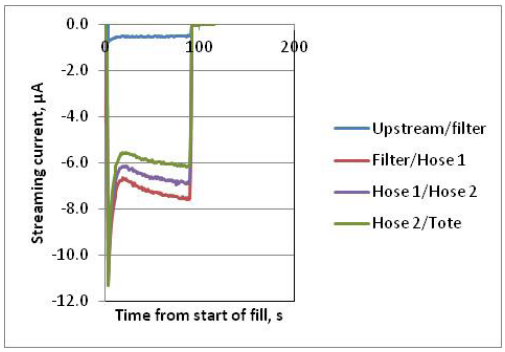

Element B, 120 USGPM

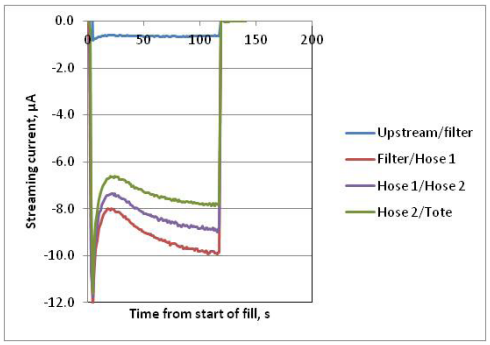

Element B, 120 USGPM, empty tote

Table G.4: Streaming currents in Phase 2 tests: 2" elements (continued)

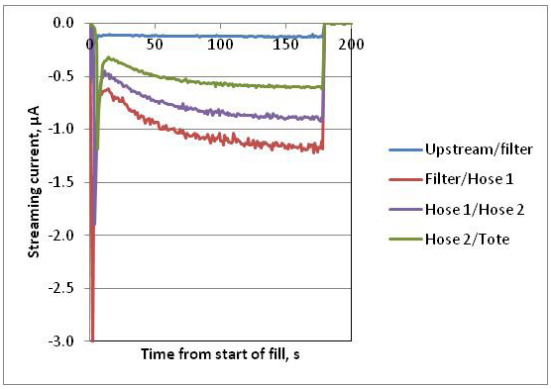

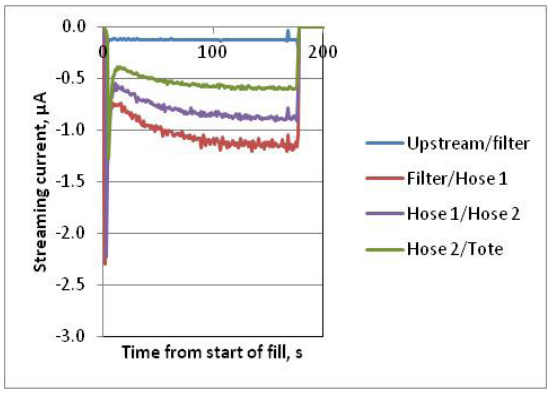

Element C, 60 USGPM

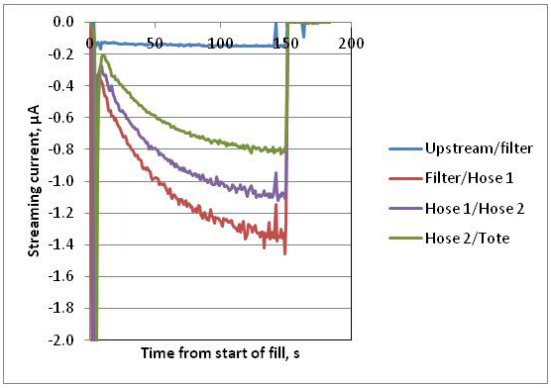

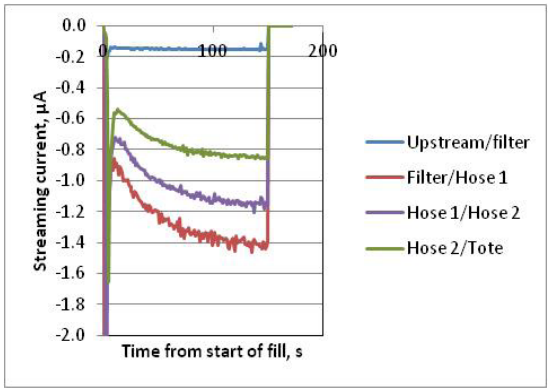

Element C, 72 USGPM

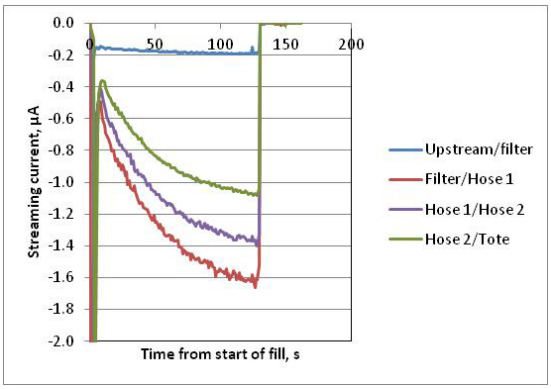

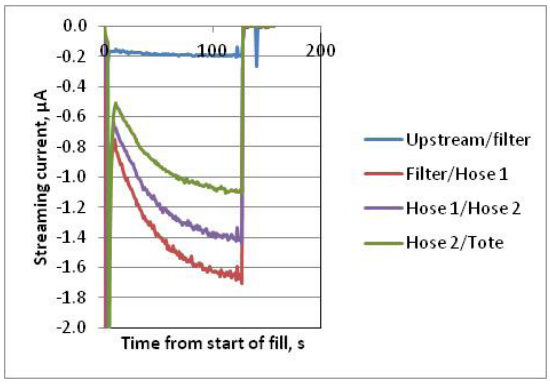

Element C, 84 USGPM

Table G.4: Streaming currents in Phase 2 tests: 2" elements (continued)

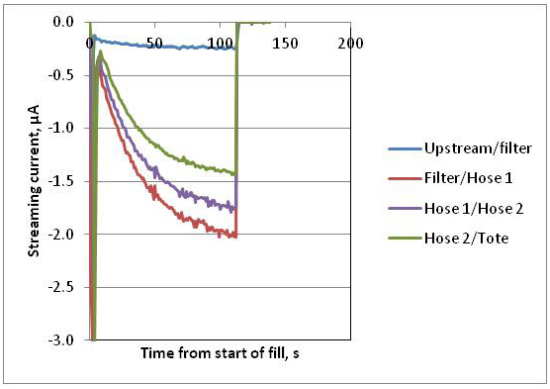

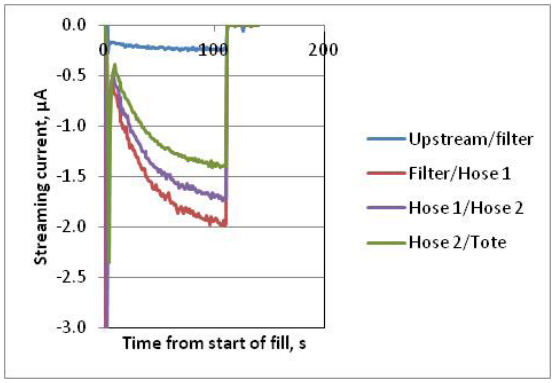

Element C, 96 USGPM

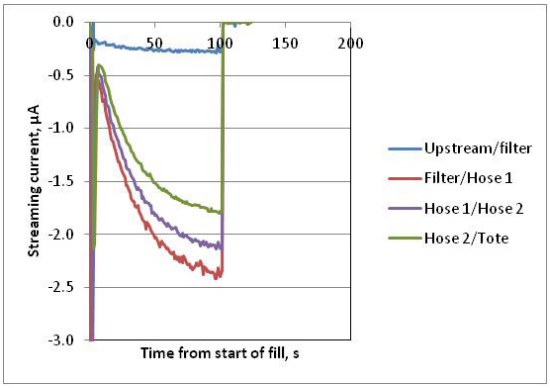

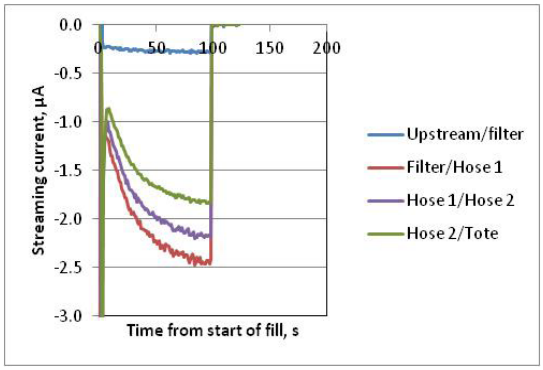

Element C, 108 USGPM

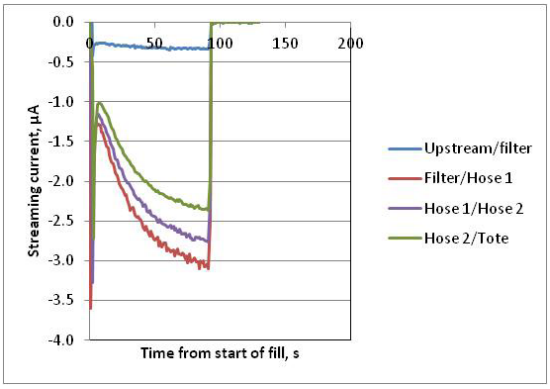

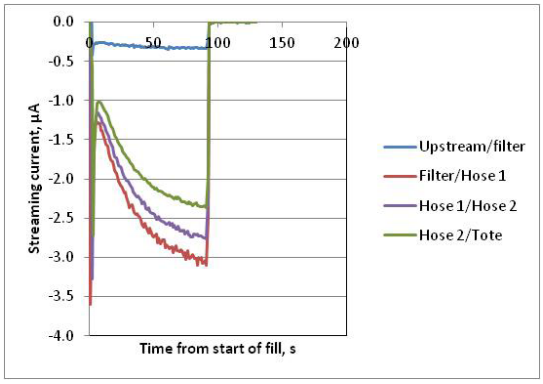

Element C, 120 USGPM

ANNEX H: PHASE 1 STREAMING CURRENTS AND CHARGE DENSITIES

Table H.1: Effective streaming current and charge density at filter section exit and tote inlet

Condition	Effective current				Effective charge density			
	Maximum		Final		Maximum		Final	
	Filter exit	Tote inlet	Filter exit	Tote inlet	Filter exit	Tote inlet	Filter exit	Tote inlet
S01	–0,31	–0,22	–0,23	–0,20	–55	–39	–41	–35
S02	–17,5	–9,1	–9,5	–5,9	–3 131	–1 623	–1 702	–1 058
S03	–16,4	–8,3	–6,1	–3,9	–2 920	–1 472	–1 089	–692
S04	–12,7	–7,4	–5,2	–2,6	–2 294	–1 329	–932	–476
TC01A	11,3	4,7	6,9	3,5	2 017	840	1 239	620
TC01B	1,6	1,3	1,5	1,3	299	248	285	237
TC01C	1,7	1,4	1,7	1,4	304	257	304	257
TC02A	2,6	2,0	2,6	2,0	454	352	454	352
TC02B	3,2	2,4	3,1	2,2	609	448	587	426
TC02C	4,7	3,1	4,6	3,0	853	561	833	549
TC03A	4,2	1,8	3,6	1,6	755	325	653	279
TC03B	–3,3	–1,9	–3,2	–1,8	–604	–335	–577	–317
TC03C	–4,2	–2,4	–4,1	–2,4	–745	–437	–734	–423
TC04A	–5,3	–3,3	–5,1	–3,1	–936	–581	–909	–559
TC04B	–3,0	–2,9	0,37	0,10	–550	–523	67	18
TC04C	–7,1	–3,6	–5,4	–2,9	–1 279	–655	–971	–516
TC05A	12,9	2,9	2,2	0,6	2 287	518	386	100
TC05B	–5,6	–1,1	–2,0	–0,3	–999	–200	–354	–53
TC05C	–7,7	–1,9	–6,2	–1,4	–1 376	–332	–1 101	–247

Table H.1: Effective streaming current and charge density at filter section exit and tote inlet (continued)

Condition	Effective current				Effective charge density			
	Maximum		Final		Maximum		Final	
	Filter exit	Tote inlet	Filter exit	Tote inlet	Filter exit	Tote inlet	Filter exit	Tote inlet
TC06A	–8,8	–2,0	–3,8	–0,8	–1 548	–361	–667	–146
TC06B	–3,9	–0,9	–1,3	–0,26	–703	–165	–241	–46
TC06C	–10,9	–2,7	–1,4	–0,32	–1 953	–481	–259	–58
TC07A			–1,2	–0,11			–207	–19
TC07B			–0,53				–93	–0,45
TC07C			–0,45	–0,005			–80	–0,91
TC08A			–0,44	–0,009			–77	–1,52
TC08B			–0,16	–0,002			–29	–0,34
TC08C			–0,27	–0,005			–48	–0,93
TC09A			–0,11				–20	–0,27
TC09B			–0,07				–13	–0,15
TC09C			–0,12				–21	–0,25
TC10A			–0,11				–20	–0,31
TC10B			–0,05				–9	–0,16
TC10C			–0,10				–17	–0,27
TC11A	20,4	10,0	19,4	9,6	3 611	1 781	3 440	1 701
TC11B	–1,1	–1,1	–0,85	–0,83	–196	–206	–155	–152
TC11C	–0,23	–0,20	–0,19	–0,18	–41	–36	–34	–33
TC12A	17,8	5,1	4,8	2,2	3 148	899	848	399
TC12B	–1,1	–1,0	–0,51	–0,52	–196	–186	–93	–94
TC12C	–0,23	–0,22	–0,21	–0,20	–41	–39	–37	–36
TC13A			–0,05				–9,0	0,05

Table H.1: Effective streaming current and charge density at filter section exit and tote inlet (continued)

Condition	Effective current				Effective charge density			
	Maximum		Final		Maximum		Final	
	Filter exit	Tote inlet	Filter exit	Tote inlet	Filter exit	Tote inlet	Filter exit	Tote inlet
TC13B			–0,02				–2,8	0,01
TC13C			–0,04				–7,4	0,16
TC14A			–0,02				–3,9	0,10
TC14B			–0,01				–1,9	–0,44
TC14C			–0,01				–2,3	0,45
TC15A	5,9	2,4	5,6	2,3	1 043	415	985	401
TC15B	–16,7	–9,6	–12,9	–9,2	–2 972	–1 703	–2 290	–1 635
TC15C	–16,7	–10,6	–16,6	–10,2	–2 980	–1 898	–2 975	–1 826
TC16A	–7,5	–5,2	–6,3	–4,5	–1 341	–925	–1 120	–797
TC16B	–13,7	–7,5	–7,9	–5,6	–2 433	–1 343	–1 406	–1 002
TC16C	–25,4	–13,3	–13,3	–8,0	–4 636	–2 425	–2 425	–1 459
TC17A	7,5	3,8	6,3	3,3	1 348	684	1 130	587
TC17B	0,11	0,11	0,11	0,11	20	19	20	19
TC17C	0,56	0,51	0,56	0,51	99	91	99	91
TC18A	4,4	2,4	3,4	2,2	774	418	605	381
TC18B	1,1	0,94	1,1	0,94	206	170	206	170
TC18C	1,9	1,5	1,8	1,4	332	263	325	258
TC19A	5,7	1,5	2,5	0,62	1 010	264	454	111
TC19B	–14,7	–6,9	–6,9	–3,8	–2 610	–1 224	–1 227	–677
TC19C	–15,6	–8,2	–13,7	–8,2	–2 748	–1 448	–2 417	–1 446
TC20A	–13,3	–6,1	–4,0	–2,5	–2 367	–1 074	–702	–452
TC20B	–7,4	–2,7	–2,1	–1,2	–1 306	–480	–365	–218
TC20C	–14,2	–5,6	–3,4	–2,0	–2 583	–1 014	–613	–361

Table H.2: Absolute values of maximum and final streaming current and charge density at filter section exit and tote inlet

Test condition	Element code	Absolute current, μA				Absolute charge density, μC/m³			
		Maximum value		Final value		Maximum value		Final value	
		Filter	Tote	Filter	Tote	Filter	Tote	Filter	Tote
1	A	12,1	5,48	6,76	2,95	4 064	970	1 211	530
1	B	1,64	1,35	1,56	1,14	352	254	300	219
1	C	1,78	1,30	1,76	1,10	325	235	320	199
2	A	2,62	1,98	2,59	1,63	643	350	462	291
2	B	3,34	2,20	3,32	1,91	875	407	618	353
2	C	5,00	2,80	4,93	2,69	908	506	894	488
3	A	5,93	2,36	3,80	1,59	1 129	418	681	285
3	B	7,33	4,12	2,78	1,62	1 721	724	495	288
3	C	11,1	4,25	4,02	2,38	4 133	754	721	427
4	A	4,77	3,06	4,73	2,98	1 053	543	845	532
4	B	6,28	2,86	0,50	0,13	2 948	508	92	24
4	C	8,85	3,85	5,49	2,94	2 347	687	995	533
5	A	13,3	3,01	2,48	0,54	2 921	530	443	96
5	B	9,49	2,11	2,07	0,33	2 315	371	369	58
5	C	11,4	2,54	6,29	1,42	3 450	448	1 124	253
6	A	9,39	2,33	3,70	0,87	2 449	408	658	155
6	B	8,19	1,82	1,54	0,33	2 376	318	278	60
6	C	11,9	2,92	1,09	0,30	4 020	513	197	55
7	A	2,84	0,01	0,57	0,011	651	3,61	101	1,93
7	B	2,49	0,01	0,42	0,0023	933	1,38	74	0,42
7	C	2,59	0,01	0,28	0,0038	667	1,27	51	0,68
8	A	1,50	0,01	0,28	0,0085	365	2,13	50	1,52

Table H.2: Absolute values of maximum and final streaming current and charge density at filter section exit and tote inlet (continued)

Test condition	Element code	Absolute current, μA				Absolute charge density, μC/m³			
		Maximum value		Final value		Maximum value		Final value	
		Filter	Tote	Filter	Tote	Filter	Tote	Filter	Tote
8	B	0,71	0,0052	0,073	0,0016	217	1,17	13	0,29
8	C	1,13	0,0078	0,17	0,0046	321	1,51	31	0,83
9	A	0,12	0,0030	0,093	0,0014	21	0,53	17	0,25
9	B	0,086	0,0021	0,061	0,00028	31	0,37	11	0,05
9	C	0,14	0,0033	0,10	0,0014	37	0,58	17	0,25
10	A	0,070	0,0027	0,054	0,00091	25	0,48	10	0,16
10	B	0,070	0,0023	0,031	0,00076	19	0,52	5,8	0,14
10	C	0,079	0,0033	0,063	0,0016	27	1,26	11	0,29
11	A	27,8	12,0	20,9	10,1	6 914	2 120	3 744	1 799
11	B	2,20	1,85	0,82	0,71	550	321	154	134
11	C	0,23	0,24	0,17	0,17	105	42	31	31
12	A	23,1	9,11	4,83	2,21	10 499	1 606	862	395
12	B	1,42	1,28	0,16	0,17	301	226	29	31
12	C	0,57	0,40	0,18	0,19	188	67	33	35
13	A	0,070	0,0053	0,050	0,00013	12	2,7	9,0	0,024
13	B	0,039	0,0057	0,0091	0,00039	101	8,7	1,7	0,074
13	C	0,40	0,0060	0,062	0,000060	70	2,0	12	0,011
14	A	0,030	0,0035	0,019	0,000030	5,4	0,6	3,4	0,0054
14	B	0,011	0,0042	0,0045	0,00012	2,6	0,80	0,87	0,023
14	C	0,041	0,0047	0,0073	0,00033	6,9	3,6	1,4	0,065
15	A	7,3	2,57	6,20	2,32	2 664	453	1 093	409

Table H.2: Absolute values of maximum and final streaming current and charge density at filter section exit and tote inlet (continued)

Test condition	Element code	Absolute current, μA				Absolute charge density, μC/m³			
		Maximum value		Final value		Maximum value		Final value	
		Filter	Tote	Filter	Tote	Filter	Tote	Filter	Tote
15	B	21,2	12,5	12,7	9,25	6 612	2 200	2 274	1 658
15	C	19,9	11,7	16,3	10,2	6 747	2 050	2 936	1 879
16	A	9,30	6,26	6,13	4,61	2 396	1 119	1 099	826
16	B	19,9	13,1	7,80	5,74	5 914	2 304	1 396	1 028
16	C	28,0	14,8	13,5	7,94	7 493	2 636	2 524	1 473
17	A	11,8	5,31	6,25	2,78	4 978	944	1 125	501
17	B	0,37	0,26	0,16	0,17	88	45	29	30
17	C	0,67	0,50	0,63	0,47	161	90	112	85
18	A	6,99	3,52	3,53	1,91	2 832	613	624	337
18	B	1,27	0,93	1,24	0,83	233	168	226	154
18	C	2,27	1,31	1,97	1,25	407	233	355	221
19	A	7,36	1,60	3,03	0,65	1 463	283	544	117
19	B	16,6	8,84	6,75	4,01	7 171	1 561	1 208	718
19	C	20,6	10,3	13,3	8,20	7 443	1 799	2 362	1 451
20	A	14,5	6,77	3,59	2,64	4 801	1 189	640	471
20	B	10,4	4,37	1,52	1,26	3 149	743	271	224
20	C	16,0	6,86	3,03	2,05	8 710	1 224	555	377

ANNEX I: MAXIMUM ELECTRIC FIELDS, DECAY TIMES AND EQUIVALENT CONDUCTIVITIES FOR EACH RUN BELOW 200 pS/m

Table I.1: Electric field decay times, effective conductivities and maximum fields

Run label	Conductivity, pS/m			Decay time, s			Maximum field, kV/m	
	Measured	From initial field decay time	From final field decay time	From measured conductivity	Initial	Final	Measured	Estimated at flat roof
S01	5	3,2	3,4	3,7	5,8	5,5	–4,8	–1,5
S02	5	3,3	2,8	3,7	5,7	6,7	–80	–25
S03	5	3,0	2,4	3,7	6,1	7,7	–62	–19
S04	5	2,0	1,5	3,7	9,3	12	52	16
TC01	0	0,87	0,58		21	32	161	49
TC01	3	1,4	0,7	6,2	13	26	75	23
TC01	0	0,80	0,54		23	34	99	30
TC02	2	0,80	0,35	9,3	23	53	139	43
TC02	0	0,83	0,43		22	44	113	35
TC02	1	0,90	0,24	19	21	77	127	39
TC03	4	3,8	3,4	4,6	4,9	5,5	25	7,7
TC03	3	3,0	3,9	6,2	6,1	4,8	–38	–12
TC03	3	3,3	3,0	6,2	5,7	6,3	–50	–15
TC04	3	3,2	2,5	6,2	5,9	7,5	–82	–25
TC04	4	3,6	4,4	4,6	5,1	4,2	–3,0	–0,9
TC04	2	2,7	2,5	9,3	7,0	7,6	–85	–26
TC05	18	10,3	9,5	1,0	1,8	2,0	1,9	0,6
TC05	23	6,5	11,5	0,8	2,9	1,6	–0,42	–0,13
TC05	20	7,4	12,5	0,9	2,5	1,5	–2,0	–0,6

Table I.1: Electric field decay times, effective conductivities and maximum fields (continued)

Run label	Conductivity, pS/m			Decay time, s			Maximum field, kV/m	
	Measured	From initial field decay time	From final field decay time	From measured conductivity	Initial	Final	Measured	Estimated at flat roof
TC06	18	7,7	10,4	1,0	2,4	1,8	–2,9	–0,9
TC06	20	8,3	11,4	0,9	2,2	1,6	–0,5	–0,2
TC06	15	7,5	11,5	1,2	2,5	1,6	–2,4	–0,7
TC11	0	1,9	0,16		10	117	193	59
TC11	0	0,66	0,061		28	305	–147	–45
TC11	0	0,13	0,083		145	225	–88	–27
TC12	0	0,71	0,050		26	375	195	60
TC12	0	0,21	0,086		90	215	–73	–23
TC12	0	0,12	0,063		151	297	–94	–29
TC15	4	2,2	1,7	4,65	8,5	11	54	16
TC15	4	2,2	1,2	4,65	8,5	15	–154	–47
TC15	5	3,6	2,5	3,72	5,2	7,5	–116	–36
TC16	2	1,9	1,0	9,30	9,8	19	–142	–43
TC16	1	2,2	1,1	18,59	8,6	16	–168	–52
TC16	4	2,7	1,7	4,65	6,9	11	–138	–42
TC17	0	1,2	0,13		15	145	169	52
TC17	0	0,072	0,010		259	1 897	38	12
TC17	0	0,40	0,083		46	224	120	37
TC18	0	0,55	0,067		34	277	178	55

Table I.1: Electric field decay times, effective conductivities and maximum fields (continued)

Run label	Conductivity, pS/m			Decay time, s			Maximum field, kV/m	
	Measured	From initial field decay time	From final field decay time	From measured conductivity	Initial	Final	Measured	Estimated at flat roof
TC18	0	0,54	0,040		35	465	123	38
TC18	0	0,89	0,070		21	265	143	44
TC19	8	3,7	5,6	2,32	5,0	3,3	3,1	0,94
TC19	11	4,3	4,8	1,69	4,3	3,8	–40	–12
TC19	5	4,5	3,7	3,72	4,1	5,1	–62	–19
TC20	5	1,9	1,8	3,72	9,6	10	–101	–31
TC20	5	4,1	3,5	3,72	4,5	5,3	–22	–6,8
TC20	4	2,0	2,6	4,65	9,2	7,1	–79	–24

Energy Institute
61 New Cavendish Street
London W1G 7AR, UK

t: +44 (0) 20 7467 7100
f: +44 (0) 20 7255 1472
e: pubs@energyinst.org
www.energyinst.org

9780852939758

ISBN 978 0 85293 975 8
Registered Charity Number: 1097899